1.0

4.5
5.0
5.6

2.8

2.5

3.2

2.2

3.6

1.1

4.0

2.0

1.8

1.25

1.4

1.6

MICROCOPY RESOLUTION TEST CHART

NATIONAL BUREAU OF STANDARDS-1963-

ARG 12931.2-EX

LEVEL II

EXPERIMENTAL AND THEORETICAL STUDIES ON MODEL HELICOPTER ROTOR NOISE

by

Krishnaswamy S. Aravamudan
and
Wesley L. Harris

Department of Aeronautics and Astronautics
Fluid Dynamics Research Laboratory
Massachusetts Institute of Technology
Cambridge, Massachusetts 02139

DDC

RECEIVED

MAY 2 1979

A

January, 1978

79 04 27 054

REPORT DOCUMENTATION PAGE	READ INSTRUCTIONS BEFORE COMPLETING FORM

1. REPORT NUMBER M.I.T. Fluid Dynamics Research Laboratory Report No. 78-1	2. GOVT ACCESSION NO.	3. RECIPIENT'S CATALOG NUMBER

4. TITLE (and Subtitle) Experimental and Theoretical Studies on Model Helicopter Rotor Noise	5. TYPE OF REPORT & PERIOD COVERED Interim Report March 1976 - December 1977
	6. PERFORMING ORG. REPORT NUMBER 83852-1

7. AUTHOR(s) Krishnaswamy S. Aravamudan Wesley L. Harris	8. CONTRACT OR GRANT NUMBER(s) 1) USARO DAAG 29-C-0027 2) NASA NSG 2095

9. PERFORMING ORGANIZATION NAME AND ADDRESS Massachusetts Institute of Technology Dept. of Aeronautics and Astronautics Fluid Dynamics Research Laboratory Cambridge, MA 02139	10. PROGRAM ELEMENT, PROJECT, TASK AREA & WORK UNIT NUMBERS Contract does not supply this information

11. CONTROLLING OFFICE NAME AND ADDRESS U.S. Army Research Center P.O. Box 12211 Research Triangle Park, NC 27709	12. REPORT DATE January 1978
	13. NUMBER OF PAGES

14. MONITORING AGENCY NAME & ADDRESS(if different from Controlling Office) Same as controlling office	15. SECURITY CLASS. (of this report) Unclassified
	15a. DECLASSIFICATION/DOWNGRADING SCHEDULE

16. DISTRIBUTION STATEMENT (of this Report)

Distribution of this document is unlimited

17. DISTRIBUTION STATEMENT (of the abstract entered in Block 20, if different from Report)

Distribution of this abstract is unlimited

19. KEY WORDS (Continue on reverse side if necessary and identify by block number)

Helicopter, rotor acoustics, rotational noise, broadband noise, Mach number scaling of helicopter rotor noise, turbulence

20. ABSTRACT (Continue on reverse side if necessary and identify by block number)

A simplified Mach number scaling law is obtained for rotational and broadband noise components of a model helicopter rotor. The broadband noise sources are further classified into low frequency and high frequency components. The scaling laws are based on the geometric and performance parameters of the rotor and characteristics of the flow field.

The existing theory of Lowson and Ollerhead is used deriving the (cont.)

DD FORM 1 JAN 73 1473 EDITION OF 1 NOV 65 IS OBSOLETE

20.

conventional sixth power law for the rotational noise of geometrically similar blades operating in similar flow environ. The knowledge of unsteady aerodynamics has been exploited to yield analytical formulation for the low frequency broadband radiation. The ambiguous state of the art regarding the origin and nature of high frequency broadband noise does not permit such a straightforward scaling law for this frequency regime. The vortices are assumed to be shed at unknown Strouhal frequency and the scaling law is derived by simply integrating the blade sectional velocity over the span. The MIT 5 x 7½

The M.I.T. 5 X 7 1/2 foot anechoic wind tunnel facility was used to perform experiments at controlled flow environ. The turbulence was generated at the inlet of the tunnel with the aid of biplanar grids and simultaneous measurements of acoustic and turbulence signals were made. The experimentally obtained results are compared with the computed intensities and spectra of rotational noise, low frequency broadband noise and high frequency broadband noise from model rotors.

EXPERIMENTAL AND THEORETICAL STUDIES

ON MODEL HELICOPTER ROTOR NOISE

Krishnaswamy S. Aravamudan

and

Wesley L. Harris

Department of Aeronautics and Astronautics

Fluid Dynamics Research Laboratory

Massachusetts Institute of Technology

Cambridge, Mass. 02139

January 1978

79 04 27 054

ABSTRACT

A simplified Mach number scaling law is obtained for rotational and broadband noise components of a model helicopter rotor. The broadband noise sources are further classified into low frequency and high frequency components. The scaling laws are based on the geometric and performance parameters of the rotor and characteristics of the flow field.

The existing theory of Lowson and Ollerhead is used deriving the conventional sixth power law for the rotational noise of geometrically similar blades operating in similar flow environ. The knowledge of unsteady aerodynamics has been exploited to yield analytical formulation for the low frequency broadband radiation. The ambiguous state of the art regarding the origin and nature of high frequency broadband noise does not permit such a straightforward scaling law for this frequency regime. The vortices are assumed to be shed at unknown Strouhal frequency and the scaling law is derived by simply integrating the blade sectional velocity over the span.

The M.I.T. 5 X 7 1/2 foot anechoic wind tunnel facility was used to perform experiments at controlled flow environ. The turbulence was generated at the inlet of the tunnel with the aid of biplanar grids and simultaneous measurements of acoustic and turbulence signals were made. The experimentally obtained results are compared with the computed intensities and spectra of rotational noise, low frequency broadband noise and high frequency broadband noise from model rotors.

ACKNOWLEDGEMENTS

TABLE OF CONTENTS

LIST OF FIGURES

LIST OF TABLES

LIST OF SYMBOLS

$a_{\lambda T}$, $b_{\lambda T}$ — Fourier coefficients of λth harmonic sound radiation due to thrust

$a_{\lambda D}$, $b_{\lambda D}$ — Fourier coefficients of λth harmonic sound radiation due to Drag

$a_{\lambda c}$, $b_{\lambda c}$ — Fourier coefficients of λth harmonic sound radiation due to Centrifugal force

B — number of blades

b — blade span

C_f — force coefficient

C_n — Complex Fourier coefficient of Sound radiation

$C_{\lambda T}$ — Complex Fourier coefficient of Thrust

C_{pb} — base pressure coefficient

c — blade chord

c_0 — speed of sound

$D_r(\phi,f)$ — power spectra density of the dipole radiation

$d_r(\phi)$ — source strength of dipole radiation

$E(k)$ — three dimensional energy function of turbulence

F_r — unsteady force acting on the blade

F_w — three dimensional Fourier component of turbulence upwash

f — frequency, HZ

$H(k)$ — incompressible Sear's function

K — aerodynamic transfer function

$\vec{k}$ — wave number vector of turbulence upwash

k_x, k_y, k_z — component of wave number vector in x, y, z, direction respectively

k_e — wave number range of energy containing eddies

k_c, k_s	wave number components in chordwise and spanwise direction
L	unsteady lift function
M_0	rotational mach number at R_0
M_c	convection mach number
M_e	Effective rotational Mach number
M_{or}	the component of forward Mach number in observer direction
M_s	$= (1 + \mu)M_t$
M_t	rotor tip Mach number
m	rotational harmonic
P_i	instantaneous pressure on the airfoil
$\vec{Q}$	velocity vector
R_{LL}	unsteady lift correlation function
R_0	radial location of the effective velocity
$R_{e\theta}*$	Reynolds number based on momentum thickness
r, r_1	observer locations
S	Strouhal number
S_{eff}	effective Sears function
$S_\theta*$	wake Strouhal number
$<S(f)>$	power spectral density
$<S_{pp}(\vec{x}, f)>$	one dimensional spectra
t	thickness of blade section
t_ξ	convection time for an eddy
U_0	rotational velocity at R_0
u_∞	free stream velocity
V_t	tip velocity
v_c	blade sectional velocity

w	turbulence upwash
$\vec{x}, \vec{x}'$	coordinate systems
α	observer location
α_S	shaft angle
β	$\sqrt{1 - M}$
ΔL	spanwise correlation length for shed vortices
δ_L	laminar boundary layer thickness
δ^*	displacement thickness
θ	momentum thickness
Λ	integral scale of turbulence
Λ_f, Λ_g	longitudinal and vertical integral scales of turbulence
λ	loading harmonic
μ	advance ratio
ν	kinematic coefficient of viscosity
ρ_0	ambient density
Φ	function to account for phase difference
$\Phi_{LL}(f)$	power spectral density of unsteady lift function
Φ_{uu}, Φ_{ww}	axial and vertical spectrum of turbulence
ϕ	Azimuthal angle
Ω	rotational speed

CHAPTER I

INTRODUCTION

Helicopter rotors generate complex acoustic signatures. A variety of mechanisms are responsible for the radiated acoustic energy and only a few of these mechanisms are understood.

The sound radiated by a lifting rotor at low to moderate tip speeds is essentially due to the time varying pressure distributions on the blade. This, often termed as "rotational noise", was originally studied by Gutin [1], where only steady azimuthally constant blade loads were considered. These discrete frequency components occur at multiples of blade passage frequency and the unsteady nature of the blade forces prevents the harmonics from decaying, as originally predicted by Gutin. Random noise formerly was called "vortex noise", but investigators now prefer "broadband noise", since vortex shedding itself is not believed to be the principal mechanism.

At higher tip speeds and/or high flight speed, the flow over the blade section may exceed sonic velocity and result in generation of a local shock. These are termed as "shock noise" and are characterized by sharp peaks in the acoustic pressure time history, resulting in highly annoying banging sounds. Another dominant noise source is due to "blade-vortex interaction". A blade that passes close to a wake vortex filament experiences [2,3] a rapid change in the aerodynamic loading. This, often termed as "blade slap", is dependent on the geometry of the wake. Both these noise sources are impulsive in nature and occur only at certain flight conditions of a helicopter. In the absence of these mechanisms,

the discrete and broadband noise dominate the rotor noise spectra.

Whereas the "rotational" or "discrete" noise from the rotors is fairly well understood, the situation for broadband noise is most unsatisfactory. Almost nothing can be said unequivocally about the broadband noise and this is simply because of the difficulty in pinpointing the noise sources experimentally. Opinions regarding the origins and behavior of broadband noise vary somewhat among investigators, but there is general agreement that turbulence in the flow seen by rotor blades is the basic physical mechanism responsible for broadband noise.

Two similar bodies placed in an otherwise smooth flow generate sound most efficiently when one lies in the turbulent wake of the other. The first person to record such an effect appears to have been G.I. Taylor [4], who waved a toasting fork through the air and observed a louder "singing" when the plane of the prongs lay in the direction of motion than when it was perpendicular to the motion. A later experiment by Kramer [5] ingeniously demonstrated the Taylor effect for airfoil sections by rotating a single blade of high aspect ratio at zero angle of attack, such that the blade passed through its own wake. The overall noise level was about 3dB higher with this arrangement than when the blade was given a certain angle of attack in either direction. Recent experimental data for a full scale helicopter rotor obtained by Leverton [6] and Leverton and Pollard [7] seems to suggest that the broadband noise is dependent only on the nature of turbulence. Thus, the turbulence may be due to inflow, the boundary layer of the blades, or the wake itself - generating an unsteady lift on the airfoil and hence the noise. Principal areas of uncertainty include the effects of

velocity and the size scale of turbulence on the intensity and spectra of the broadband noise. The work of Leverton [6] fails to show any kind of Strouhal frequency scaling with velocity for full scale rotors.

Much of the recent impetus to study the rotational and broadband noise comes from improved data processing technique and equipment. Narrowband analysis of rotor noise data has shown discrete frequency components extending well beyond 150 Hz, which historically was believed to be the transition region between rotational noise and broadband noise for typical helicopter rotors. Work by Lowson, Whatmore, and Whitfield [10] and by Leverton [6] emphasize that low frequency broadband noise could have different causative physical mechanisms and acoustic behavior than high frequency broadband noise. It is generally believed that the inflow turbulence interaction with the rotor blades is responsible for the low frequency broadband noise. The high frequency component is attributed to the vortex shedding by the airfoils. In Figure 1.1 is shown a typical 6% bandwidth acoustic spectrum of a model rotor. Identified in this figure are the regions of rotational noise, low frequency broadband noise, and high frequency broadband noise.

To obtain the relationship between flow field characteristics and the sound radiated lifting rotors, it is necessary to determine which mechanism is primarily responsible for the radiation. Each postulated mechanism leads to a particular characterization of the sound field and of its relationship to the flow field characteristics. Empirical measurements and similarity arguments can then be used to establish a posteriori verification of the choice of the mechanism. To this end,

we assume that (i) the steady and unsteady loading harmonics are responsible for radiation of rotational noise, (ii) the intensity and size scale of turbulence are the governing factors for low frequency broadband noise radiation, and (iii) the periodic vortex shedding is the dominant mechanism responsible for radiation of high frequency broadband noise. The major contribution of the research effort described in this report is the development of appropriate Mach number scaling laws for model helicopter rotor noise and experimental verification of these laws. Equally important has been the obtainment of a definition of the effects of helicopter performance parameters on model helicopter rotor noise.

Here, an attempt has been made to study the influence of free-stream disturbances on the acoustic signatures generated by model helicopter rotors. Appropriate theoretical modelling for rotational, low frequency broadband and high frequency broadband noise are made exploiting the existing knowledge of acoustic radiation from a rotating dipole source and unsteady aerodynamics associated with rotating blades. In Chapter II is presented a detailed description of the MIT Anechoic Wind Tunnel and model rotor facility, the instrumentation used for acquisition and processing of various rotor noise components. Here we have discussed the nature of the artificially generated tunnel turbulence and the appropriate theoretical modelling of its spectrum. In Chapter III is derived a simple Mach number scaling procedure to describe to rotational noise characteristics. Chapter IV contains a formal theoretical analysis of the low frequency broadband noise radiation. We have compared the experimentally obtained data with the

computed intensity and spectra of low frequency broadband noise. In Chapter V the nature of the high frequency broadband noise is discussed in detail. An order of magnitude study has been made to predict the peak intensity of the high frequency broadband noise and its location in the frequency domain. The effects of inflow turbulence on the high frequency broadband noise radiation are postulated and the results are compared with experimentally obtained data. Chapter VI provides the scaling results appropriate for the radiation of low rotational frequency broadband noise and the high frequency broadband noise. We have also made an attempt to compare our model results with the full scale results obtained by Leverton [6]. The conclusions of our efforts are discussed in Chapter VII.

CHAPTER II

DESCRIPTION OF THE EXPERIMENTS

2.1 Introduction

The M.I.T. anechoic wind tunnel facility was used to study the effects of controlled free stream turbulence on the low frequency and the high frequency broadband noise radiation from a model helicopter rotor. The parameters under study were the variation of helicopter performance characteristics such as number of blades, thrust and advance ratio. In addition, we also studied the effects of intensity and size scales of injested turbulence on the intensity and spectra of broadband noise. Turbulence was generated at the tunnel inlet by placing biplanar grids of varying size. In this chapter, the experimental apparatus used in obtaining and analyzing both turbulence and acoustic data are described. The nature of the injested turbulence and the appropriate theoretical modelling of the spectrum for evaluation of the acoustic spectra are discussed at length.

2.2 The M.I.T. Anechoic Tunnel & Rotor Facility

The 5 x 7 1/2 foot open Jet wind tunnel was used for the study of effects of free stream turbulence on model rotor generated noise. The maximum speed of the tunnel is 75 mph and the open jet section of the tunnel is enclosed in a 12 x 12 x 24 foot anechoic chamber. The sides of the chamber were covered with Cremer blocks and the floor of the chamber was covered with 6 inch thick polyurethene foam. The anechoic properties of the tunnel were measured and the acoustic cut off frequency above which

free field conditions prevail was found to be 160 HZ. The effect of the shear layer of the open jet on refraction and scattering of acoustic waves were studied by using aeolian tones as sound source and were found to be insignificant under the present test conditions. The details of the aerodynamic and acoustic calibrations of the wind tunnel facility are described in References [11] and [12].

The model helicopter rotor system consists of a 4.17 foot diameter rotor and has blades made of fiber glass. The rotor hub is designed to take up to 8 blades and is connected to a thrust measuring dynamometer. The dynamometer consists of four sets of BLH SPB 3-20-35 semi-conductor strain gages mounted on two sets of flexures. Lebow slip ring was used to transmit the signals from the rotating dynamometer. The details of the dynamometer system and its calibration may be obtained from Reference [12]. The rotor shaft is driven by a 5.8 HP hydraulic motor which has a maximum rpm of 1200. The rotor shaft has a tilt capability of $\pm$ 20°. The details of the model rotor are summarized in Table 2.1.

Controlled turbulence was generated with the aid of biplanar grids mounted in the upstream section of the tunnel. Figure 2.1 shows a photograph of the model rotor system with an upstream turbulence generator in the background. The steady velocity in the test section was set using a pitot static probe and the read out was made on a vertical manometer. The pressure variation was minimal for the test conditions reported here. The fluctuating velocity signals were measured with the aid of a hot wire sensor. In Figure 2.2 is shown a photograph of the set up. Identified within the figure are the location of the probes for measuring steady and fluctuating velocity signals.

2.3 Instrumentation

Data flow for all the experiments performed for this study was from microphones and hot wire sensors to a magnetic tape and later from the magnetic tape to appropriate spectrum analyzers.

The acoustic measurements were made along a circular arc at a radius of 52 inches from the rotor disc plane, perpendicular to the direction of the wind and passing through the axis of the rotor. Acoustic signals were measured using a 1/2 inch B & K microphone type 4133 with a cathode follower type 2614. The signals were amplified by a B & K microphone amplifier and were recorded on magnetic tape using a P.I. 4 channel tape recorder model 6204 in direct mode. The microphones were calibrated using a B & K piston phone type 4220. In addition to the acoustic signal, a timing pulse at a period of $1/B\Omega$ was also recorded on one of the channels of the tape recorder. The steady thrust measurements were made simulta- neously with the aid of a digital volt meter. In Figure 2.3 is shown a schematic of the instrumentation utilized in acquisition of acoustic data.

The fluctuating velocity signals were measured with an X-type hot wire sensor type DISA 55P51. The probe was placed 7.5" directly above the rotor plane 4" aft the axis of the rotor. Flow Corporation constant temperature anemometer type 900-1 were used in conjunction with Flow Corporation linearizers type 900-4 and type 4835-C. An attenuator was used with the latter linearizer in order to adjust the sensitivity of both the wires to be same. The probe was calibrated over anticipated test velocities and the responses of both wires were found linear. The linearized signals were processed through a Flow Corporation sum and difference unit to yield the longitudinal and vertical components of

velocities. These signals were further passed through a Flow Corporation suppressor filter unit type 900-3 to yield only the fluctuating quantities of the signal. All the signals were constantly monitored with the aid of a Flow Corporation digital volt meter type 900-2D. The fluctuating signals were then recorded on two F.M. channels of a P.I. 4 channel tape recorder type 6204. The r.m.s. values of the signals were measured by using HP 3400A RMS volt meters. In Figure 2.4 is shown a schematic of instrumentation used in acquisition of turbulence data. The acoustic and turbulence measurements were made simultaneously.

The measured acoustic signals were processed with the aid of a B & K audio Frequency analyzer type 2107 and a B & K graphic level recorder type 2305. Figure 2.5 depicts a schematic of the instrumentation used for analyzing the acoustic data. The turbulence data was analyzed using a Federal Scientific UA-15A Spectrum Analyzer together with a 1015 averager. In Figure 2.6 is shown a schematic of instrumentation for analyzing the turbulence data.

2.4 Turbulence Measurements

The grids employed in this study were designed based on the data of Baines and Peterson [13]. The grids were biplanar consisting of bars of 3/4 inches with a mesh size of 6 inches and bars of 3 1/2 inches with a mesh size of 20 inches. The grid solidity were 0.23 and 0.32 respectively. The grid Reynolds number based on the lowest tunnel velocity were 9×10^4 and 3×10^5 respectively. As noted in Reference [13], the turbulence down stream of a biplanar grid becomes practically isotropic in an axial distance of about 5 to 10 mesh lengths.

In the present series of experiments, the grids were located 96 inches from the axis of the rotor. This corresponds to about 16 mesh lengths for the smaller grid and 4.8 mesh lengths for the larger grid. The longitudinal and vertical integral scales Λ_f and Λ_g of the grid generated turbulence were determined near the axis of rotor. For convenience, we estimated from the Eularian Integral time scale τ_e. The values of τ_e were determined from the extrapolated zero intercept of the power spectra of longitudinal and vertical velocities. The length scales, then are given by

$$\Lambda_f = U_0 \tau_{ef} \; ; \; \Lambda_g = U_0 \tau_{eg}$$

Figure 2.7 shows the typical variation of measured longitudinal integral scale in the presence of as well as in the absence of turbulence generating grids. The longitudinal scale is roughly independent of the free stream velocity when the grids are present. In the absence of grids, the measured Eularian time scales were quite large and fluctuating. This resulted in large length scales that are varying considerably with the free stream velocity. However, the variation of the length scale does not seem to follow any definite pattern. For convenience in the theoretical analysis we assumed that the scale of turbulence was in-dependent of the free stream velocity. To this end, we obtained an average value of the scale which is plotted in dotted lines in Figure 2.7. In Figure 2.8 is shown the measured vertical integral scale as a function of free stream velocity. Once again, we observe that the fluctuations in the measured scales are large in the absence of grids. In Table 2.2 are given the averaged values of longitudinal and vertical

length scales for the three different cases. From the table, it is seen that the ratio of vertical scale to longitudinal scale is slightly greater than the expected value of 0.5 for isotropic, homogeneous turbulence.

In Figures 2.9 and 2.10 are the measured power spectral density of the longitudinal and vertical components of turbulence as a function of wave number respectively. In plotting these figures, Taylor's hypothesis of frozen turbulence has been applied to convert the turbulence spectrum from an experimentally obtained temporal frame to a spatial frame. The axial wave number is related to frequency by $k_x = 2\pi f/U_0$ and this is nondimensionalized with respect to k_e as $3k_x/8\pi k_e$. Here k_e is the wave number range of energy containing eddies and is related to the longitudinal integral scale Λ_f by $k_e \simeq 0.75/\Lambda_f$. Also shown in the figures is the empirical isotropic turbulence spectrum derived from von Karman's interpolation formula. The nondimensionalized power spectral densities for longitudinal and vertical components of turbulence are given as follows

$$\Phi_{uu}(k_x) = \Phi_{uu}(0) \, / \, [1 + k_x^2/k_e^2]^{5/6} \tag{2.2}$$

$$\Phi_{ww}(k_x) = \frac{\Phi_{ww}(0) \, [1 + {}^8/_3 \, k_x^2/k_e^2]}{[1 + k_x^2/k_e^2]^{11/6}} \tag{2.3}$$

The measured data shows good agreement with the von Karman spectrum including a -5/3 power decrease at high frequencies. However, in the absence of grids, the tunnel turbulence seems to deviate slightly from

the predicted von Karman spectrum. In Figure 2.11 is shown the variation
of fluctuating axial and vertical components of turbulence as a function
of free stream velocity. From the Figure 2.11 we infer than an average
turbulence intensity of 11% for the larger grid and 6.25% for the smaller
grid is very reasonable. In absence of grids, the tunnel turbulence
seems to average to about 1.7% of the free stream velocity.

2.5 Acoustic Measurements

Extensive measurements of the background noise for the M.I.T. anechoic
wind tunnel facility has been made by Harris and Lee [15].
However, it is very likely that an upstream turbulence generator would alter
the background noise spectra of the tunnel. To ensure that the acoustic
measurements were not affected by such noise, a survey of the tunnel back-
ground noise was made at various tunnel speeds with and without the
turbulence generating grids in place.

To isolate the low frequency rotational noise components of the
rotor from the relatively high intensity tunnel background noise, a periodic
sampling technique was used. This technique involves the use of a PAR wave-
form eductor, Model TDH-9. The waveform eductor samples the repetitive
input and stores them in a 100 channel capacitance memory. After a suffi-
cient number of sweeps have occurred, the noise from non-repetitive sources
(background noise in the present case) will be suppressed since their average
value will approach zero. The processed rotor data will contain only the
rotational noise. The timing pulse of $\frac{1}{B\Omega}$ was used to average the waveform
of the signal. The spectrum was obtained by using a Federal Scientific UA-15A
Spectrum Analyzer with a 1015 averager. In Figure 2.12, the instrumentation
used for processing the rotational noise data is shown. In Figure 2.13, the

typical waveforms and the resulting spectra with and without the use of periodic sampling technique are shown.

Since some of our studies involve the influence of free stream disturbances on the low frequency and high frequency broadband noise sources, it was necessary to ensure that (i) the rotational harmonics do not contribute significantly to the broadband noise generated by the rotor and (ii) the background noise level in the tunnel is low enough to yield the necessary signal to noise ratio. The first task was accomplished with the use of the periodic sampling technique.

In Figure 2.14 are plotted the 6% bandwidth spectra for a two bladed rotor operating at 672 rpm and an advance ratio of 0.3. The 3/4" x 6" turbulence generating grid was located upstream and the Figure compares the spectra obtained with and without waveform eductor. The rotational harmonic obtained from the periodic sampling technique are very distinct and they decay very rapidly. As can be seen from Figure 2.14, above 200 HZ, which we assume as the transition from rotational noise to broadband noise, the levels of broadband noise are significantly higher than those of rotational harmonics.

The second task was accomplished by measuring the acoustic signals at a given observer location with and without the rotor system operating. Figures 2.15 and 2.16 show the measured 6% bandwidth sound pressure levels for 3/4" x 6" grid and 3 1/2" x 20" grid respectively. Also drawn in these figures is the typical noise spectra with the model rotor operating in the tunnel. From the Figures 2.15 and 2.16 it is evident that the background noise in the wind tunnel does not affect the rotor generated noise.

In the absence of turbulence generating grids, the background noise of the wind tunnel seem comparable to the intensity of low frequency broadband noise. Hence, we have not used this experimentally obtained low frequency broadband noise data in our prediction techniques. The background noise, however, drops significantly above 2000 HZ. Thus the experimentally obtained high frequency broadband noise data has been used.

CHAPTER III

DISCRETE NOISE RADIATION FROM MODEL ROTORS

3.1 Introduction

The low frequency 'rotational' or 'discrete' noise radiated by
lifting rotors is essentially due to steady and unsteady pressure
distributions on the blade. These periodic sources occur at integral
multiples of the blade passage frequency and the unsteady nature of
the forces prevent the higher harmonics from decaying. The rotational
noise spectra of typical helicopter rotors are strongly dependent on
the blade tip Mach number, in addition to other helicopter performance
parameters. Most model rotor systems cannot simulate the high tip Mach
numbers of real helicopters. In this chapter, we have attempted to use
the existing theories of discrete tone radiation from subsonic rotors
[16 , 17, 18] to yield a simplified Mach number scaling formula for
the intensity of rotational noise harmonics. The contents of this
chapter are largely an extension of recent work by Aravamudan, Lee,
and Harris [19]. In Section 3.2 is discussed the relative importance
of various source terms contributing to the rotational noise radiation.
In Section 3.3 is derived the theoretical Mach number scaling formula.
The experimental verification of the scaling procedure is discussed in
Section 3.4.

3.2 Rotation Noise Sources

The rotational noise of subsonic rotors is mainly attributed to
force and thickness effects. The relative importance of force and thick-

ness terms depend on the rotor blade Mach number. The source strength of the force term is larger than that of the thickness term. However, the acoustic efficiency of the thickness source radiation is far greater than that due to the force. Thus, which mechanism dominates the acoustic field is essentially a question of whether the added acoustic efficiency of the thickness source can overcome its inherently weak strength. Since the acoustic efficiency decays rapidly with decreasing Mach number, there is a rapid fall-off in acoustic effectiveness for blade stations inboard of the tip. Hence, in the following order-of-magnitude considerations on the force and thickness effects, only tip regions need to be considered.

For each source, its effective Mach number $M_e = M_t \sin\alpha/(1 - M_{or})$ is maximum in a direction straight ahead of the rotor. The factor $(1 - M_{or})$ is minimum for the advancing blade and hence the sources in the vicinity of the advancing blade contribute more. The front rotor disc plane is chosen as the observer location since the thickness noise is most intense in this location. We further assume that the tip Mach numbers are below the critical Mach numbers and hence compressibility corrections are omitted. Hawkings and Lowson [18] found the acoustic source strength of thickness, direct force and force derivative terms to be of the order of $\rho_0 \Omega^2 t$, $\Omega F_r/c_0$, and $1/c_0 (\partial F_r/\partial\tau)$. The thickness source term $\rho_0 \Omega^2 t$ may be rewritten as $(\rho_0 c_0 \Omega) (M_t c/b)(t/c)$. Ignoring the directional properties of F_r, one can rewrite the second term as $1/2 \, C_f M_s^2 (\rho_0 c_0 \Omega)$ where $M_s = (1 + \mu)M_t$ for the advancing blade. Based on quasi-steady approximations, Hawkings and Lowson [18] suggested an order of $0.1 \, \rho_0 c_0 \Omega$ for force derivative term. For typical helicopter

rotors, $b/c \sim 12$, $t/c \sim 0.12$, $C_f \sim 0.06$, and the order of magnitude of these sources are $0.01 M_t \rho_0 c_0 \Omega$, $0.03 M_s^2 \rho_0 c_0 \Omega$, and $0.1 \rho_0 c_0 \Omega$, respectively. Based on calculations of Hawkings and Lowson, the approximate expressions for the acoustic efficiency of each of these sources are given by $2.6 \times 10^4 M_e^{11 \cdot 4}/(1 - M_1)^3$, $2.2 \times 10^2 M_e^{8 \cdot 4}/(1 - M_1)^2$ and $1.8 \times 10^2 M_e^{6 \cdot 3}/(1 - M_1)^2$, respectively. Combining the source strength and its acoustic efficiency, the ratio of acoustic pressure due to thickness, force, and force derivative is given as follows:

$$260 M_e^{6 \cdot 1} : 6.6 M_s^2 M_e^{2 \cdot 1} : 18$$

For a typical helicopter with an advance ratio of 0.3, $M_e = 0.6$, $M_s = 0.65$, and the second term is of the order of unity. The thickness and force derivative terms are equally important at a value of $M_e = 0.65$ where both the terms are of same order. However, as the Mach number is decreased to about 0.60, the thickness term is about 4dB less than the corresponding force derivative term and at $M_e = 0.5$, it is about 14dB less. Hence, in our Mach number scaling formulation, we need consider only force derivative terms and the formulation would still be valid for relatively high up Mach numbers; the tip Mach number is limited by 0.65.

3.3 Mach Number Scaling of Rotational Noise

Lowson and Ollerhead [16] derived the expressions for the far field acoustic radiation due to a rotating fluctuating point force. The complex Fourier coefficient C_n of sound radiation from a source at a

distance R from the axis of rotation is given by:

$$C_n = \sum_{\lambda=0}^{\infty} \frac{(i)^{-(n-\lambda)}}{4\pi} \left[\frac{n\Omega X}{c_0 r_1^2} \left[ia_{\lambda T}(J_{n-\lambda} + (-)^\lambda J_{n+\lambda}) \right. \right.$$

$$\left. - b_{\lambda T}(J_{n-\lambda} - (-)^\lambda J_{n+\lambda}) \right] - \frac{ia_{\lambda D}}{Rr_1} \left[(n-\lambda)J_{n-\lambda} + (-)^\lambda(n+\lambda)J_{n+\lambda} \right]$$

$$- \frac{b_{\lambda D}}{Rr_1} \left[(n-\lambda)J_{n-\lambda} - (-1)^\lambda(n+\lambda)J_{n+\lambda} \right]$$

$$+ \frac{n\Omega y}{c_0 r_1^2} \left[a_{\lambda C}(J'_{n-\lambda} + (-1)^\lambda J'_{n+\lambda}) + ib_{\lambda C}(J'_{n-\lambda} - (-)^\lambda J'_{n+\lambda}) \right] \right] \qquad (3.1)$$

In Equation (3.1), the subscripts T, D, and C refer to Fourier coefficients of thrust, drag, and radial forces corresponding to a loading harmonic λ and the argument of Bessel functions is nMy/r_1. The coordinate system is shown in Figure 3.1. The effect of blade number may be included by replacing n by mB, where m is a positive integer. For $\lambda=0$, we obtain the case of steady blade loading and Equation (3.1) is reduced to the classical propeller noise study of Gutin. The effect of forward velocity may be included by replacing r_1 by $r_1(1 - M_{\text{or}})$. It should be noted that this transformation applied to the retarded position of the rotor, i.e., the position of the rotor when the sound was emitted.

In order to obtain the desired scaling formula, it is necessary to

study the characteristics of the two terms $J_{n+\lambda}$ and $J_{n-\lambda}$ appearing repeatedly in Equation (3.1). The typical values of n and λ are much larger than unity except for the case of steady blade loading and low harmonics. It has been shown that the range of loading harmonic λ contributing significantly to the sound radiation lies between $n(1 - KM y/r)$ where $K \sim 1.36$. For this range of λ, $J_{n+\lambda} << J_{n-\lambda}$ and hence, the former can be ignored. This result can be explained physically as follows. The $J_{n+\lambda}$ term represents the slow rotational mode, rotating at a speed of $n\Omega/(n+\lambda)$ while the $J_{n-\lambda}$ term represents a mode rotating with a speed of $n\Omega/(n-\lambda)$. Since the faster modes have higher efficiency, the contribution of slower modes may be neglected. Further, the proportions of the thrust, drag, and radial forces of a typical helicopter rotor is of the order of 10:1:1. Hence, over the efficient region of radiation, the contribution of drag and the radial forces may be ignored. In fact, the numerical computation of the noise radiation of each of these sources given by Lowson and Ollerhead [16] justify such a simplification except near the plane of the rotor disc where the contribution of the lift component would be zero and the drag and centrifugal forces dominate the acoustic field. Hence, over the range of angles except the plane of the rotor, with these simplifications, Equation (3.1) reduces to

$$C_n = \sum_{\lambda=0}^{\infty} \frac{(i)^{-(n-\lambda)}}{4\pi} \frac{n\Omega X}{c_0 r_1^2} [ia_{\lambda T} - b_{\lambda T}] J_{n-\lambda}(nMy/r_1) \qquad (3.2)$$

For the case of a helicopter rotor, the observed sound is the result of the continuous distributed loading along the blade span. Therefore,

the power spectral density of radiated sound $P(\vec{x},n)$ at an observer location $\vec{x}$ is given by

$$P(\vec{x},n) = \lim_{T\to\infty} \frac{1}{T} \int_0^T dt \iint_{\eta\eta'} C_n(\vec{x},\eta)C_n^*(\vec{x},\eta')d\eta d\eta' \qquad (3.3)$$

where C_n^* is the complex conjugate of C_n. To this end, we define the following non-dimensional parameters. Let

$$\xi = \eta/b \qquad (3.4)$$

Then,

$$nMy/r_1 = (nM_t y/r_1)\xi$$

Let,

$$(a_{\lambda T}^2 + b_{\lambda T}^2)^{1/2} = \frac{1}{2}\rho_0(\eta\Omega)^2 c\, C_{\lambda T}$$

Then,

$$ia_{\lambda T} - b_{\lambda T} = (\frac{1}{2}\rho_0 b^2\Omega^2 c)\xi^2 C_{\lambda T}e^{i\Phi_\lambda} \qquad (3.5)$$

where Φ_λ is a function to account for the phase difference. Combining Equations (3.3), (3.4), and (3.5), we obtain

$$P(\vec{x},n) = \frac{1}{4\pi} \left[\frac{n\Omega X}{c_0 r_1^2} \right]^2 \left[\frac{1}{2} \rho_0 b^2 \Omega^2 c \right]^2 b^2 \sum_{\lambda=0}^{\infty} \sum_{\lambda^T=0}^{\infty} \int_0^1\int_0^1 C_{\lambda T} C_{\lambda^{\cdot} T} \xi^2 \xi_1^2$$

$$\cdot e^{i[\Phi_\lambda - \Phi_{\lambda^\cdot}]} J_{n-\lambda}(nM_t y/r_1 \xi) J_{n-\lambda^\cdot}(nM_t y/r_1 \xi_1) d\xi d\xi \tag{3.6}$$

The term $e^{i[\Phi_\lambda - \Phi_{\lambda^\cdot}]}$ accounting for the phase difference is independent of the tip Mach number M_t and the observer location. The term $C_{\lambda T}$ may be interpreted as the unsteady sectional lift coefficient and, in general, is a function of the blade geometry. For geometrically similar blades, the quantities inside the summation sign remain unchanged provided $[M_t(y/r_1)]_1 = [M_t(y/r_1)]_2$. Hence, the Mach number scaling formula reduces to

$$P(\vec{x}_2,n,M_{t_2}) = P(\vec{x}_1,n,M_{t_1}) \left(\frac{M_{t_2}}{M_{t_1}} \right)^6 \left(\frac{c_2}{c_1} \right)^2 \left(\frac{r_1}{r_2} \right)^2 \left(\frac{\sin\alpha_2}{\sin\alpha_1} \right)^2 \tag{3.7}$$

where $\sin\alpha = x/r_1$.

In the case of forward flight, r_1 should be replaced by $r_1(1 - M_{or})$ where M_{or} is the component of forward flight Mach number in the direction of the observer. With reference to Figure 3.1, we have:

$$M_{or} = M_1 \cos\beta = \mu M_t \cos\beta = -\mu M_t \cos\phi\cos\alpha \tag{3.8}$$

Further, the factors x/r_1^2 and $M_t y/r_1$ must be replaced by:

$$\frac{X}{r_1^2} \rightarrow \frac{X}{r^2(1 + \mu M_t \cos\phi\cos\alpha)^2} = \frac{\sin\alpha}{r_1(1 + \mu M_t \cos\phi\cos\alpha)^2}$$

$$(3.9)$$

$$\frac{M_t y}{r_1} \rightarrow \frac{M_t y}{r_1(1 + \mu M_t \cos\phi\cos\alpha)} = \frac{M_t \cos\alpha}{(1 + \mu M_t \cos\phi\cos\alpha)}$$

With these, the equation for power spectral density becomes:

$$P(\vec{x},n) = \left[\frac{1}{4\pi} \frac{nM_t \sin\alpha}{r_1(1 + \mu M_t \cos\phi\cos\alpha)^2}\right]^2 \left[\frac{1}{2}\rho_0 M_t^2 c\right]^2$$

$$\cdot \sum_{\lambda=0}^{\infty} \sum_{\lambda'=0}^{\infty} \int_0^1\int_0^1 C_{\lambda T} C_{\lambda' T} \; \xi^2\xi_1^2 \; e^{i[\Phi_\lambda - \Phi_{\lambda'}]}$$

$$\cdot J_{n-\lambda}(nM_t\cos\alpha/(1 + \mu M_t\cos\phi\cos\alpha)\xi)$$

$$\cdot J_{n-\lambda'}(nM_t\cos\alpha/(1 + \mu M_t\cos\alpha\cos\phi)\xi_1)\,d\xi d\xi_1 \qquad (3.10)$$

Once again, when the arguments of the Bessel function in Equation (3.10) are equal, the Mach number scaling formula becomes:

$$P(\vec{x}_2,n,M_{t_2}) = P(\vec{x}_1,n,M_{t_1})\left(\frac{M_{t_2}}{M_{t_1}}\right)^6 \left(\frac{c_2}{c_1}\right)^2 \left(\frac{r_1}{r_2}\right)^2 \left(\frac{\sin\alpha_2}{\sin\alpha_1}\right)^2$$

$$\cdot \left(\frac{1 + \mu_1 M_{t_1}\cos\alpha_1\cos\phi_1}{1 + \mu_2 M_{t_2}\cos\alpha_2\cos\phi_2}\right)^4 \qquad (3.11)$$

A special case arises when the observer location is above the axis of the rotor. In this case, $y/r_1 = 0$, and hence the only term in (3.1) contributing to the entire sound field will be when $n = \lambda$. Hence, both (3.7) and (3.11) reduce to:

$$P(\vec{x}_2, n, M_{t_2}) = P(\vec{x}_1, n, M_{t_1}) \left(\frac{M_{t_2}}{M_{t_1}}\right)^6 \left(\frac{c_2}{c_1}\right)^2 \left(\frac{r_1}{r_2}\right)^2 \tag{3.12}$$

which is the conventional sixth power Mach number scaling law.

3.4 Experimental Results and Discussion

To verify the validity of the Mach number scaling formula derived in the preceeding section, a detailed experimental program was carried out in the MIT Anechoic Wind Tunnel facility. The details of the Wind Tunnel facility and the instrumentation utilized in data acquisition and data processing are given in Chapter II of this report. A periodic sampling technique was used in determining the intensity of rotational harmonics.

In Figures 3.2 and 3.3 are shown the results of the Mach number scaling formula for lower and higher rotational harmonics of a two bladed rotor on axis. The experimental results at a tip Mach number of 0.15 were used to predict the sound pressure levels at other Mach numbers. As can be seen from Figures 3.2 and 3.3, the theoretical Mach number scaling formula given by Equation (3.12) yields better comparison with the experimentally obtained data for higher rotational harmonics. The discrepancy of the scaling formula for lower rotational harmonics is attributed to the fact that the measurements were made in

the acoustic near field because of the physical limitations of the wind tunnel facility. In Figures 3.4 and 3.5 are shown the scaling results for the lower and higher harmonics of a two bladed rotor off axis. Here the experimental results of the rotor operating at a tip Mach number of 0.15 and at an angle of 59° were used to predict the sound pressure levels at other Mach numbers. In Figures 3.6 and 3.7 are shown the Mach number scaling results for a three bladed rotor on axis and off axis, respectively. Once again, we observe that the predictions for the lower harmonics are poorly correlated as compared to those at higher rotational harmonics.

Figures 3.8 and 3.9 depict the directivity of lower and higher harmonics of a two bladed rotor. In Figure 3.10 is shown the directivity of rotational harmonics of a three bladed rotor. The directivity data were obtained by positioning the microphones at 10° intervals and using the periodic sampling technique described in Chapter II. As can be seen from these figures, the directivity is dependent on the harmonic number and becomes all the more important for the off axis Mach number scaling law derived in Section 3.3.

CHAPTER IV

LOW FREQUENCY BROADBAND NOISE RADIATION FROM MODEL ROTORS

4.1 Introduction

Since the broadband noise often appears to follow roughly a M_0^6
dependence, it is natural to postulate that unsteady, but random, forces
on blades are responsible for its generation. Lowson and Ollerhead [16],
Ffowcs Williams and Hawkings [20] and Morfey and Tanna [21] have
theoretically related the radiated broadband acoustic spectrum from
a single blade to the blade load spectrum, without specifying how the
loads are generated. Their results take no account of blade-to-blade
correlations which might exist in practical applications. Lowson [22]
has tried to account for this by postulating a frequency independent
spatial correlation scale. Rotational harmonics are generated by the
passage of blades through steady asymmetric velocity variations in the
plane of the rotor. The broadband noise, on the other hand, is generated
by passage of blades through a turbulent - and thus a randomly varying
velocity field. The essential difference between the harmonic loading
and random loading is the bandwidth of excitation. The origin of tur-
bulence, in most cases seems rather inconsequential. It is mainly due
to atmospheric inhomogeneities, but upstream obstructions such as fuse-
lage and/or the wakes shed by the moving airfoil might very well be the
culprit. A lifting rotor produces a mean downward velocity field which
draws the atmospheric eddies through the rotor plane with a convecting
velocity V_c. This random variation in "up wash" induces a random

variation in the angle of incidence and hence a fluctuating blade load.
As atmospheric turbulence contains a spectrum of wave number components,
the resulting loading spectrum affects tha acoustic spectrum over the
entire range of frequencies.

In this chapter, an attempt has been made to study the effects of
inflow turbulence on the intensity and spectrum of low frequency broad-
band noise. Here, we have exploited the existing theories of radiation
from subsonic rotors and the knowledge of aerodynamic transfer functions
to yield appropriate formulae for the radiation of the low frequency
broadband noise. In Section 4.2 is described the effects of blade-to-
blade correlation. In Section 4.3 is given a brief account of the
formulation. Section 4.4 is given an account of blade loading due to
turbulence. To facilitate comparison of experimentally obtained results
with the theoretically predicted ones, we have chosen von Karman's
spectrum for turbulence upwash. The details of the spectrum and aero-
dynamic transfer functions are given in Section 4.5 and the associated
numerical calculations are given in Section 4.6. The numerically ob-
tained results are compared with experimentally obtained data and a
detailed discussion of results are given in Section 4.7.

4.2 Effects of Blade-to-Blade Correlation

Many of the possible mechanisms for broadband noise generation by
a single stationary airfoil in a moving stream have been subject of
various investigators. The non-uniform velocity field associated with
turbulence leads to an unsteady blade load that is dipole in nature.

Amiet [23] studied the resulting noise pattern by using the non-station-ary airfoil theory of Sears [24]. However, in the case of rotating blades, the problem becomes more complex. The very fact that the blades are rotating can be looked at in terms of Doppler shifts in frequency [16]. The presence or absence of a blade at various spatial locations may in fact be interpreted as temporal variations seen in the observer coordinates. Thus, a wide range of frequencies are generated at a single blade passage harmonic $mB\Omega$.

A hovering or low forward speed rotor also modifies any ingested turbulence due to the distortion of fluid elements drawn into the rotor plane. The eddies, in general, are elongated in the direction of con-vection velocity and often are chopped several times as they pass through the rotor plane. For example, an atmospheric eddy of length scale of about 10 ft. will take the order of one second to be drawn through a rotor plane with a convection velocity of about 10 ft./sec. Thus, for a two bladed rotor at 5 HZ, about twenty blade passages will encounter parts of the same eddy. Thus blade-to-blade correlation effect allows positive and negative interference between acoustic waves genera-ted by various blades. This loading variation phenomenon can also be looked at as a slow time modulation of the loading seen by the blades passing a given point. This low frequency amplitude modulation will then add narrow side bands to each blade passing harmonic. On the other hand, the smaller eddies which are associated with high frequency sound spend less time passing through the rotor plane because of their smaller spatial extent. In the above cited example, an eddy of length scale of

a foot or less will completely pass through the plane of the rotor between consecutive blade passage. The resulting rapid modulation of the high frequency blade loading implies wider side bands and hence the radiated sound spreads over a large part of the spectrum. Hanson [25] studied this phenomenon for the case of a stationary fan and observed "partially coherent' blade loading which leads to partially coherent or narrow band random noise that are characterized by "hay stacking" at higher harmonics of blade passage. Homicz and George [26] derived expressions for radiated high frequency noise which included blade-to-blade correlations and inferred that the sums and integrals involved in a modal analysis theory had to be centered over a range of loading harmonics, Doppler shift terms and azimuthal component terms. The large number of terms required a prohibitive computation time for evaluation of the spectra beyond 500 to 1000 HZ for typical Helicopter rotors. In a subsequent article, George and Kim [27] and Amiet [28] gave simpler formulations to specialize the radiation due to atmospheric turbulence. Our analysis follows closely the one proposed by Homicz and George [26] and George and Kim [27].

4.3 Formulation

Figure 4.1 depicts the rotor geometry showing the definitions of symbols and convection velocity of a turbulent eddy. The time interval Δt for equally spaced blades to pass a fixed point on the rotor plane is given by

$$\Delta t = \frac{2\pi R_0/B}{2\pi \Omega R_0} = \frac{1}{\Omega B} \qquad (4.1)$$

On the other hand, the time scale for an eddy of wave length λ_ξ to be convected past a given point in the rotor plane is given by

$$t_\xi = \frac{\lambda_\xi}{V_c} \qquad (4.2)$$

Here the eddy wavelength λ_ξ is given by $2\pi\Lambda/_\xi$, where ξ is the turbulent wave number and Λ is the turbulence integral scale. Thus the ratio of blade passage time to convection time is

$$\frac{\Delta t}{t_\xi} = \frac{1}{2\pi} \frac{\xi V_c}{B \Lambda \Omega} \qquad (4.3)$$

The far field radiated sound for loading due to a turbulent upwash given by Homicz and George [26] is of the form:

$$< S(f) > \sim \int\limits_{\xi_{min}}^{\infty} \left[G(\xi,n,m) \sum_n \sum_m J^2_{nB-m} \left(\frac{fR_0 \cos\phi}{c_0} \right) \right.$$

$$\left. J^2_m \left(\frac{M_0}{M_c} \sqrt{\left(V_c/\Lambda\Omega \right)^2 \xi^2 - \left(\frac{f}{\Omega} - nB \right)^2} \right) \right] d\xi \qquad (4.4)$$

The two series involving Bessel's Function arise because of the resolution of the turbulence in the polar coordinates and because of the Doppler shifts in frequency due to motion of the blades. The frequency f_0 beyond which (4.4) predicts a smooth spectrum is given by

$$\frac{f_0}{\Omega} \simeq \frac{B \ (1 + M_0/M_c)}{2(1 - M_0 \cos \phi \ )} \tag{4.5}$$

Also, the values of turbulent wave number   which make signigicant con-
tributions to the spectrum at a given frequency f are given by [26].

$$\frac{(f/\Omega) \ (1 - M_0 \cos \phi)}{(V_c/\Lambda\Omega \ )(1 + M_0/M_c)} < \xi < \frac{(f/\Omega)(1 + M_0 \cos \phi)}{(V_c/\Lambda\Omega \ )} \tag{4.6}$$

Combining (4.5) and (4.6) the lower limit for ξ which makes significant
contributions for $f > f_0$ is obtained as

$$\xi_{f_0} \ > \ \frac{B \ \Lambda \ \Omega}{2V_c}$$

Similarly, for $f \gg f_0$, we have

$$\xi_f \ \gg \ \frac{B \ \Lambda \ \Omega}{2V_c} \tag{4.7}$$

Using (4.3), this result may be interpreted as

$$\frac{\Delta t}{t_\xi} \gg 1 \qquad \qquad f \ \gg f_0$$

This result implies that the small turbulent eddies which generate
sound at frequencies $f > f_0$ will completely pass through the rotor plane
before the next blade arrives. Under such circumstances, we may assume
that there is no significant blade-to-blade correlation and hence the
total radiation is given by simply adding the uncorrelated sound power

spectral densities of each of the blades. The radiation of a single blade approximated by a rotating point dipole has been given by Ffowcs Williams and Hawkings [20] as

$$<S_{pp}(\vec{x},f)> = \frac{f^2}{4\rho_0 c_0^3 r^2} \sum_{n=-\infty}^{\infty} D_r (\phi, f - n\Omega)J_n^2 (\frac{fR_0\cos \phi}{c_0})$$

(4.8)

where $D_r(\phi,f)$ is the power spectral density of the dipole strength in the radiation direction.

For a dipole $d_r(\phi)$ fluctuating in amplitude with frequency f and rotating with a frequency Ω along a circular path, the force derivative terms will certainly outweigh the acceleration terms provided $f \gg \Omega$ and the source Mach number is subsonic. Further discussion of this point is given by Morfey and Tanna [21]. This leads to $2\pi i f d_r(\phi)$ for a single frequency component force and hence the intensity spectrum given by equation (4.8) contains f^2. However, any given component of load spectrum radiates over a range of Doppler shifted frequencies. Conversely, the acoustic spectrum at a frequency f will contain load fluctuations at frequencies shifted from f by a range of harmonics $\lambda\Omega$. The amplitudes of the Doppler shifted contributions are seen to be proportional to $J_n^2 (fR_0\cos \phi/c_0)$ which become progressively smaller for $n \geq fR_0\cos \phi/c_0$. Thus, the primary Doppler effects are shifts $\Delta f \simeq n\Omega$ of less than approximately $fR_0\cos \phi/c_0$ or $\Delta f/f \lesssim M_0\cos \phi$. Hence the acoustic spectrum at frequency f is affected by the dipole forces over a range of frequencies of width $2fM_0\cos\phi$ centered at f. A special case of interest arrives when the observer is directly above the axis of

rotation. For this case, $\phi = 90°$ and the radiation at any frequency is affected by the load fluctuation only at that frequency as in the case of a stationary airfoil. For observer locations other than this, a large part of the loading harmonics contribute to the acoustic radiation.

To this end, we are left with equation (4.8) where the only unknown is the power spectral density of the dipole source field $D_r(\phi, f-n\Omega)$. The dipole source field is a direct consequence of the unsteady lift acting on the airfoil surface. Hence, a knowledge of the unsteady aerodynamics is essential to evaluate the source strength terms occurring in equation (4.8). Further, we assume that the rotating dipole is situated at 80% of the blade span, where the maxima of the steady lift occurs [16]. In the following section, we shall discuss the effects of the incident turbulence on blade loading.

4.4 Blade Loading Due to Incident Turbulence

We next find the unsteady lift distribution on a blade moving relative to a fluid containing a homogeneous, randomly varying upwash field w. We define coordinates fixed with respect to the fluid as x', y', z' and coordinates with respect to the airfoil as x, y, z. Figure 4.2 shows the chosen coordinate system. Now, the four-dimensional Fourier representation of the turbulence upwash with respect to the fluid is given as follows

$$w(\vec{x'}, t) = \int_{-\infty}^{\infty} d^3k \int_{-\infty}^{\infty} F_w(\vec{k}, f) \, e^{2\pi\vec{k}\cdot\vec{x'}} e^{i2\pi ft} \, df \qquad (4.9)$$

where $\vec{k}$ is the wave number vector of the incident turbulent field. Referring to Figure 4.2, we see that the blade moves with the velocity $\vec{Q}$ with respect to the fluid where $\vec{Q} = (U_0, 0, -V_c)$. Hence the relationship between the coordinate systems $\vec{x}$ and $\vec{x}'$ is given by $\vec{x}' = \vec{x} - \vec{Q}t$. At this stage, we make Taylor's hypothesis that the turbulent upwash field is frozen - that is it does not vary during the time of a blade passage. This may be represented in terms of the Fourier components of the spectra as

$$F_w(\vec{k}, f) = F_w(\vec{k})\delta(f)$$

With this, the turbulent upwash field in blade fixed coordinates becomes

$$w(\vec{x}, t) = \int_{-\infty}^{\infty} d^3k \, F_w(\vec{k})e^{i2\pi[\vec{k}\cdot\vec{x} - \vec{k}\cdot\vec{Q}t]} \tag{4.10}$$

The fluctuation in the upwash produces a fluctuation in the lift generated by the airfoil. To this end, we define the elemental lift response function of the airfoil as

$$\Delta L(\vec{k}) = K(k_c, k_s) \, dw(\vec{k}) \tag{4.11}$$

where K is the aerodynamic lift response function at a moving point of the rotating blade to a unit amplitude of turbulent upwash and k_c and k_s are the wave number components in chordwise and spanwise directions respectively. The total lift generated by the blade can then be expressed as follows

$$L(t) = \int_{-\infty}^{\infty} d^3k \, F_w(\vec{k}) \, K(k_c, k_s)e^{-i2\pi\vec{k}\cdot\vec{Q}t} \tag{4.12}$$

Since the turbulent upwash is isotropic, the coordinate system may be rotated in such a way that in the new coordinate system $\vec{x}$ is parallel to $\vec{Q}$ as shown in Figure 4.2. This transforms equation (4.12) to

$$L(t) = \int_{-\infty}^{\infty} d^3k \, F_w(\vec{k}) \, K(k_x, k_y) \, e^{i2\pi k_x Qt} \tag{4.13}$$

where $Q = |\vec{Q}|$

In order to obtain the lift spectral density, we define a lift correlation function

$$R_{LL}(t, t + \tau) = \overline{L(t) \, L^*(t + \tau)}$$

Under the assumption of a stationary random process, this becomes only a function of the time delay τ and the power spectral density of lift may be expressed as follows

$$\Phi_{LL}(f) \triangleq \int_{-\infty}^{\infty} R_{LL}(\tau) \, e^{-2\pi i f \tau} d\tau$$

Substituting for $L(t)$ from equation (4.13), we obtain

$$\Phi_{LL}(f) = \int_{-\infty}^{\infty} d^3k \int_{-\infty}^{\infty} d\tau \Phi_{ww}(\vec{k}) \, |K(k_x, k_y)|^2$$

$$e^{i2\pi(k_x Q - f)\tau}$$

Noting the mathematical identity that

$$\int_{-\infty}^{\infty} \exp\left[i2\pi(k_x Q - f)\tau\right] d\tau = \delta(k_x Q - f)$$

we have the one sided power spectral density for $f \gg 0$ as follows

$$\Phi_{LL}(f) = \frac{2}{Q} \int_{-\infty}^{\infty} \int_{-\infty}^{\infty} dk_y dk_z \, \Phi_{ww}(f/Q, k_y, k_z) \, |K(f/Q, k_y)|^2 \tag{4.14}$$

Equation (4.14) is general in the sense that any known turbulence upwash spectrum or an aerodynamic transfer function may be used to yield the power spectral densities. To facilitate comparison of the theoretical calculations with experimentally obtained results, we use von Karman's turbulence spectrum. The approximate values of the aerodynamic transfer function K are based on Osborne's [29] extension of the two dimensional Sear's function.

The blade loading spectrum derived above is that for a fluctuating lift force which is actually oriented at a slight angle α_S to the axis of the rotor. This gives rise to a fluctuating torque component in addition to the fluctuating thrust components. Since the angle α_S is rather small (~6°) for typical helicopter rotors, the contributions of the torque components are negligible. Since the thrust is along the axis by definition, its contribution to force in an observer direction is simply $T\sin\phi$. The corresponding torque component is $T\cos\phi\tan\alpha_S$ which is at least one order less than the lift component. Hence the dipole strength may simply be chosen as that of the lift component alone which is given by $D_r \sim \Phi_{LL} \sin^2\phi$.

The influence of spanwise correlation length of turbulence on radiated acoustic intensity may be accounted for by estimating the appropriate correlation lengths for atmospheric turbulence induced loads. Variations in the phase of the spanwise load distribution can lead to significant acoustic interference effects for particular combination of k, f and ϕ. However, these effects can be calculated only with substantially more detailed knowledge of the spanwise aerodynamic loading than is presently available. Further more, one would expect that the inherent randomness of the problem would tend to mask such a behavior.

4.5 Turbulence Spectra & Aerodynamic Transfer Function

Referring to the coordinate system described in Figure 4.2, calculation of the cross power spectral density of the vertical component of turbulence w in the lateral direction is required. This is a function of the axial wave number and spanwise separation distance. The general expression for the energy spectrum tensor yields for the three wave number spectrum of the vertical component as [30]

$$\Phi_{ww}(\vec{k}) = \frac{E(k)}{4\pi k^2} \left(1 - \frac{k_z^2}{k^2}\right) \tag{4.15}$$

Adopting the empirical von Karman's interpolation formula, the three dimensional energy function of the turbulence, E(k) is given by

$$E(k) = \frac{55}{9\pi} \frac{\Gamma(5/6)}{\Gamma(1/3)} \frac{\overline{w}^2}{k_e} \frac{(k/k_e)^4}{\left[1 + (k/k_e)^2\right]^{17/6}} \tag{4.16}$$

where k_e is the wave number range of energy containing eddies. Integration of (4.15) over wave number k then yields the two wave number spectrum of the vertical component

$$\Phi_{ww}(k_x, k_y) = \int_{-\infty}^{\infty} \Phi_{ww}(\vec{k}) \, dk_z$$

$$= \frac{4\overline{w^2}}{9\pi \, k_e^4} \frac{(k_x^2 + k_y^2)}{\left[1 + (k_x^2 + k_y^2)/k_e^2 \right]^{7/3}} \tag{4.17}$$

The wave number range of energy containing eddies k_e is given by

$$k_e = \frac{\sqrt{\pi}}{\Lambda_f} \frac{\Gamma(5/6)}{\Gamma(1/3)} \simeq 0.7468/\Lambda_f \tag{4.18}$$

Substitution of (4.18) into (4.17) yields the two dimensional turbulence spectrum for the vertical component as

$$\Phi_{ww}(k_x, k_y) = 0.4548 \, \overline{w^2} \Lambda_f^4 \frac{k_x^2 + k_y^2}{[1 + 1.793\Lambda_f^2 (k_x^2 + k_y^2)]^{7/3}} \tag{4.19}$$

By taking Fourier transform of equation (4.19) with respect to k_y, we obtain a cross spectrum at a given frequency which would be measured by two probes separated by a distance y in the spanwise direction. By integrating the cross spectrum over y, a spanwise correlation length may be obtained. Amiet [23] has shown that this correlation length for high frequency limits may roughly be estimated as k_x^{-1}. We assume that each such strip radiates independently of its neighbors with random phase correlation between them. This means that their respective acoustic intensities may be added directly. The radiated intensity will then be

proportional to the square of the area, $c^2 k_x^{-2}$ and total from bk_x such regions along the span will scale as $c^2 bk_x^{-1}$. For a point dipole, where $k_x b \ll 1$, the appropriate scaling factor is $(cb)^2$. Hence we see that the radiation for finite correlation lengths is reduced by a factor $(k_x b)^{-1}$. With this, a spanwise correction factor for the estimate of the acoustic power spectral density, will be $(1 + k_x b)^{-1}$ or $(1 + bf/Q)^{-1}$.

If we assume that at every instant, each rotor blade behaves like a two dimensional airfoil in rectilinear motion through a three dimensional sinusoidal upwash pattern, the three governing parameters for the aerodynamic transfer function are k_T, Γ and M_0. Here

$$k_T = \sqrt{k_c^2 + k_s^2} = (k_x^2 + k_y^2)^{\frac{1}{2}}$$

$$\Gamma = \tan^{-1}(k_y/k_x)$$

(4.20)

These quantities will depend on the magnitude and direction of the turbulent wave vector $\vec{k}$ as well as the azimuthal angle of the blade. During each revolution, a blade will encounter some region in which Γ approaches $\pi/2$ or zero implying nearly steady but a three dimensional flow or nearly two-dimensional but unsteady flow respectively. In either case, the loading is reduced below that predicted by quasi steady two-dimensional theory. Homicz and George [26] calculated the load response to a convected sinusoidal upwash pattern for two extreme values of $\Gamma = 0$ and $\Gamma = \pi/2$ and inferred that the influence of Γ may be ignored as compared to the effect of k_T and M_0. Osborne [29] gave the asymtotic expres-

sions for compressible two-dimensional Sears function for $\Gamma = 0$ as follows

$$|S_{eff}| = \left|H(\pi c k_T/\beta^2)\right|\left[J_0^2(\frac{M_0\pi c}{\beta^2}k_T) + J_1^2(\frac{M_0^2\pi c}{\beta^2}k_T)\right]^{\frac{1}{2}} \tag{4.21}$$

where $\beta = \sqrt{1 - M_0^2}$ and $|H(k)|$ is the magnitude of the original incompressible Sears function [24] which to a very good approximation may be given as

$$|H(k)| \simeq (1 + 2\pi k)^{-\frac{1}{2}} \tag{4.22}$$

Hence the aerodynamic transfer function to be used in conjunction with equation (4.14) is given by

$$|K(k_x,k_y)| = \frac{1}{2}\rho_0 Q b c \frac{\frac{2\pi}{\beta}[J_0^2(\frac{M_0^2\pi c}{\beta^2}k_T) + J_1^2(\frac{M_0^2\pi c}{\beta^2}k_T)]^{\frac{1}{2}}}{[1 + \frac{2\pi^2 c}{\beta^2}k_T]^{\frac{1}{2}}} \tag{4.23}$$

It was pointed by Mugridge [31], that the net lift response of a two dimensional thin airfoil to a convected three dimensional upwash is less than the two dimensional upwash response. If the length scale of turbulence is small compared to the span of the blade, the end effects, in general are negligible.*

For an upwash pattern given by

$$w \exp \left[i(2\pi f t - k_x x + k_y y) \right]$$

where $k_y = {}^{mb}/2$ and $k_x = \pi f c /_U$, the lift response function is given by

$$\left| C_L^2(k_x, k_y) \right| = 4b^2 \overline{w}^2 \pi^2 \left[\left(\frac{1}{1 + 2\pi k_x} \right) \left(\frac{k_x^2 + \frac{2}{\pi^2}}{k_x^2 + \frac{2}{\pi^2} + k_y^2} \right) \left(\frac{\sin k_y}{k_y} \right)^2 \right] \tag{4.24}$$

It may be noted that as $k_y \to 0$, this expression corresponds to the original Sears function. Order of magnitude estimates of the use of Mugridge's function in place of the two dimensional Sears function in equation (4.23) were made. This resulted in reduction of about 3.5 dB at a frequency of 200 HZ. The difference between the two responses above 500 Hz were less than a dB.

4.6 Numerical Calculations

Introducing equations (4.23),(4.19) in (4.14) and then in (4.8), we obtain the final expression for the spectrum of low frequency broadband noise as follows

$$< S_{pp}(\vec{x}, f) > = \frac{f^2 \sin^2 \phi}{2Q c_0^3 r^2 \rho_0 (1 + bf/Q)} \sum_{n=-\infty}^{\infty} D_r(f - n\Omega) J_n^2 \left(\frac{f R_0 \sin \phi}{c_0} \right) \tag{4.25}$$

where

$$D_r(f) = \frac{\pi^2 \rho^2 Q^2 b^2 c^2 (0.4548)}{\beta^2} \; \overline{w}^2 \; \Lambda_f^4$$

$$\int_0^\infty dk_y \frac{[(f/Q)^2 + k_y^2] \; [J_0^2(\frac{M_0^2 \pi c}{\beta^2} \sqrt{(f/Q)^2 + k_y^2}) + J_1^2(\frac{M_0^2 \pi c}{\beta^2} \sqrt{(f/Q)^2 + k_y^2})]}{[1 + \frac{2}{\beta^2} \pi^2 c \sqrt{(f/Q)^2 + k_y^2}] \; [1 + 1.793 \; \Lambda_f^2 \{(f/Q)^2 + k_y^2\}]^{7/3}} \qquad (4.26)$$

Before we proceed to the actual computation of equation (4.25), we need to make two approximations. Firstly, the infinite summation over the loading harmonics has to be reduced to a finite summation. George and Kim [27] have demonstrated that the resulting error would be less than one percent if the series were truncated at

$$n_{min}, n_{max} = \pm 1.2 \frac{f}{\Omega} M_0 |\cos \phi |$$

Secondly, in the evaluation of the integral of the unsteady lift function and the upwash turbulence spectrum, the integration must be truncated at a finite wave number K_y. The integration was performed numerically up to a certain value K_y using Simpson's rule and then the upper limit of integration was increased by a predetermined quantity. The integration scheme automatically terminated the integration when subsequent increase in the upper limit yielded less than 0.1 percent increase in the value of integral.

4.7 Results and Discussion

Numerical calculations were performed for the measured values of turbulence intensities and integral scales for various advance ratios and tip Mach numbers.

Figures 4.3 and 4.4 compare the predicted and the measured narrow band spectra for the large and the small turbulence generating grids respectively. The acoustic spectra obtained is corrected for the experimentally obtained two bladed rotor results and with a 6% bandwidth analysis by adding 3 db to the entire spectrum. The experimental plot is deliberately terminated around 3000 Hz, beyond which is assumed to be the region of high frequency broadband noise. As can be seen from Figures 4.3 and 4.4, the agreement between measured and the predicted Spectra is better for the larger grid with an integral scale of about 5" than for the smaller grid with an integral scale of 3.3". The results of the rotor operating with no upstream turbulence generator are not plotted because at these frequencies the background noise was comparable to the intensity of the low frequency broadband noise. In Figure 4.5 are plotted the effect of advance ratio on the predicted peak intensity of the low frequency broadband noise. As can be seen from the figure, a doubling of advance ratio result in an increase of peak sound pressure level of about 8 db. This result is not surprising because of the increased r.m.s. value of turbulence in the tunnel with increasing forward speed. Since the theory predicts a 6 db increase in doubling the turbulence velocity, only the remainder must be thought of as the true influence of advance ratio. Caution must be exercised in comparing these results with those of full scale rotors since increase in advance ratio

does not significantly change the turbulence encounter.

In Figures 4.6, 4.7 and 4.8 are drawn the influence of tip velocity on the predicted spectra of the low frequency broadband noise. The corresponding integral scales are 11.8", 5" and 3.3" respectively. An examination of these figures indicates that both the spectrum and intensity of low frequency broadband noise are strongly affected by the scale of turbulence as well as the rotational Mach number.

In Figure 4.9, we have plotted the peak intensity of the low frequency broadband noise as a function of the relative tip velocity. In plotting this figure, we removed the effect of the increase in the r.m.s. turbulence levels by taking out $20 \log \frac{w_2}{w_1}$ from the predicted sound pressure levels. The levels are normalized with respect to the predicted sound pressure level at a Mach number of 0.1. Also plotted in the figure are measured sound pressure levels for a two bladed rotor operating with a 0.75" x 6" grid. As can be seen from the figure, a 12 db increase per doubling velocity seems to fit the predicted and the measured data very well. Including the effect of increase in r.m.s. turbulence levels would result in the conventional M^6 power law. The location of the peak intensity in the frequency domain increases with increase in tip velocities. In Figure 4.10 are plotted the predicted sound pressure levels as a function of the turbulence integral scale for a fixed value of the tip Mach number of 0.25. Once again, we observe that the location of the peak intensity in the frequency domain decreases with an increase in the integral scale of turbulence. In Figure 4.11 are plotted the peak intensity of LFBN as a function of the longitudinal integral scale Λ_f, of turbulence. Here, the

effect of the rotational velocity and the increase in turbulence intensity are removed. As can be seen from the figure the peak intensity is a very weak function of Λ_f. This weak dependence can be readily explained by an examination of equation (4.26). For relatively large values of frequency, we may approximate the denominator of equation (4.26) as

$$[1 + \frac{2\pi^2 c}{\beta^2} \sqrt{(f/Q)^2 + k_y^2}] [1.793 \Lambda_f^2 \{(f/Q)^2 + k_y^2\}]^{7/3}$$

Since the integral is independent of Λ_f we readily obtain a scaling factor based on Λ_f as

$$D_r(f) \sim \Lambda_f^{-2/3}$$

which would result in a reduction of approximately 2 db per doubling the integral scale.

An examination of Figures 4.3 to 4.11 suggest that the location of the peak intensity of the LFBN in the frequency domain can easily be scaled with reference to a Strouhal number defined as follows

$$S = \frac{f_p \Lambda_f}{V_t}$$

In Figure 4.12 is plotted the spectra of sound pressure levels for various Mach numbers and size scale of turbulence. It is interesting to see how the entire data collapses to a single curve defining a normalized acoustic spectra as a function of Strouhal number. The peak intensity location seems to appear at a Strouhal number of about 1.5.

CHAPTER V

HIGH FREQUENCY BROADBAND NOISE RADIATION FROM MODEL ROTORS

5.1 Introduction

In the preceeding chapter we discussed the possible mechanisms of
low frequency broadband noise radiation from rotating airfoils and arrived
at an acceptable Strouhal frequency scaling to predict intensity and
spectrum of such a radiation. It was observed that at high enough fre-
quencies, this radiation decays approximately like f^{-2}. Therefore, in ab-
sence of any other mechanism of radiation, the intensity of rotor generated
noise would be insignificant at frequencies well beyond the peak of low
frequency broadband noise radiation. But, our experimentally obtained
model data as well as the full scale rotor data of Leverton [6] do not
exhibit such a decrease in the measured acoustic spectra. In fact, the
evidence of existence of another mechanism which radiates efficiently over
the frequency range well beyond low frequency broadband noise peak is
overwhelming. In this chapter we shall discuss the possible mechanisms
appropriate for such high frequency radiation.

As mentioned before, the broadband part of the rotor noise spectrum
is attributed to the non-periodic time dependent loads. These fluctuations
in force may arise as a result of (i) free stream disturbances generating
a fluctuating angle of incidence (ii) a turbulent boundary layer on the
surface of the airfoil and (iii) a spanwise vorticity in the wake of the
airfoil. These mechanisms, in general, interact through nonlinear fluid
mechanical processes. However, under certain conditions, it is possible

to consider them as being mutually independent.

The interaction of the turbulent boundary layer with the trailing edge of an airfoil imparts momentum fluctuations to the surrounding media and the total radiated spectrum may be divided into turbulent boundary layer dominated components and wake dominated components. Chanaud and Hayden [32] have shown that when the dimensions of the radiating surface are small compared to the acoustic wave length, the contributions of the turbulent boundary layer to the total acoustic intensity are usually negligible relative to the contributions from the inflow turbulence or wake. In the absence of signigicant inflow turbulence, the wake generated noise would dominate the high frequency regime of the acoustic spectra.

Several independent experiments by Hersh and Hayden [33], Paterson, Vogt, Fink and Munch [34] and Clark [35] revealed that discrete tones are emitted from isolated airfoils under certain operating conditions. Over a wide range of Reynolds number based on the chord of the airfoil, the total radiated sound could be dominated by these discrete tones. Further, the frequencies of these tones appear to be a well defined function of free stream velocity and form an organized pattern. There is a considerable amount of difference of opinion regarding the Strouhal frequency scaling of these discrete tones. Hersh and Hayden [33] and Paterson, et al. [34] have all attributed the generation of these tones to the classical vortex shedding along the span of the airfoil. The shed vortices generate a periodic pressure fluctuation over the airfoil at that particular Strouhal frequency, resulting in a edge dipole radiation. Tam [36], on the other hand believes that there is very little compelling

evidence to suggest a direct relationship between the vorticity in the wake and the generated discrete tones. He postulates that these tones are a direct consequence of a self excited feedback loop of aerodynamic origin formed by the acoustic wave, boundary layer and the wake flow of the airfoil.

In our efforts to understand the nature of High Frequency broadband noise, we performed a series of experiments involving the influence of performance parameters on the intensity and spectra of High Frequency Broadband Noise (HFBN). The performance parameters chosen were (i) the steady thrust acting on the model rotor system, (ii) the advance ratio and (iii) the number of blades. In addition, we also examined the effect of serrations on the nature of HFBN. In section 5.2 is described the effects of leading edge and pressure surface serrations on the intensity and spectra of the HFBN. Section 5.3 describes the dependency of HFBN on the chosen performance parameters. In the light of these measurements, we discuss the Strouhal frequency scaling procedures adopted by various investigators in section 5.4. The appropriate amplitude scaling formulae and the experimental results to verify the proposed scaling procedure are discussed in section 5.4. A qualitative analysis of the influence of the free stream disturbances on the high frequency radiation from rotating airfoil is discussed in section 5.5. The contents of section 5.2 and 5.4 are largely due to Lee, Aravamudan, Bauer and Harris [37] and Aravamudan, Lee and Harris [19].

5.2 Seration Studies

Serrations made of masking tape were used as boundary layer tripping devices. The effect of serrations on the high frequency broadband noise

were studied by attaching serrations of various lengths and thicknesses along the blade suction surface, pressure surface and leading edge. In all these cases the rotor rotational speed was held constant at 1100RPM and the acoustic measurements were made at 52 inches (1.32 m) directly above the rotor disc.

5.2.1 Suction Surface Serration

Single layer serrations of 2 inches (5cm) to 15 inches (38 cm) in length were attached to the suction surface of both the blades of a two bladed rotor. The serrations were 3/8 inch (9.5 mm) aft leading edge. Little or no change in the HFBN was observed. The thickness of the tripping serrations was increased by increasing the number of layers. Figure 5.1 shows the effect of increasing the thickness of serrations of 15 inches in length on the spectrum of HFBN.

As can be seen from the figure, little or no change in the intensity of HFBN occurs for serrations up to 4 layers and significant reduction occurs for serrations of 6 layers. However, this proved to be of very little practical interest since the total thrust generated by the rotor also decreased. The acoustic spectrum had an even larger change when a spoiler type serration of 15 inches in length was attached to the blades. The HFBN peak disappeared completely but a significant increase in the low frequency broadband noise was observed. The thrust of the blades also decreased sharply and the blades were believed to be fully stalled. Paterson et al [34] obtained similar results for the case of an isolated airfoil.

5.2.2 Leading Edge Serration

The noise spectra of a two bladed rotor with serrations of various

lengths along the leading edge were measured. Figure 5.2 depicts the
effect of length of serration on the HFBN. The serrations were found
to be effective in reducing the HFBN, but increased the low frequency
broadband noise considerably. A 12 inch (30 cm) serration almost
eliminated the HFBN peak, but increased the low frequency broadband
noise by about 5 db. This increase in low frequency broadband noise
may be attributed to the increased level of turbulence and the conse-
quent random loading on the blades. A further increase in serrations
did not prove effective in reducing the HFBN peak. This seems to
suggest that the significant contributions to HFBN comes from the
outboard 1/2 portion of the blades. This finding is consistant with
that of Hersh and Hayden [33] for the case of low speed propellers.

5.2.3 Pressure Surface Serration

Figure 5.3 shows the influence of serrations of various lengths
located 3/8" aft the leading edge on the pressure surface of the airfoil.
It may be observed from the figure that a 15 inch serration reduces the
HFBN by about 10 db without increasing the low frequency broadband noise.
With a 6 inch serration the peak level was found to decrease by about
3 db. The surface pressure measurements of Paterson, et al [34] indicate
that the pressure surface boundary layer is laminar and the boundary layer
on the suction surface is turbulent. The serrations tripped the boundary
layer on the pressure surface. Consequently the intensity of shed vortices
were reduced and hence the HFBN. Since there was no appreciable increase
in the turbulence intensity, the low frequency broadband noise remain un-
affected. The boundary layer noise is increased, but since its relative

magnitude with other sources is small, the increase is not noticeable.

Figure 5.4 shows the effect of a 4 inch serration located at various distances from the tip of the rotor blade. As can be seen from the figure, the serrations are most effective when they are spread around 75% of the blade span. Location of the serrations beyond this point seem to reduce the efficiency of the process. Serrations beyond 12 inches from the blade tip seemed to have no effect on the HFBN peak. This seems to suggest that the HFBN peak comes from the outboard 1/2 blade span.

Figure 5.5 shows the effects of pressure surface and leading edge serrations on the steady thrust generated by rotor. As can be seen from Figure 5.5, the serrations had little or no effect on the total thrust although it is believed that the drag may increase slightly due to the existence of a turbulent boundary layer on both sides of the blades.

5.3 Parametric Studies

The effects of rotor thrust, advance ratio and number of blades on the intensity and spectrum of HFBN were investigated. The tip path angle was held constant at 9° during the entire set of experiments. Both narrow-band and 6% bandwidth analysis of the data were made. The directivity of two and three bladed rotors were measured along the rotor axis in a plane perpendicular to the wind direction.

5.3.1 The Effects of Collective Pitch and Thrust

Experiments were conducted at tunnel speeds of 44 fps and 73 fps with a rotor speed of 1100 rpm. The rotor collective pitch was set to be 0, 2, 5, 8 and 11.2 degrees at the tip. Figure 5.6 shows noise spectrum shapes for different collective pitches. A line representing the 6th power fre-

quency dependence (f^6) was drawn on each spectrum. This power law would result if each blade section along the span were radiating in a two dimensional manner according to local speed. For low collective pitch, such an approximation seems valid. It should be noted that blade-slap due to blade vortex interaction occurs at 5 deg. and 8 deg. collective pitch settings. This implies that the two-dimensional vortex shedding does not prevail at these conditions. Ham [38] has shown that flow separation is likely to occur during blade-vortex interaction. The separated flow may randomize the vortex shedding and consequently will reduce the intensity of HFBN.

Figure 5.7 shows the 6% bandwidth analysis of HFBN under increasing thrust conditions at constant advance ratio without blade slap. It may be noted from Figure 5.7 that neither the peak frequency location nor the amplitude of HFBN is a strong function of steady state thrust. However, increase in thrust results in a narrowing of the width of the HFBN hump. Also, a "drag dipole" radiation which occurs at approximately twice the vortex shedding frequency becomes more noticeable with increase of thrust.

5.3.2 The Effects of Advance Ratio

To determine the effect of advance ratio on the spectrum and intensity of HFBN, the tunnel speed was varied from 29.3 ft./sec. to 58.7 ft./sec. maintaining the rotor rotational speed constant at 672 rpm. This corresponds to a variation in advance ratio from 0.2 to 0.4 at an increment of 0.05. The mean thrust developed by the rotor was kept constant at 2.84 lbs. by changing the collective pitch of the rotor blades. The tip path angle was

maintained at 9° by changing the shaft angle. Figure 5.8 shows the 6%
bandwidth spectrum of the HFBN at various advance ratios. It may be noted
from Figure 5.8 that the location of the peak is not seriously affected
by increasing the advance ratio. However, the peak seems to broaden with
increase of advance ratio which would tend to increase the spectral
content in the corresponding 1/3 octave band. In addition, the intensity
of the peak by itself is increasing with increasing advance ratio.

In Figure 5.9 is shown variation of the peak intensity in 6.3 kHZ
1/3 octave band as a function of increasing advance ratio. A 8 db
per doubling advance ratio seems like a good approximation for estimating
the influence of advance ratio on the intensity of HFBN.

5.3.3 The Effects of Number of Blades

To determine the effect of number of blades on HFBN, a series of
tests were conducted with 2, 3, 4, 5 and 6 blades. Once again the thrust
was maintained constant at 3.04 lbs. by changing the collective pitch
of the rotor blades. The tip path angle was maintained at 9° by changing
the shaft angle and the rotational speed of the rotor was held constant
at 672 rpm. Figure 5.10 depicts the 6% bandwidth spectrum of HFBN for
various number of blades. Figure 5.10 seems to indicate an increase in
the intensity of HFBN as well as widening of the spectra with increase
in number of blades. Since the increase in number of blades is likely
to cause increased vortex shedding and consequently an increased blade-
shed vortex interaction, these results appear consistent. Since the

increase in the intensity of HFBN is not confined to a narrow frequency band, an octave band analysis was performed on the same data. Figure 5.11 shows the variation of the intensity of HFBN in 6.3 kHZ octave band as a function of increasing number of blades. A 3 db per doubling blade number seems like a fair approximation to account for the variation in number of blades.

5.3.4 Directivity Patterns:

The directivity of two and three bladed rotors were measured on a plane normal to the tunnel wind axis at 10° intervals. These results are plotted in Figure 5.12. Also shown in Figure 5.12 is the directivity of a vertical dipole source for comparison.

5.4 Scaling of High Frequency Broadband Noise

As mentioned above, there is considerable amount of difference of opinion among various investigators regarding the Strouhal frequency scaling of the discrete tones generated by airfoils. In this section, we have reviewed some of the existing scaling procedures. In view of the experimental results obtained in Section 5.2 and Section 5.3, we have proposed a simple scaling formula relating the frequency of discrete tones to the geometric properties of the airfoil.

The serration studies of an isolated airfoil by Hersh and Hayden [33] and Paterson, et al. [34] revealed that the intensity of the discrete tones were reduced considerably by a boundary layer trip wire located at about 80% of the chord on the pressure surface of the airfoil. From this,

Paterson, et al., inferred that the pressure of a tone was associated with an undisturbed laminar boundary layer on the pressure side of the airfoil. The frequency of shed vortices are then given by [34],

$$f = \frac{SV}{2\delta_L} \tag{5.1}$$

Using the results of the laminar boundary layer for a flat plate, the expression for the tone frequency was given by

$$f = \frac{KV^{3/2}}{(c\nu)^{1/2}} \tag{5.2}$$

where Patterson et al [34] chose the factor K as a parameter to fit their experimental data.

It was noted by Tam [36] that the observed growth, saturation and decay of the intensity of the discrete tones was typical of an acoustically excited feedback loop of aerodynamic origin. The loop consists of an unstable laminar boundary layer on the pressure side of the airfoil which upon merging with the boundary layer in the suction side forms the near wake region as shown in Figure 5.13. Forced by the acoustic waves that impinge on the boundary layer, the disturbances are initiated in the wake flow at the sharp trailing edge of the airfoil - point A in Figure 5.13. The disturbances, in the form of large scale unstable waves, grow in amplitude as they propagate downstream along the wake. When these disturbances acquire sufficiently large amplitude, they cause the wake to vibrate laterally. Since the acoustic waves are produced by the actual

unsteady lateral displacement of the wake, the noise source region in the present case is highly localized - say point B in Figure 5.13. Thus generated acoustic waves propagate in all directions including the pressure side of the airfoil near the trailing edge where they force the boundary layer to oscillate. In this way the feedback loop is completed.

According to the feedback model above, disturbances are continuously being initiated at the sharp trailing edge of the airfoil. The fluid dynamic oscillations could be the Tollmein-Schlichting instability waves within the pressure surface laminar boundary layer. The instability requirement of these waves will now yield the frequencies of the discrete tones generated by the airfoil. Figure 5.14 depicts the stability criteria for the Tollmein-Schlichting waves for a Blasius profile. When the boundary layer oscillations are measured at constant frequency and different streamwise locations, maximum amplitude is found to occur at a Reynolds number corresponding to the right branch of the neutral stability curve shown in Figure 5.14. With this, Fink [39] obtained the expression for the frequency of tone radiation as

$$f = (2\pi)^{-1} \left(\frac{\beta\delta^*}{V}\right) \left(\frac{\nu}{\delta^*}\right) \tag{5.3}$$

where δ^* is the displacement thickness and $\beta\delta^*/V$ is the reduced frequency. The value of reduced frequency decreases from 0.17 to roughly 0.10 as the Reynolds number based on chord is increased from 1×10^5 to 2×10^6. Since the Reynolds number for a rotor blade varies along the span, the resulting radiation is confined in a frequency band.

Hanson [40] made extensive measurements of the near wake properties which lead to the generation of vortex shedding sound from airfoils. The airfoils belonged to the NACA 16 series with various trailing edge modifications. He measured the mean and fluctuating base pressure and the velocity profile in the wake and related them to the measured far field acoustic spectra. The frequency scaling of the periodic vortex noise was given as follows

$$S_\theta^* = 0.0728 \left(1 - \frac{1038}{R_{e\theta}^*}\right) \tag{5.4}$$

where

$$S_\theta^* = \frac{f\theta}{u_s}$$

$$R_{e\theta}^* = \frac{u_s \theta}{\nu}$$

Here S_θ^* and Re_δ^* are wake Strouhal numbers and Reynolds numbers based on the momentum thickness θ of the near wake region. The velocity u_s was given as

$$u_s = u_0 \sqrt{1 - C_{pb}} \tag{5.5}$$

where C_{pb} was the measured base pressure coefficient.

5.4.1 Peak Frequency Consideration:

So far we have considered various theories describing the frequency scaling characteristics of the trailing edge noise from stationary airfoils.

It should be noted that no two theories described herein predict the same frequency and thus exists a controversy regarding the noise generating mechanism. Several independent experimental investigations have confirmed the use of a shear layer thickness as the appropriate length scale [35, 40, 45] to predict the frequency of discrete tones from isolated airfoils. Wake measurements for rotating airfoils are not available as of now and would indeed be desirable information. Lee [14] made measurements of the peak frequency location of the high frequency broadband noise of the present model rotor system, operating at various speeds. Based on his measurements, he defined a Strouhal number

$$S = \frac{ft}{V_e}$$

where V_e was the rotational velocity measured at 75% of the blade span. His experimental results lead to a Strouhal number of about 1.

Following Lee's [14] argument that there is a need for a frequency scaling based more on geometrical parameters of the system than on the fluid dynamical characteristics, we define *a priori* a frequency scaling law as

$$f = \frac{SV}{t} \tag{5.6}$$

The velocity V is chosen to be the tip velocity. Based on our experimental results, the existence of such a relationship will be demonstrated later in Section 5.4.3.

5.4.2 Pressure Field Consideration

By developing the known ideas of Lighthill [41] concerning the aerodynamic generation of sound by unlimited turbulent flow, Curle [42] obtained the expressions for the acoustic radiation from a surface S immersed in turbulent flow as follows:

$$\rho - \rho_0 = \frac{1}{4\pi c_0^2} \left[\frac{\partial^2}{\partial x_i \partial x_j} \int_{volume} \frac{T_{ij}}{r} d\tau(\vec{y}) - \frac{\partial}{\partial x_i} \int_s \frac{(p_i - \rho v_i v_n)}{r} d\tau S(\vec{y}) \right.$$

$$\left. - \int_s \frac{\partial}{\partial t} (\rho v_n) \frac{d\tau(\vec{y})}{r} \right] \tag{5.7}$$

For an acoustically compact source, the far field sound radiation is given by Curles' extension of Lighthill's theory.

$$p(\vec{x},t) = - \frac{1}{4\pi c_0} \frac{x_i}{x^2} \frac{\partial}{\partial \tau} \int_s p_i(y, \tau - x/c_0) \, ds(y) \tag{5.8}$$

Using the coordinate system shown in Figure 5.15, we have the instantaneous pressure due to an element of the airfoil of length ΔL, over which the shed vortices are assumed to be correlated, given by

$$p = - \frac{1}{4\pi c_0} \frac{\cos\theta}{r_1} \frac{\partial}{\partial \tau} P_i(\tau) \, (c\Delta L)$$

The shed vortices cause a periodic variation of P_i, the frequency being given by Equation (5.6). To this end we have,

$$P_i \simeq p_0 \cos (2\pi f \tau)$$

Normalizing p_0 with respect to the blade sectional velocity $\rho_0 v_c^2/2$, we have the mean square pressure variation as

$$(\Delta p)^2 \simeq \frac{S^2 c^2 \rho_0^2 \cos^2 \theta \, v^2 v_c^4 (\Delta L)^2}{c_0^2 \, r_1^2 \, t^2} \qquad (5.9)$$

The blade sectional velocity v_c at the chordwise location is given by

$$v_c = v + u_\infty \cos \phi$$

which may be rewritten in terms of the advance ratio as

$$v_c = v \left[1 + \mu \left(\frac{b}{R}\right) \cos \phi \right] \qquad (5.10)$$

This has a maximum value at the azimuthal angle of $\phi = 0$, and substituting the maximum value of (5.10) into (5.9), we obtain

$$(\Delta p)^2 \cong \frac{S^2 c^2 \rho_0^2 \cos^2 \theta \, v^6 \, [1 + \mu \, b/R]^4 \, (\Delta L)^2}{c_0^2 \, r_1^2 \, t^2}$$

The total pressure is therefore the sum of the elementary emitting surfaces or sources and is given by

$$S_{pp}(f) = \sum (\Delta p)^2 \simeq \frac{S^2 c^2 \rho_0^2}{c_0^2 t^2} \sum_{k=1}^{b/\Delta L} \frac{v_k^6 (1 + \mu\, b/R_k)^4 (\Delta L_k)^2}{r_k^2} \tag{5.11}$$

Here, the subscript k denotes the quantities corresponding to a kth element. Noting that

$$v_k = \Omega R_k = \Omega k \Delta L$$

$$r_k^2 = x^2 + R_k^2$$

$$\cos^2\theta_k = x^2/(x^2 + R_k^2)$$

we can rewrite Equation (5.11) as follows:

$$S_{pp}(f) \cong \frac{S^2 c^2 \rho_0^2}{c_0^2 t^2} \quad \frac{\Omega^6 (\Delta L)^8}{x^2} \quad \sum_{k=1}^{b/\Delta L} \frac{k^6 [1 + \mu (\frac{b}{\Delta L}) \frac{1}{k}]^4}{[1 + (\frac{k\Delta L}{x})^2]^2} \tag{5.12}$$

Here we have assumed that the correlation length ΔL is constant along the span: For the farfield solution, in general, $R_k/x < 1$; hence the term in the denominator of summation may be approximated to unity. Further, since ΔL is small compared to b, $b/\Delta L$ is a large number, say N. Then the Equation (5.12) becomes

$$S_{pp}(f) \simeq \frac{S^2 c^2 \rho_0^2}{c_0^2 t^2} \quad \frac{\Omega^6}{x^2} (\Delta L)^8 \sum_{k=1}^{N} k^6 [1 + 4\mu \frac{N}{k} + 6\mu^2 \frac{N^2}{k^2} + \cdots]$$

The summation is given by standard formulae in [43] and for large N's, may be approximated as follows

$$\sum_{k=1}^{N} k^6 \simeq N^7/7$$

$$N \sum_{k=1}^{N} k^5 \simeq \frac{N^7}{6}$$

$$N^2 \sum k^4 \simeq \frac{N^7}{5}$$

Hence, we obtain the total pressure field as

$$S_{pp}(f) \simeq \frac{S^2 c^2 \rho_0^2 b \; v_t^6 \Delta L}{c_0^2 t^2 x^2} \quad [\; 1 + \frac{14}{3} \mu + \frac{42}{5} \mu^2] \tag{5.13}$$

With this, the Mach number scaling formula for the total high frequency broadband noise generated by rotors in similar flow environ is given by:

$$S_{pp}(x_2, f_2) = S_{pp}(x_1, f_1) + 60 \log \frac{V_{t_2}}{V_{t_1}} + 20 \log \left(\frac{c_2 t_1}{c_1 t_2} \right)$$

$$+ 10 \log \left(\frac{b_2}{b_1} \right) - 20 \log \left(\frac{x_2}{x_1} \right) + 10 \log \left(\frac{\Delta L_2}{\Delta L_1} \right)$$

$$+ 10 \log \left[\frac{ \{ 1 + \frac{14}{3} \mu_2 + \frac{42}{5} \mu_2^2 \} }{ \{ 1 + \frac{14}{3} \mu_1 + \frac{42}{5} \mu_1^2 \} } \right] \tag{5.14}$$

and the corresponding peak frequency locations f_1 and f_2 are given by (5.6). The effect of blade number may be included by adding $10 \log B_2/B_1$

to Equation (5.14).

Mugridge [44] and Clark, et al [45] demonstrated experimentally that the correlation lengths over a stationary airfoil are directly proportional to the displacement thickness of the turbulent boundary layer. In the case of a rotating airfoil, the thickness of the boundary layer is influenced by the local Reynolds number as well as by the spanwise flow. Realistic estimates of correlation lengths for rotating airfoils are not presently available. However, since the mechanism is similar to that of a stationary airfoil, we assume for scaling purposes that the correlation length behaves in a manner similar to the boundary layer displacement thickness at a representative spanwise location. Since the displacement thickness for the turbulent boundary layer varies like $c/(R_e)^{0.2}$, the high frequency broadband noise levels vary like $V_t^{5.8}$.

5.4.3 Experimental Results and Discussion

To verify the validity of the frequency and amplitude scaling procedures developed in the previous sections, we performed a series of experiments in the M.I.T. anechoic wind tunnel facility. The data was analyzed using a B & K spectrum analyzer with 6% band width. In Figure 5.16 are plotted typical HFBN spectra for various rotational speeds at constant advance ratio for a 2 bladed rotor. As noted above in Section 5.3, the advance ratio had no significant effect on the peak frequency location, and this justifies use of rotational tip velocity in equation (5.6) for Strouhal scaling of shed vortices.

- 75 -

Figure 5.17 shows a plot of peak frequency as a function of the blade
tip velocity. As can be seen from Figure 5.17, the peak frequency is
directly proportional to the blade tip velocity with a proportionality
constant of 54. At higher tip speeds, the high frequency broadband noise
is spread over a narrow range of frequencies and hence there is some scatter
in the measured data. Using maximum blade thickness in Equation (5.6), the
resulting Strouhal frequency is 1.08. Although a wake characteristic
length such as displacement of momentum thickness should be the appropriate
length scale to be used, a simple relationship based on the geometrical
parameter may be very useful in practical applications.

In Figure 5.18, an estimate of the peak sound pressure levels calcu-
lated using the measured values of a two bladed rotor operating at 550
rpm as a base, is plotted. The three bladed rotor data is normalized
with respect to the two bladed rotor data by taking out $10 \log B_2/B_1$ from
measured sound pressure levels. As can be seen from Figure 5.18, the
prediction scheme presented in Section 5.4.2 gives good correlations with
the measured two blade and three blade data except at very low rotational
velocities. It was observed that at these low velocities, corresponding
to a rotational speed of 300 and 400 rpm, the measured high frequency
broadband noise spectra showed intense peaks. This probably is due to
a fairly laminar flow on both sides of the airfoil resulting in more
intense shedding of vortices. The peak intensity decreased slightly as
we increased the rotational velocity to about 500 rpm, and then started in-
creasing according to the postulated power law. Also observed at these

low velocities were multiple tones at twice and thrice the fundamental peak of high frequency broadband noise. These peaks were 15 to 20 db less than the intensity of primary tone and disappeared as we increased the rotational speed to about 500 rpm. At present, we have not been able to establish a physical mechanism responsible for such secondary radiation at multiples of primary vortex shedding frequency.

When the advance ratio was kept constant, the prediction scheme seemed to yield excellent correlation with measured data. The central region in Figure 5.18 corresponds to a variation in advance ratio which again seems to cause a slight difference between predicted and the measured sound pressure levels. Considering the number of approximations made in the scaling procedure, the general agreement between the theoretical prediction scheme and the experimental results may be regarded as highly favorable.

5.5 Effects of Free Stream Turbulence

It was observed in Section 5.4 that the intensity of high frequency broadband noise is dependent on the spanwise correlation length of shed vortices. It was also assumed that these correlation lengths are proportional to the displacement thickness of the boundary layer.

The influence of free stream disturbances on the development of a turbulent boundary layer on a flat plate has been studied by McDonald and Kreskovsky [46] and Evans and Horlock [47]. Using an existing integral boundary layer calculation to predict the turbulent boundary layers developing in a turbulent free stream, Evans and Horlock [47] concluded

that the displacement thickness decreased with increasing free stream turbulence intensity. Extending their results to the scaling procedure developed in Section 5.4, we conclude that the increase in the intensity of free stream turbulence would in general tend to decrease the intensity of the high frequency broadband noise. In Figure 5.19 is shown the effect of free stream turbulence on the 6% bandwidth high frequency spectrum of a two bladed rotor noise. The above prediction would result in a decrease of 5.6 db for the 0.75" x 6" grid and 8.1 db for the 3.5" x 20" grid respectively from the measured intensity of high frequency broadband noise in the absence of turbulence generating grids. We further note that the location of the peak intensity of the high frequency broadband noise remains unaffected by introduction of free stream disturbances. In Figure 5.20 are plotted the predicted and measured intensities of high frequency broadband noise as a function of turbulence intensity. From Figure 5.20 it is evident that the influence of turbulence on the intensity of HFBN is indeed significant.

It should be noted that the proposed scheme to include the effect of free stream turbulence on the intensity of HFBN is only qualitative in nature. The results of Evans and Horlock [47] were obtained for low to moderate intensities of turbulence (of the order of 4%) and the validity of extending their theory to the present situation of high intensity turbulence is indeed argumentative. But in the absence of accurate information regarding development of boundary layers on rotating airfoils in presence of free stream turbulence, only a crude approximation can be made to predict the nature of broadband noise.

CHAPTER VI

CONCLUSIONS AND RECOMMENDATIONS FOR FURTHER RESEARCH

The objective of this study has been to arrive at suitable velocity dependent factors to predict the various noise components of a model helicopter rotor. To this end, we have performed a series of experiments at the M.I.T. anechoic wind tunnel facility. The rotational and the broadband noise components were isolated and studied independently. An analysis based on existing theoretical modelling of unsteady aerodynamics has been presented and the computed results have been compared with the measured data. In Section 6.1 is given the conclusions of our efforts and Section 6.2 describes some of the possible recommendations for further research in this area.

6.1 Conclusion

It is postulated that the rotational noise from model rotors is a direct consequence of steady and unsteady loading harmonics and the broad-band noise may further be classified into low frequency and high frequency components because of the inherent differences in their causative mechanisms. The low frequency broadband noise is attributed to the interaction of in-gested turbulence with the rotor blades. The high frequency broadband noise is associated with the periodic vortex shedding from the rotating airfoils.

Analytical expressions were developed to determine the spectral content of the rotational noise components using existing theories of radiation from rotating dipole sources. An order of magnitude study indicated that the contribution of force derivative terms outweigh the contributions of force and

and thickness terms for tip Mach numbers of 0.6 or less. Such an approximation yielded simpler expressions for the complex Fourier co-efficeints of sound radiation from a rotating point source. The resulting Mach number scaling formula for rotational noise is as follows.

$$
\begin{aligned}
SPL_2 = \ & SPL_1 + 60 \log \frac{M_{t_2}}{M_{t_1}} + 20 \log \frac{c_2}{c_1} \\
& - 20 \log \frac{r_2}{r_1} + 20 \log \frac{\sin\alpha_2}{\sin\alpha_1} \\
& - 40 \log \left[\frac{1 + \mu_2 M_{t_2} \cos\alpha_2 \cos\phi_2}{1 + \mu_1 M_{t_1} \cos\alpha_1 \cos\phi_1} \right]
\end{aligned}
\tag{6.1}
$$

The location in the frequency domain is simply given by the blade passage harmonic, $nB\Omega$.

Theoretical analysis of the low frequency broadband noise were made exploiting the existing knowledge of unsteady thin airfoil theory and the characteristics of the inflow turbulence. Assumptions of isotropy and homogeneity of turbulence were made to make the analysis feasible. The measured spectrum of turbulence justified the validity of such assumptions. Further, it was observed that the measured turbulence spectra could easily be interpreted in terms of von Karman's interpolation formula. With the aid of this and the two dimensional Sears function, the unsteady lift acting on the airfoil was computed. The resulting acoustic intensity and spectra were dependent on the flow and rotational Mach numbers, intensity and size scale of turbulence. The peak intensity of low frequency broad-band noise was found to be varying with the Mach number according to a M_t^4 power law, and with r.m.s. values of turbulence velocity according to

a $\overline{w}^2$ power law. The influence of size scale of turbulence on the peak intensity was found to be insignificant, approximately $\Lambda_f^{-0.33}$. However, the location of peak intensity in the frequency domain was found to be strongly dependent on the Mach number and the longitudinal scale of turbulence. To this end, we plotted the normalized acoustic intensity as a function of Strouhal frequency $f\Lambda_f/V$. It was observed that the peak intensity of LFBN occured at a Strouhal number of about 1.5. With this, a scaling law can readily be proposed to evaluate the peak intensity of low frequency broadband noise. Under similar flow environ, the sound pressure level of a rotor system 2 in terms of a rotor system 1 will then be given as follows

$$
\begin{aligned}
SPL_2 = \ & SPL_1 + 20 \log \frac{b_2 c_2}{b_1 c_1} + 10 \log \frac{\overline{w}_2^2}{\overline{w}_1^2} \\[2mm]
& + 40 \log \frac{M_{t_2}}{M_{t_1}} + 20 \log \frac{\left[(1 + \mu_2)^2 + (M_{c_2}/M_{t_2})^2\right]}{\left[(1 + \mu_1)^2 + (M_{c_1}/M_{t_1})^2\right]} \\[2mm]
& - 3.3 \log \frac{\Lambda_{f_2}}{\Lambda_{f_1}} - 20 \log \frac{r_2}{r_1}
\end{aligned}
\tag{6.2}
$$

The location of the peak intensity in the frequency domain is given by

$$
f_{p_{1,2}} = \frac{1.5 \ V_{1,2}}{\Lambda_{f_{1,2}}}
\tag{6.3}
$$

for respective rotor system.

To obtain a similar scaling procedure for high frequency broadband noise generated by a model rotor, we assumed that noise sources were acoustically compact and computed the instantaneous pressure due to an element of an airfoil where vortices are being shed. Extending experimentally obtained results for the spanwise correlation lengths for stationary airfoils to rotating airfoils and assuming that the correlation lengths vary like the displacement thickness of the boundary layer, it was observed that the peak intensity of high frequency broadband noise has a $V_t^{5.8}$ factor. An expression which scales the location of peak intensity in the frequency domain was obtained based on the rotor blade geometric parameters. The resulting scaling laws for peak intensity was found to be

$$
\begin{aligned}
SPL_2 = SPL_1 &+ 60 \log \frac{M_{t_2}}{M_{t_1}} + 20 \log \frac{c_2 t_1}{c_1 t_2} \\
&+ 10 \log \frac{b_2}{b_1} - 20 \log \frac{r_2}{r_1} + 10 \log \frac{(\Delta L)_2}{(\Delta L)_1} \\
&+ 10 \log \left\{ \frac{[1 + {}^{14}/3 \, \mu_2 + {}^{42}/5 \, \mu_2^2]}{[1 + {}^{14}/3 \, \mu_1 + {}^{42}/5 \, \mu_1^2]} \right\}
\end{aligned}
$$

(6.4)

and the peak frequency was found to be given by

$$
f_{p_{1,2}} = 1.08 \, V_{t_{1,2}} \Big/ t_{1,2}
$$

(6.5)

for the respective rotor systems. The effects of intensity and size scale of turbulence were less obvious in the study of high frequency broadband noise. One of the effects of free stream turbulence is to alter the correlation lengths of shed vortices. To this end, we used an existing integral boundary layer calculation to predict the turbulent boundary layers developing in a turbulent free stream. The results indicated that increase in the intensity of free stream turbulence in general, would tend to decrease the correlation length, thus resulting in reducing the intensity of high frequency broadband noise.

The scaling laws obtained for the intensities of rotational noise components were experimentally verified over a range of operating conditions. The measured data showed general agreement with the scaling procedure except at low rotational harmonies. It is believed that the geometric and acoustic near field effects might have caused some ambiguity in the measured rotor noise spectra at very low frequencies. The low frequency broadband noise prediction procedures were experimentally verified under various operating conditions of the rotor and varying intensity and size scale of turbulence. A comparison of predicted peak frequency and sound pressure levels with experimental data showed good agreement except for the case of effect of turbulence on the intensity of high frequency broadband noise. In this case, the data showed general agreement with the prediction technique, but the measured intensity levels were higher than the predicted levels. We further add that improvements in modelling more of the fluid mechanical aspects of the flow field are desired to place this scaling procedure on a firmer basis.

With the knowledge of the variation of the flow parameters on the
intensity and spectrum of low frequency and high frequency broadband
noise, it is indeed tempting to compare the scaling procedure with ex-
perimentally obtained full scale rotor results [6]. Since the r.m.s.
turbulence velocity and size scale are unspecified, we estimated their
values based on Leverton's [6] data for a full scale rotor operating
at 160 rpm and generating a thrust of 3050 lbs. The peak intensity was
measured to be 72 db and the frequency was 250 HZ. With this, we esti-
mated the integral scale of turbulence as 2.8 ft. and the r.m.s. turbu-
lence velocity as 1.52 ft./sec. These values were used to predict the
intensity of low frequency broadband noise for the same rotor operating
at 260 rpm generating a thrust of 700 lbs. The model rotor used in both
scaling procedures was operating at 750 rpm, generating a thrust of 3.8
lbs. and the r.m.s. velocity and size scale of turbulence were 4.1 ft./sec.
and 0.42 ft. respectively. This resulted in a prediction of 80.4 db at
a frequency of 400 HZ. The measured values were found to be 77 db at a
frequency of 350 HZ.

Caution must be exercised in comparing the high frequency broadband
noise results of the model rotor system with those of full scale tests
because of vast differences in Reynolds number. At high enough Reynolds
number, there is very little evidence that full rotors sustain a laminar
boundary layer. To determine the relevance of the present study to actual
rotor noise, we computed the intensity and spectrum of the full scale
rotor of Leverton using our model rotor running at 1000 rpm. Figure 6.1
shows the predicted and measured frequencies for the high frequency

broadband noise peak. In Figure 6.2, the estimated sound pressure levels are compared with the measured Leverton's data after accounting for atmospheric absorption. As can be seen from Figures 6.1 and 6.2, the high frequency broadband noise scaling procedure predicts the location of the peak in the frequency domain accurately, but fails to predict the proper sound pressure levels. Since the estimated turbulence intensity is very low, we attribute this discrepancy to the vast difference in the Reynolds number. The Reynolds number of the full scale rotor was 6.62×10^6 as opposed to the Reynolds number of our model rotor of 2.3×10^5. The tail rotor data of Paterson et al [34] corresponds to a Reynolds number of 2.5×10^6. A Sikorsky 5 bladed rotor operating at a design rpm of 1243 on a rotor whirl test stand radiated 90 db at 10 kHZ. Using the proposed prediction scheme and using the data of our model rotor operating at 550 rpm, we were able to obtain a sound pressure level of 90 db at 9800 HZ.

The analysis of Homicz and George [26] has placed the blade-turbulence interaction noise modelling on a firmer theoretical basis than existed previously for the generation of broadband noise. But, their claim that their theory can be used to predict the high frequency broadband noise is unrealistic. Our analysis, being a direct consequence of the method of Homicz and George yields good comparison with the measured model rotor data for low frequency broadband noise. But, their analysis predicts a constant decay of the acoustic field with increasing frequency, which does not happen in either model or full scale rotor systems. We have, therefore, used the classical vortex shedding theory in conjunction with the blade-turbulence interaction theory to predict the total acoustic spectrum of rotor noise. The principal area of uncertainty lies in the inadequacy

of classical vortex shedding theory to predict the noise generated at high Reynolds number. A better understanding of the fluid dynamics of the rotating blades are necessary to yield more realistic prediction tehcniques [19].

Our efforts in modelling the rotational noise components of the model rotor and understanding the effects of free stream turbulence on the nature of high frequency and low frequency broadband noise components have been greatly benefitted from the detailed experimental task performed by Lee [14]. The utility of our results for scaling of low frequency and high frequency broadband noise remains as demonstrated in the above comparison of predictions and data. The scaling procedures developed in this study may be considered as a first order attempt in responding to the challenge of Mach number and Reynolds number scaling of full scale rotors.

6.2 Recommendations for Further Research:

The objective of every experimental researcher is to compile data at various laboratory operating modes and to postulate prediction schemes applicable to full scale operating conditions. In this report, we have presented the results of the detailed study of the acoustic characteristics of the M.I.T. 4.17 foot diameter model rotor system. The tip Mach number and Reynolds number (based on chord) were limited to 0.25 and 2.5×10^5 respectively because of the limitations of the rotor operating system. The next logical step will be to explore the validity of the present prediction procedures at higher tip Mach numbers and Reynolds numbers. The principal areas of uncertainties in extending the present analysis are as follows:

(i)   The relative importance of force and thickness terms in the radiation of rotational noise components must be reconsidered. The order of magnitude analysis presented in Chapter III of this report indicated that the thickness and the force terms are comparable at tip Mach numbers of about 0.65. Recently Farassat and Brown [48], using a time domain approach showed that the thickness noise dominated the acoustic time history of a rotor operating at an advancing blade Mach number of 0.92.

(ii)   The effects of free stream turbulence on the intensity and bandwidth of rotational harmonics need to be studied on a formal basis. It is generally accepted that the turbulence increases the blade to blade correlation [26] and add side bands at blade passage tones. This effect was more pronounced for the case of a stationary fan studied by Hanson [25].

(iii)   The ambiguous state of the art regarding the frequency and amplitude scaling of high frequency broadband noise needs to be clarified. The aerodynamic sources of high frequency broadband noise are strongly dependent on the operating Reynolds number and has been subject of various investigations [9, 33, 34, 35, 36]. More experimental data over a wide range of Reynolds numbers is needed to place the theory of high frequency broadband noise on a firmer basis.

It is believed that blade surface pressure measurements would greatly enhance our understanding of the aerodynamic noise generating mechanisms. The simultaneous measurements of aerodynamic and acoustic signals will facilitate proper cross correlation analysis.

There is very limited experimental data available for determining the impulsive noise characteristics of a helicopter rotor. The blade-vortex interaction noise, often termed as "blade slap" and the shock-interaction noise often termed as "blade pop" are two major sources of impulsive noise. The blade slap occur only at certain operating conditions such as a decent, or a low advance ratio flight. Experiments are being conducted at the M.I.T. anechoic tunnel facility and by Schmitz at the NASA Ames Directorate [49], to gain more insight to the characteristics of glade vortex interaction noise. The shock noise or "blade pop" is often due to presence of unsteady shock waves on the blade surface. They are highly directional, loud and high pitched banging sound occuring at blade passing frequency. Recent theoretical study by Kitaplioglu and George [50] indicate that the shocks under proper circumstances, are likely to make an important contribution to helicopter noise. We believe that acquiring experimental data on shock noise would be necessary to suppliment the theoretical study already in progress.

REFERENCES

1. Gutin, L., "On the Sound Field of a Rotating Propeller", NACA TM
        1195, 1948.

2. Cox, C.R., "Aerodynamic Sources of Rotor Noise", Journal of American
        Helicopter Society, 18, pp. 3-9, 1973.

3. Morfey, C.L., "Rotating Blades and Aerodynamic Sound", Journal of
        Sound and Vibration, 28, pp. 587-617, 1973.

4. Taylor, G.I., "The Singing of Wires in Wind", in Scientific Papers,
        Vol. III, Cambridge University Press, 1963.

5. Kramer, M., "The Aerodynamic Profile as Acoustic Noise Generator",
        Journal of Aeronautical Sciences, 20, pp. 280-282, 1953.

6. Leverton, J.W., "The Noise Characteristics of a Large Clean Rotor",
        Journal of Sound and Vibration, 27, pp. 357-376, 1973.

7. Leverton, J.W. and Pollard, J.S., "A Comparison of Overall and
        Broadband Noise Characteristics of Full Scale and Model
        Helicopter Rotors", Journal of Sound and Vibration,
        30, pp. 135-152, 1973.

8. Goldstein, M.E., "Aeroacoustics", NASA SP-346, 1974.

9. Hayden, R.E., Fox, H.L., and Chanaud, R.C., "Some Factors
        Influencing Radiation of Sound from Flow Interaction
        with Edges of Finite Surfaces", NASA CR-145073 (also
        Bolt Beranek & Newman Report 2797, 1976).

10. Lowson, M.V., Whatmore, A.R., and Whitfield, C.E., "Source Mech-
        anisms for Rotor Noise Radiation", NASA CR-2077, 1973.

11. Bauer, P. and Widnall, S.E., "The Development of a Wind Tunnel
        Facility for the Study of V/STOL Noise", Flight
        Transportation Lab. Report, FTL R-72-6, M.I.T., 1972.

12. Widnall, S.E., Harris, W.L., Lee, A., and Drees, H.M., "The
        Development of Experimental Techniques for the Study of
        Helicopter Rotor Noise", NASA CR-137684, 1974.

13. Baines, W.D. and Peterson, E.G., "An Investigation of Flow Through
        Screens", Transactions of ASME, 73, pp. 467-480, 1951.

14. Lee, A., "Theoretical and Experimental Study of Helicopter Rotor
        Noise", Ph.D. Thesis, Dept. of Aeronautics and Astronautics,
        M.I.T., 1975.

15. Harris, W.L. and Lee, A., "The Development of Experimental Techniques for the Study of Helicopter Rotor Noise", AIAA paper 75-455, AIAA 2nd Aeroacoustics Conference, Hampton, Virginia, March 24-26, 1975.

16. Lowson, M.V. and Ollerhead, J.B., "A Theoretical Study of Helicopter Rotor Noise", Journal of Sound and Vibration, 9, pp. 197-222, 1969 (also Wyle Research Staff Report WR 68-9, 1968).

17. Wright, S.E., "Discrete Radiation from Rotating Periodic Sources", Journal of Sound and Vibration, 17, pp. 437-498, 1971.

18. Hawkings,D.L. and Lowson, M.V., "Noise of High Speed Rotors", AIAA paper 75-450, AIAA 2nd Aeroacoustics Conference, Hampton, Virginia, March 24-26, 1975.

19. Aravamudan, K.S., Lee, A., and Harris, W.L., "Simplified Mach Number Scaling Formula for Helicopter Rotor Noise", to appear in the Journal of Sound and Vibration.

20. Ffowcs Williams, J.E. and Hawkings, D.L., "Theory Relating to the Noise of Rotating Machinery", Journal of Sound and Vibration, 10, pp. 10-21, 1969.

21. Morfey, C.L. and Tanna, H.K., "Sound Radiation from a Point Source in Circular Motion", Journal of Sound and Vibration, 15, pp. 325-351, 1971.

22. Lowson, M.V., "Rotor Noise Radiation in Non-Uniform Flow", Proceedings of the Symposium on Aerodynamic Noise, Loughborough University, Paper D2, 1970.

23. Amiet, R.K., "Acoustic Radiation from an Airfoil in a Turbulent Stream", Journal of Sound and Vibration, 41, pp. 407-420, 1975.

24. Sears, W.R., "Some Aspects of Non-Stationary Airfoil Theory and Its Applications", Journal of Aeronautical Sciences, 8, pp. 104-108, 1941.

25. Hanson, D.B., "Spectrum of Rotor Noise Caused by Atmospheric Turbulence", Journal of Acoustical Society of America, 56, pp. 110-126, 1974.

26. Homicz, G.F. and George, A.R., "Broadband and Discrete Frequency Radiation from Subsonic Rotors", Journal of Sound and Vibration, 36, pp. 151-177, 1974.

27. George, A.R. and Kim, Y.K., "High Frequency Broadband Rotor Noise", AIAA Paper 76-561, 3rd AIAA Aero-Acoustic Conference, Palo Alto, CA, July 20-23, 1976.

28. Amiet, R.K., "Noise Produced by Turbulent Flow into a Propeller or Helicopter Rotor", AIAA Paper 76-560, 3rd AIAA Aero-acoustic Conference, Palo Alto, CA, July 20-23, 1976.

29. Osborne, C., "Unsteady Thin Airfoil Theory", AIAA Journal, 11, pp. 205-209, 1973.

30. Hinze, J.O., "Turbulence", Second edition, McGraw Hill Publications, New York, 1975.

31. Mugridge, B.D., "Sound Radiation from Aerofoils in Turbulent Flow", Journal of Sound and Vibration, 13, pp. 362-363, 1970.

32. Chanaud, R.C. and Hayden, R.E., "Edge Sound Produced by Two Turbulent Wall Jets", Paper FF-11, Spring Meeting of Acoustical Society of America, Atlantic City, New Jersey, 1970.

33. Hersh, S. and Hayden, R.E., "Aerodynamic Sound Radiation from Lifting Surfaces With or Without Leading Edge Serrations", NASA CR-114370, 1971.

34. Paterson, R.W., Vogt, P.G., Fink, and Munch, C.L., "Vortex Shedding Noise From Isolated Airfoils", Journal of Aircraft, 10, pp. 296-302, 1973.

35. Clark, L.T., "The Radiation of Sound from an Airfoil Immersed in Laminar Flow", Journal of Engineering for Power, 13, Ser. A, pp. 366-376, 1971.

36. Tam, C.W., "Discrete Tones from Isolated Airfoils", Journal of Acoustical Society of America, 55, pp. 1173-1177, 1974.

37. Lee, A., Aravamudan, K.S., Bauer, P., and Harris, W.L., "An Experimental Investigation of Helicopter Rotor High Frequency Broadband Noise", AIAA Paper 77-1339, Paper presented at the 4th Aeroacoustic Conference, Atlanta, Georgia, October 3-5, 1977.

38. Ham, N.D., "Some Preliminary Results from an Investigation of Blade Vortex Interaction", J. of American Helicopter Society, 19, pp. 45-48, 1974.

39. Fink, M.R., "Prediction of Airfoil Tone Frequencies", Journal of Aircraft, 12, pp. 118-119, 1975.

40. Hanson, C.E., "An Investigation of the Near Wake Properties Associated with Periodic Vortex Shedding from Airfoils", MIT Acoustics and Vibration Laboratory, TR76234-5, 1970.

41. Lighthill, M.J., "On Sound Generated Aerodynamically, II, Turbulence as a Source of Sound", Proceedings of the Royal Society, A, 222, 1952.

42. Curle, N., "The Influence of Solid Boundaries Upon Aerodynamic Sound", Proceedings of Royal Society, A, 231, 1955.

43. Gradshteyn, I.S. and Ryzhik, I.W., "Table of Integrals, Series and Products", Academic Press, New York, 1965.

44. Mugridge, B.D., "Turbulent Boundary Layers and Surface Pressure Fluctuations on Two Dimensional Aerofoils", Journal of Sound and Vibration", 18, pp. 475-486, 1971.

45. Clark, L.T., "A Prediction Model for Wake Related Sound Generation", Ph.D. Thesis, University of Washington, 1973.

46. McDonald, H. and Dreskovsky, J.P., "Effect of Free Stream Turbulence on the Turbulent Boundary Layer", International Journal of Heat and Mass Transfer, 17, pp. 705-716, 1974.

47. Evans, R.I., and Horlock, J.H., "Calculation of the Development of Turbulent Boundary Layers with a Turbulent Free Stream", ASME Paper 74-FE-24, 1974.

48. Farassat, F. and Brown, J.J., "A New Capability for Predicting Rotor and Propeller Noise Including the Effect of Forward Motion", NASA TMX-74037, June 1977.

49. Schmitz, F.H., and Yu, Y.H., "Theoretical Modelling of High Speed Helicopter Impulsive Noise", Paper No. 54, Third European Rotorcraft and Powered Lift Aircraft Forum, Aix-en-Provence, France, September 7 - 9, 1977.

50. Kitaplioglu, C. and George, A.R., "A Study of Far Field Sound Due to Unsteady Shocks on Rotors", AIAA paper 77-1360, 4th AIAA Aeroacoustics Conference, October 3 - 5, 1977, Atlanta, Ga.

Table 2.1

MODEL ROTOR CHARACTERISTICS

Radius (b)	25 inches (64.1 cm)
Chord (c)	2 inches (5.13 cm)
Number of blades (B)	1 to 6
Section	NACA 0012
Twist	- 8°
Shaft tilt Capability	±20°
Maximum RPM	1200
Testing RPM	Variable, from 400 RPM to 1100 RPM
Lead-lag	None
Cyclic Pitch	None
Collective Pitch	By adjusting pitch of individual blade

1.0

4.5
5.0
5.6

2.8

2.5

1.1

3.2

2.2

3.6

4.0

2.0

1.8

1.25

1.4

1.6
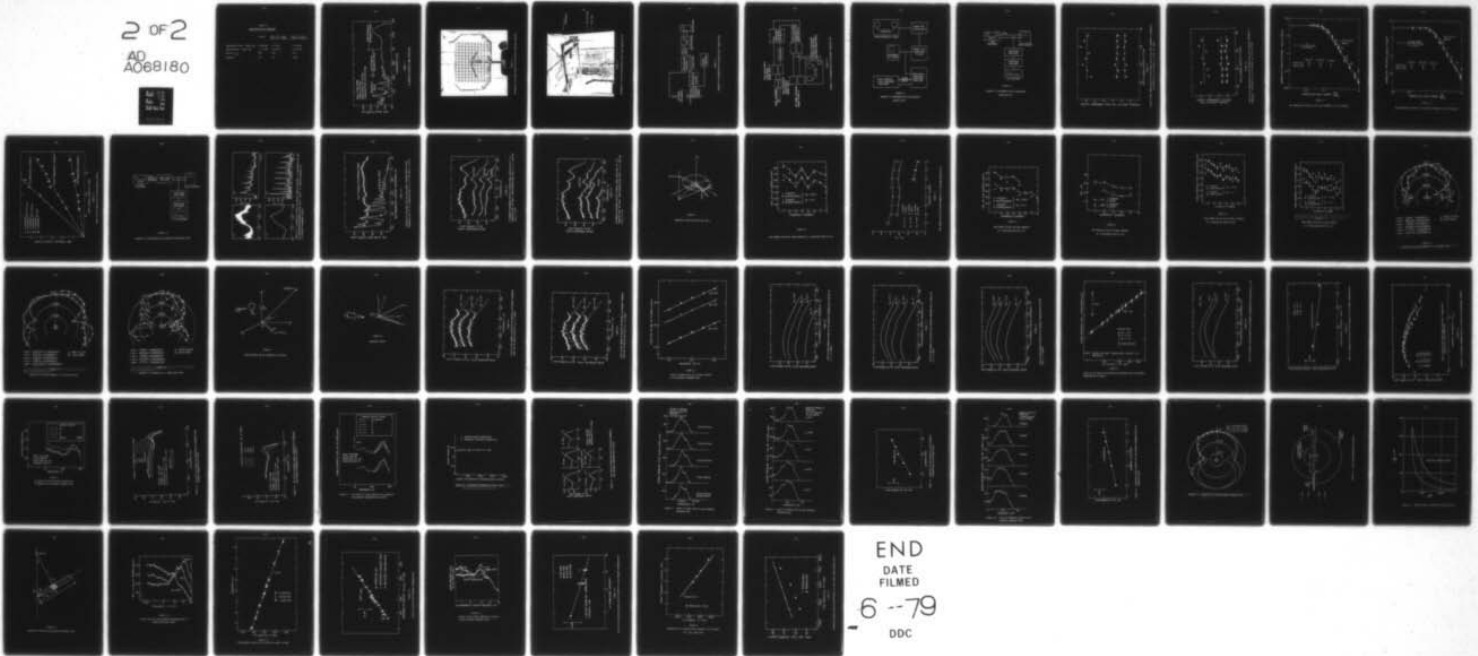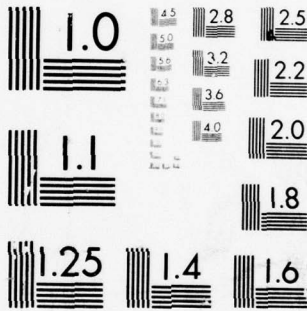
MICROCOPY RESOLUTION TEST CHART

NATIONAL BUREAU OF STANDARDS-1963-A

Table 2.2

<u>CHARACTERISTICS OF TURBULENCE</u>

	No grid	3.5" x 20 " grid (8.97 cm x 51.28cm)	0.75" x 6" grid (1.92cm x 15.38 cm)
Longitudinal Scale - inches (cm)	11.8(30.26)	5 (12.82)	3.3 (8.46)
Vertical Scale - inches (cm)	7 (17.95)	3.2 (8.21)	2.0 (5.13)
Ratio of Λ_g/Λ_f	0.59	0.64	0.61
Intensity	1.7%	11%	6.25%

FIGURE 1.1

6% BANDWIDTH SPECTRUM OF MODEL ROTOR NOISE
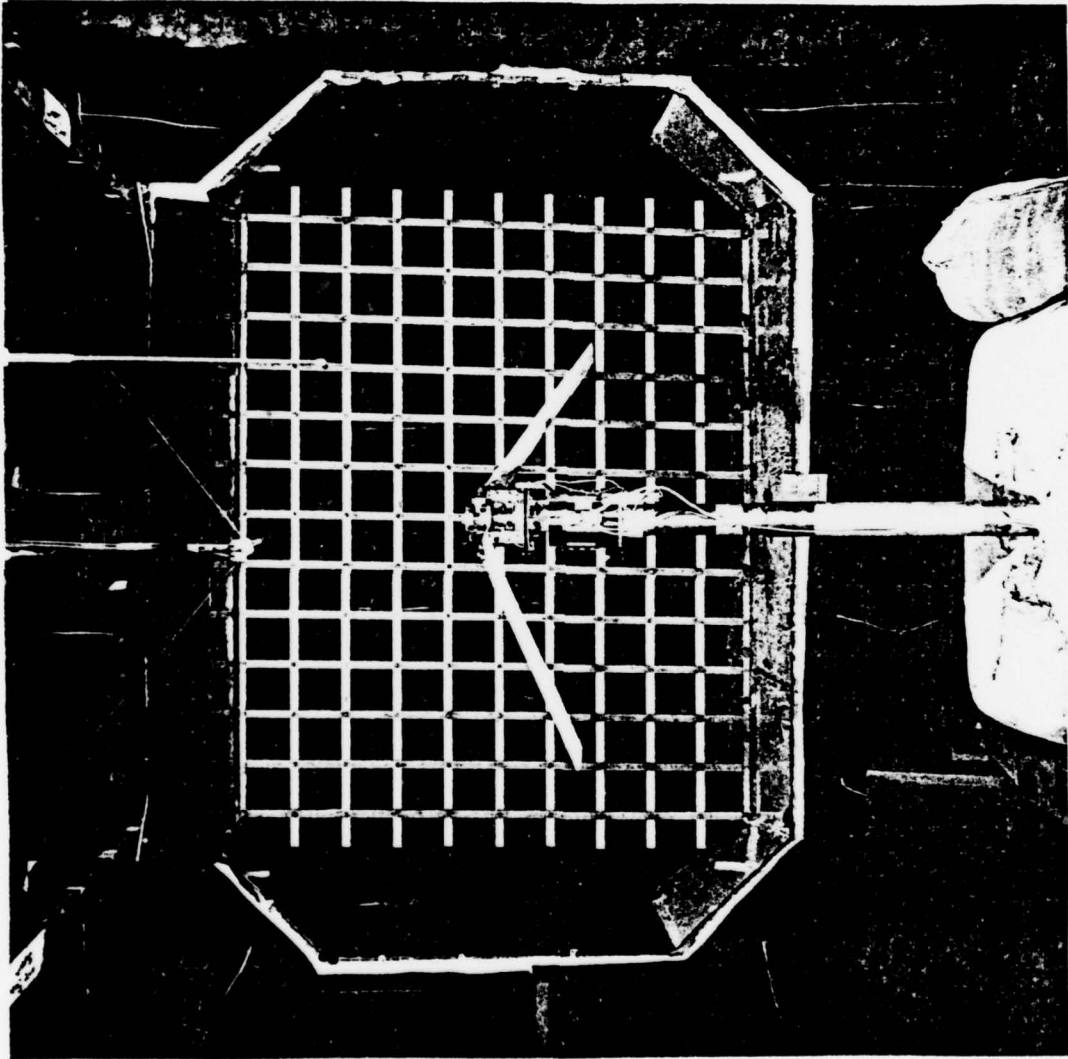
FIGURE 2.1

PHOTOGRAPH OF THE ROTOR ASSEMBLY WITH UPSTREAM TURBULENCE GENERATOR

B & K
MICROPHONES

HOT WIRE PROBE

PITOT TUBE
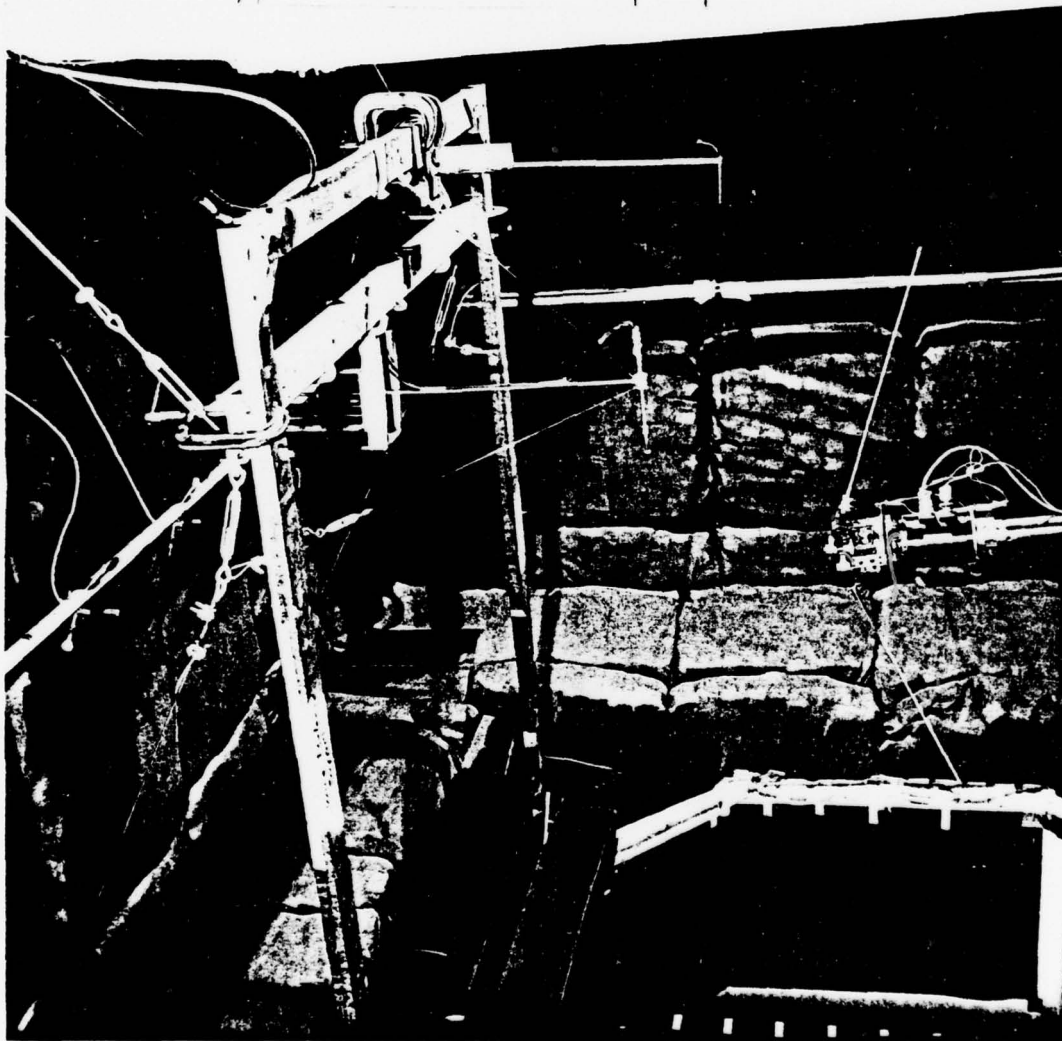
FIGURE 2.2

PHOTOGRAPH OF THE SETUP FOR MEASURING ACOUSTIC AND TURBULENCE DATA
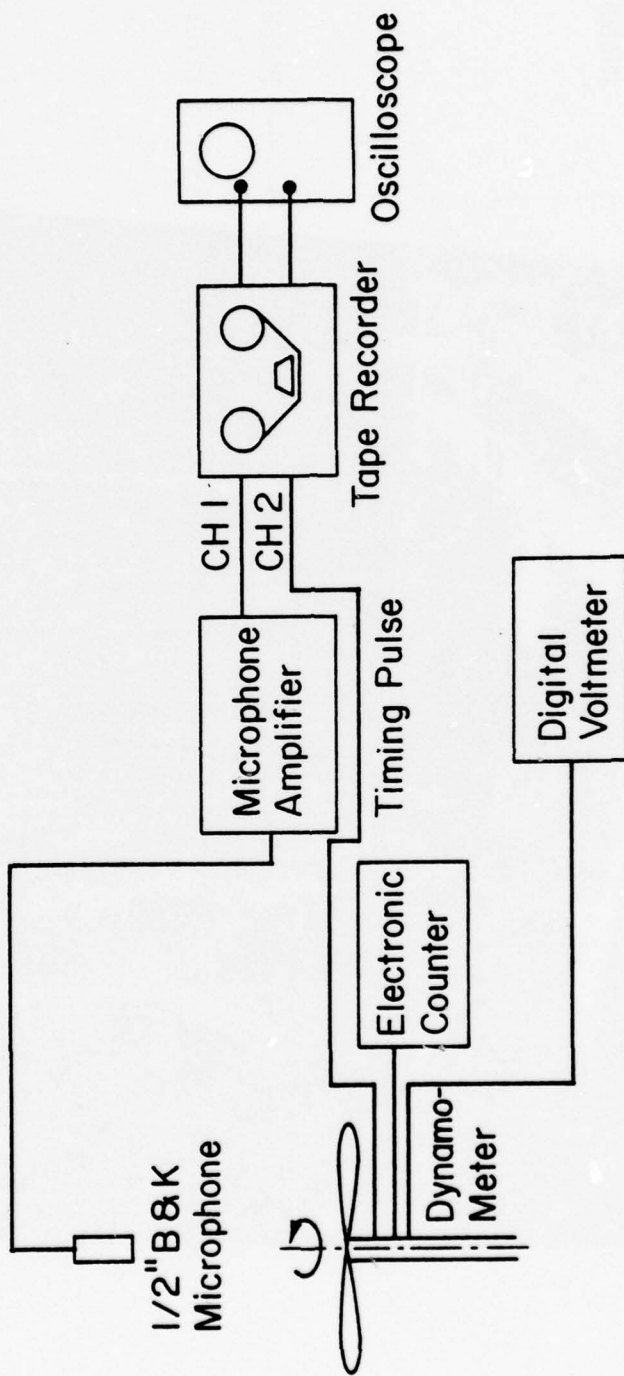
FIGURE 2.3

SCHEMATIC OF INSTRUMENTATION FOR ACQUISITION OF ACOUSTIC DATA
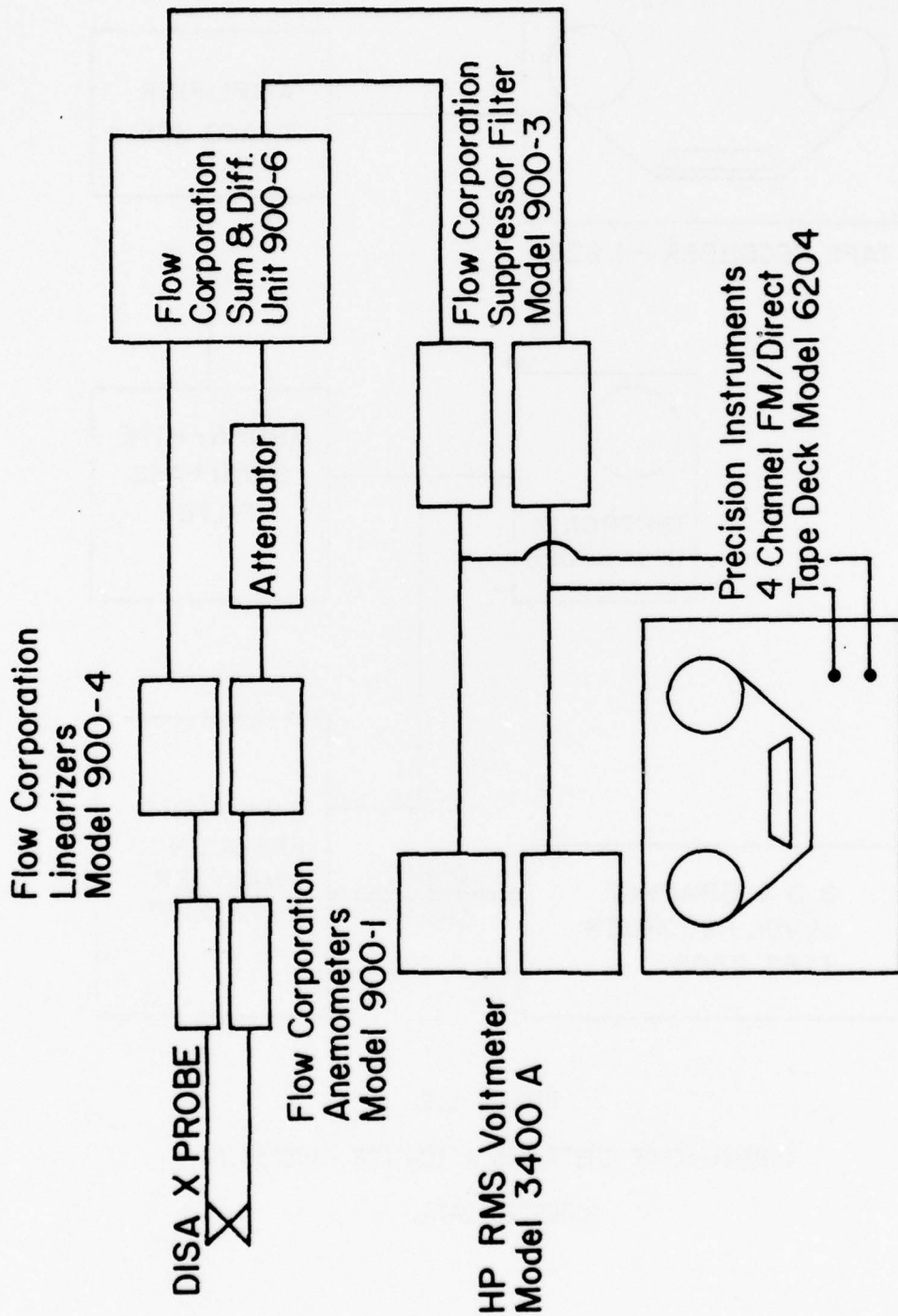
FIGURE 2.4

SCHEMATIC OF INSTRUMENTATION FOR ACQUIRING TURBULENCE DATA
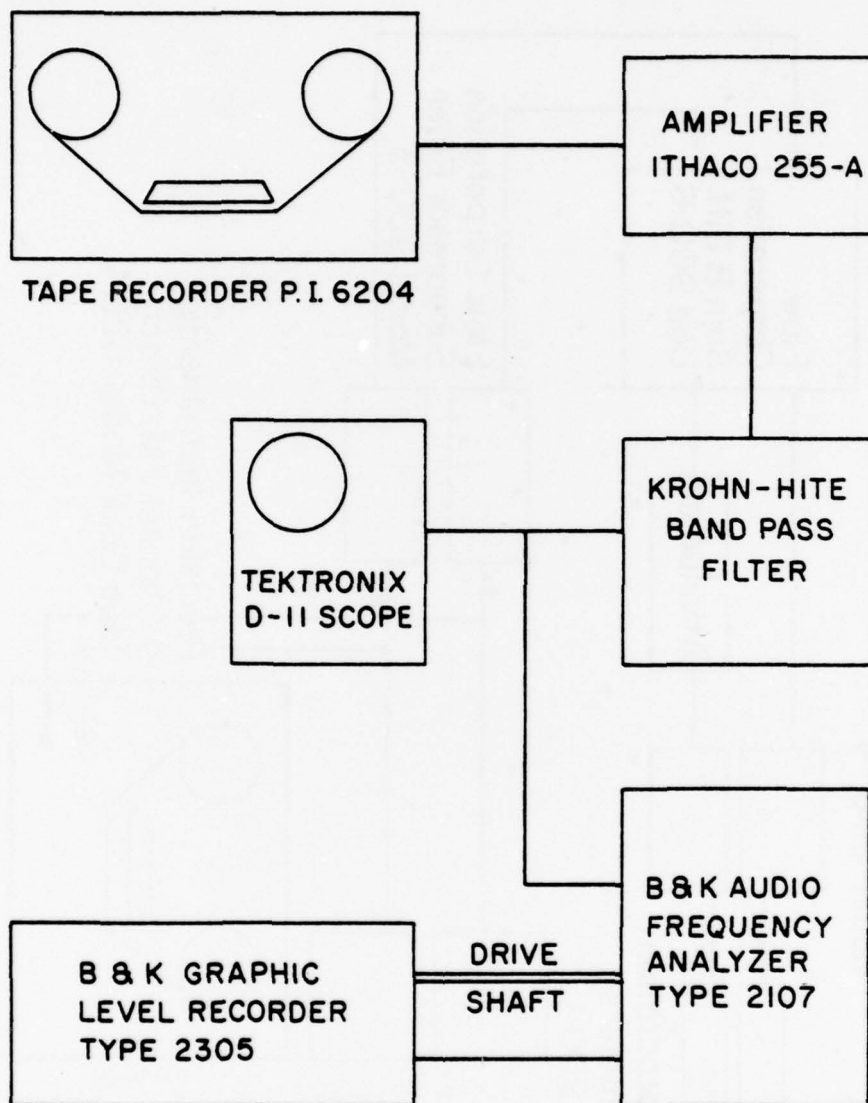
FIGURE 2.5

SCHEMATIC OF INSTRUMENTATION FOR PROCESSING

ACOUSTIC DATA.
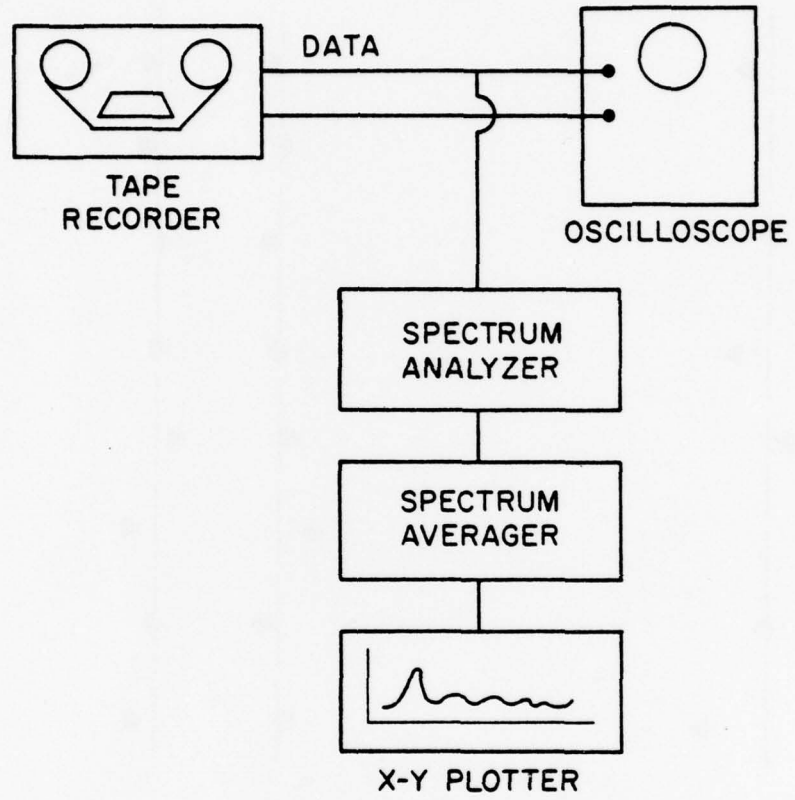
FIGURE 2.6

SCHEMATIC OF INSTRUMENTATION FOR PROCESSING

TURBULENCE DATA

FREE STREAM VELOCITY, FT./SEC.

FIGURE 2.7

INTEGRAL SCALE OF THE AXIAL COMPONENT, INCHES
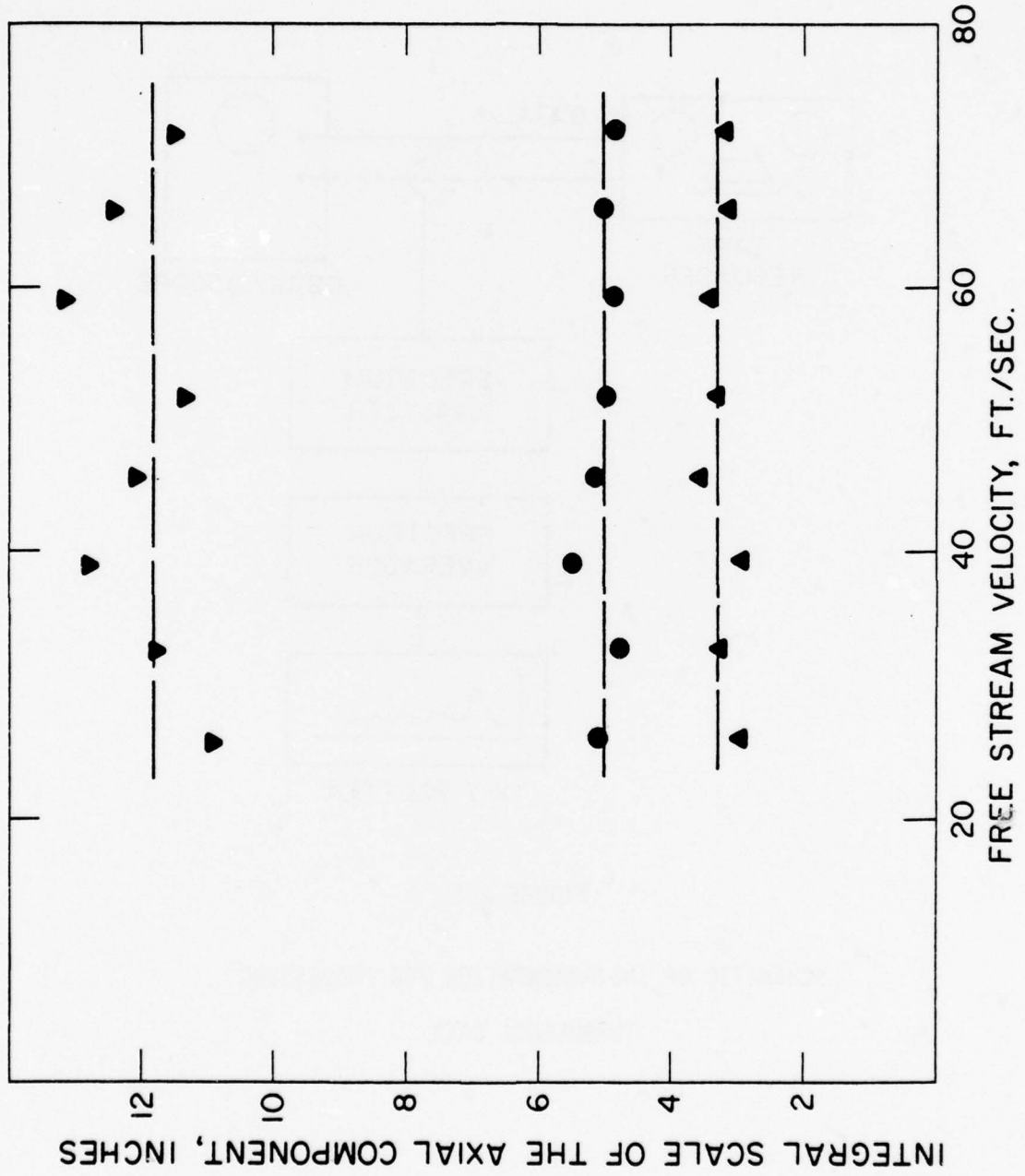
EFFECT OF FREE STREAM VELOCITY ON THE INTEGRAL SCALE OF THE AXIAL COMPONENT OF TURBULENCE,

▼ NO GRID, ● 3.5" X 20" GRID, ▲ 0.75" X 6" GRID.
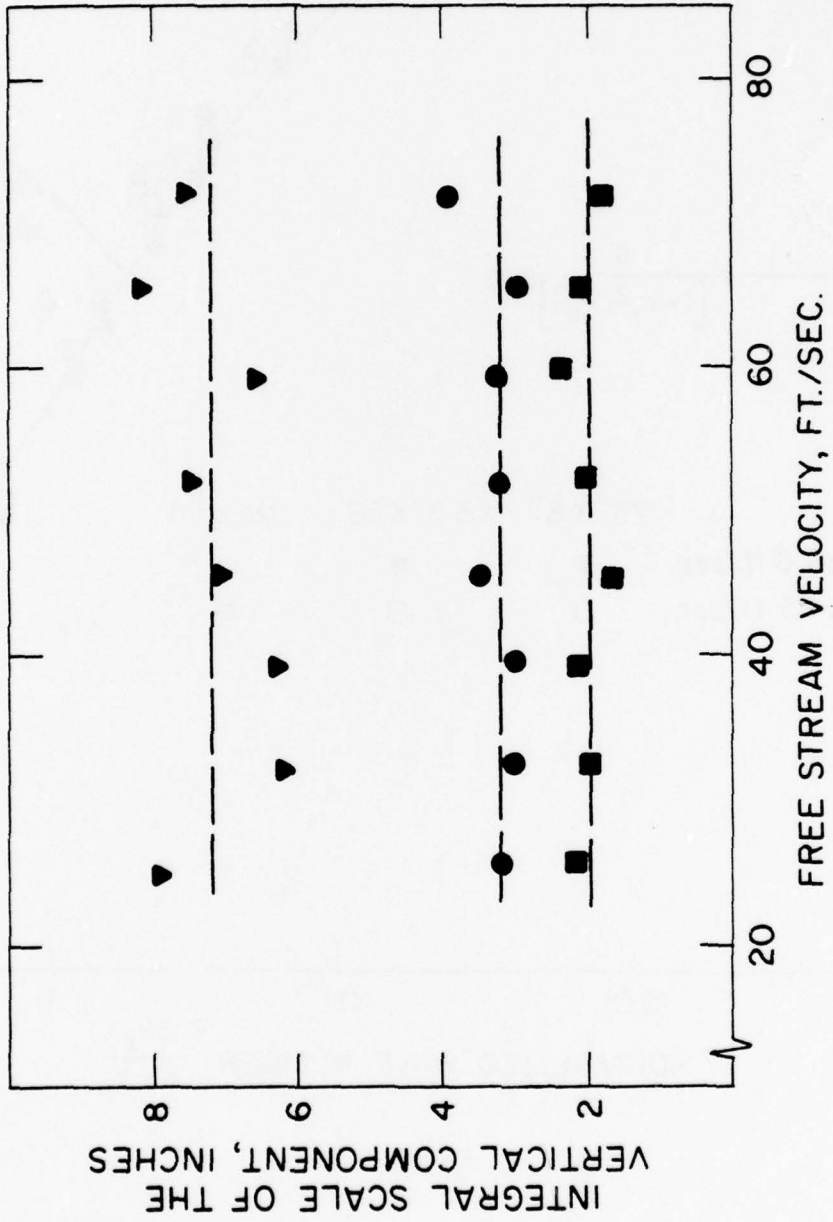
FIGURE 2.8

EFFECT OF FREE STREAM VELOCITY ON THE INTEGRAL SCALE OF THE VERTICAL COMPONENT OF
TURBULENCE, ▼ NO GRID, ● 3.5" X 20" GRID, ■ 0.75" X 6" GRID.
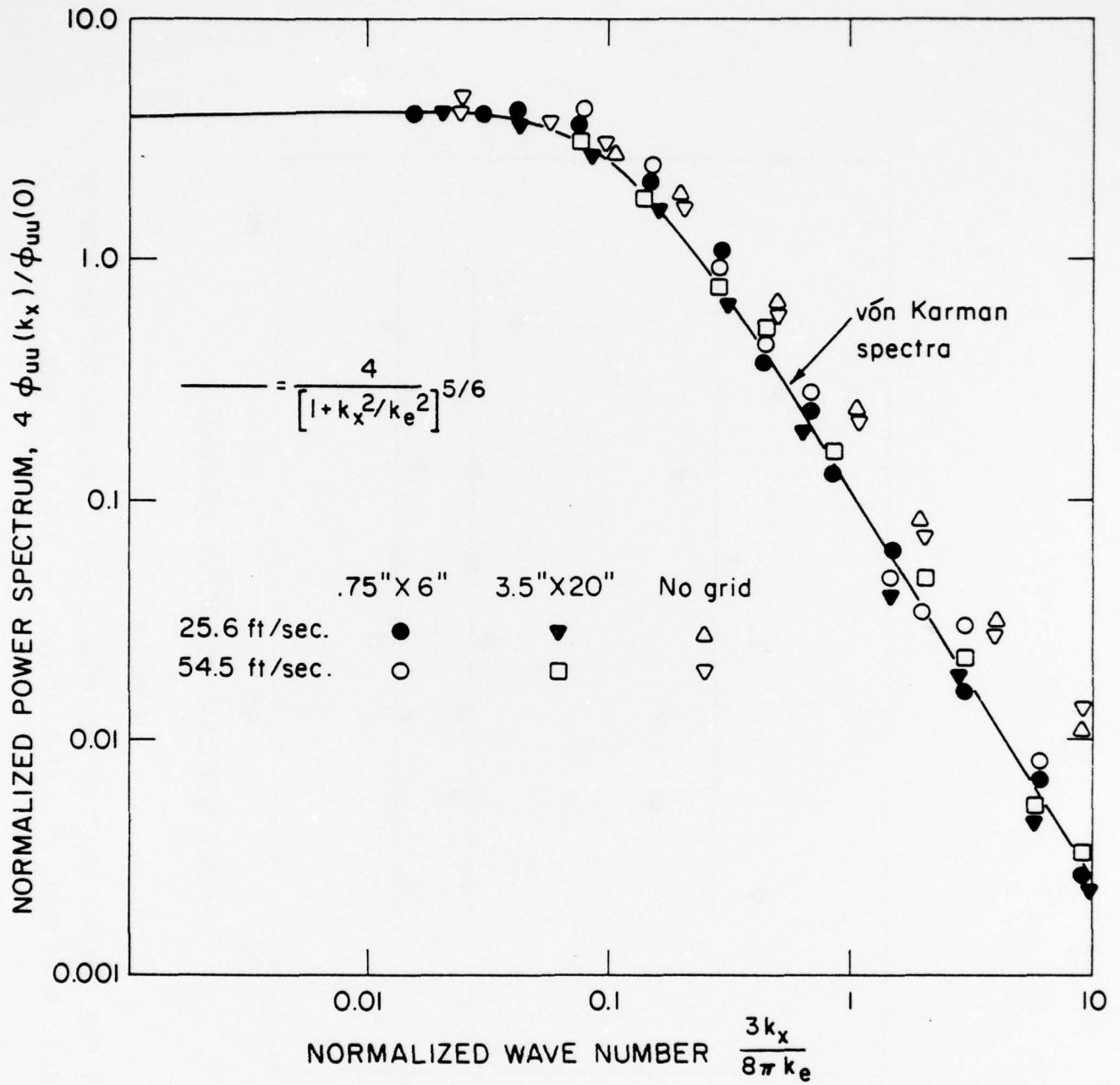
FIGURE 2.9

ONE DIMENSIONAL SPECTRUM OF THE AXIAL COMPONENT OF GRID TURBULENCE
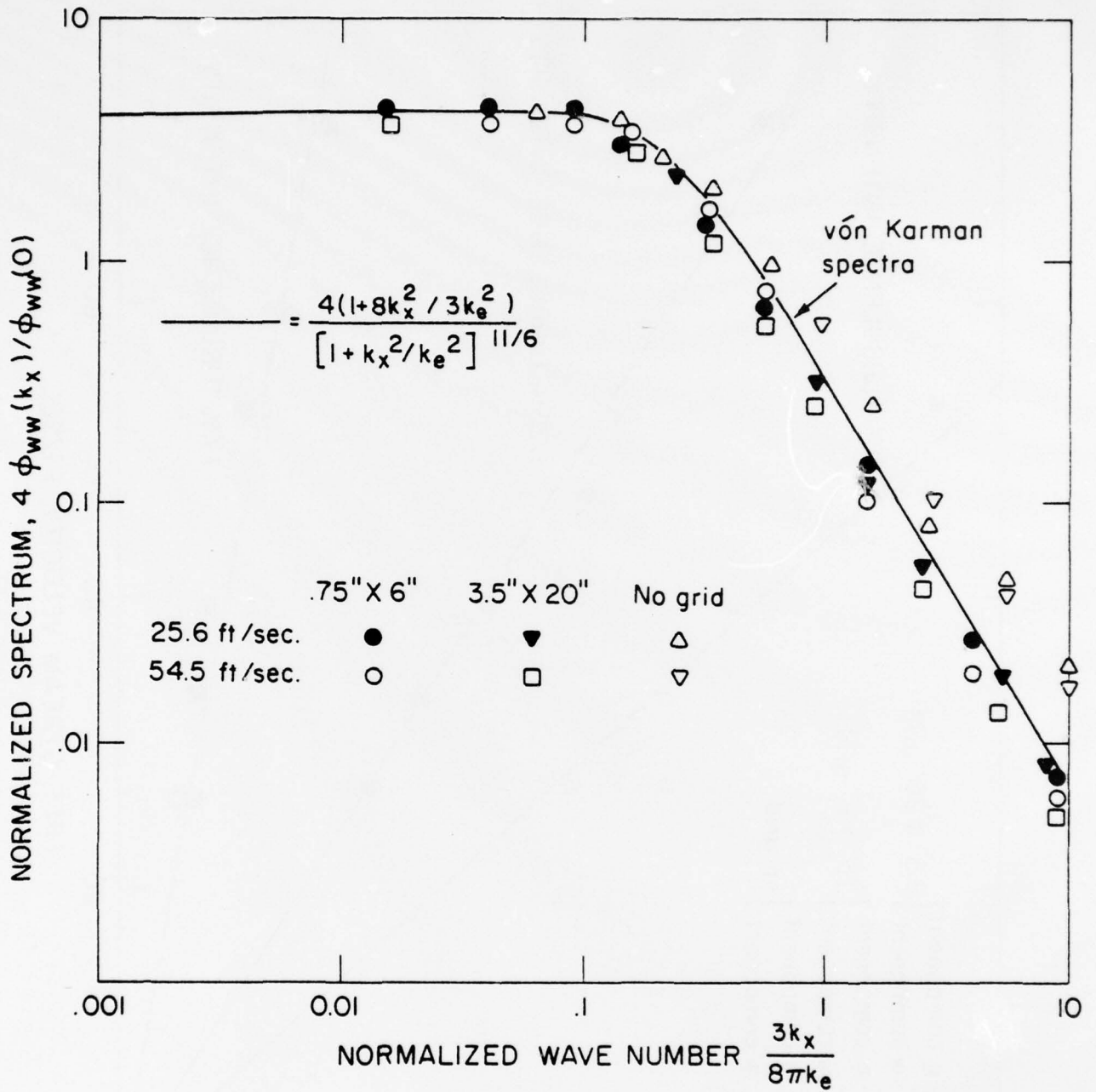
FIGURE 2.10

ONE DIMENSIONAL SPECTRUM OF THE VERTICAL COMPONENT OF GRID TURBULENCE
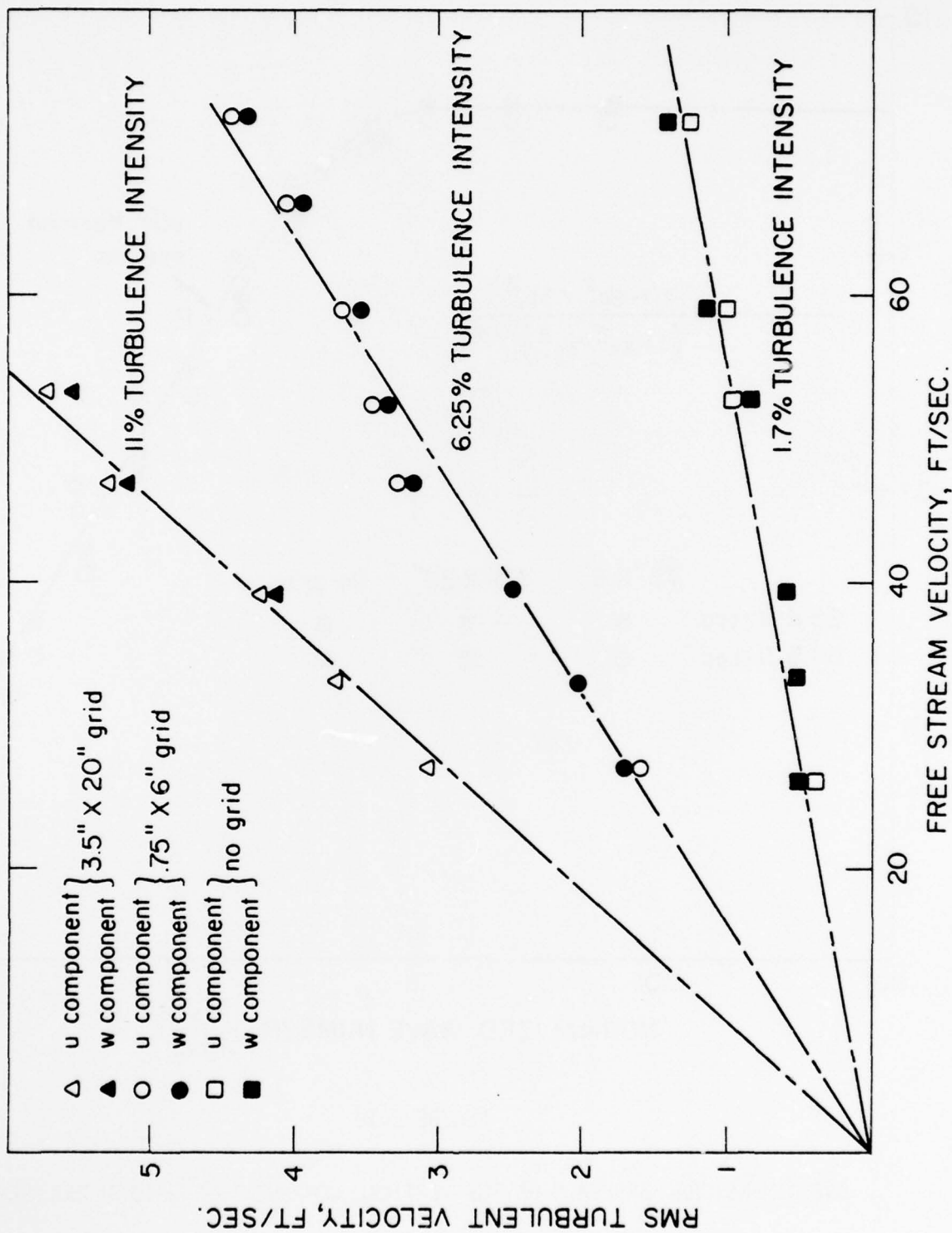
FIGURE 2.11

EFFECT OF FREE STREAM VELOCITY ON RMS TURBULENT VELOCITY
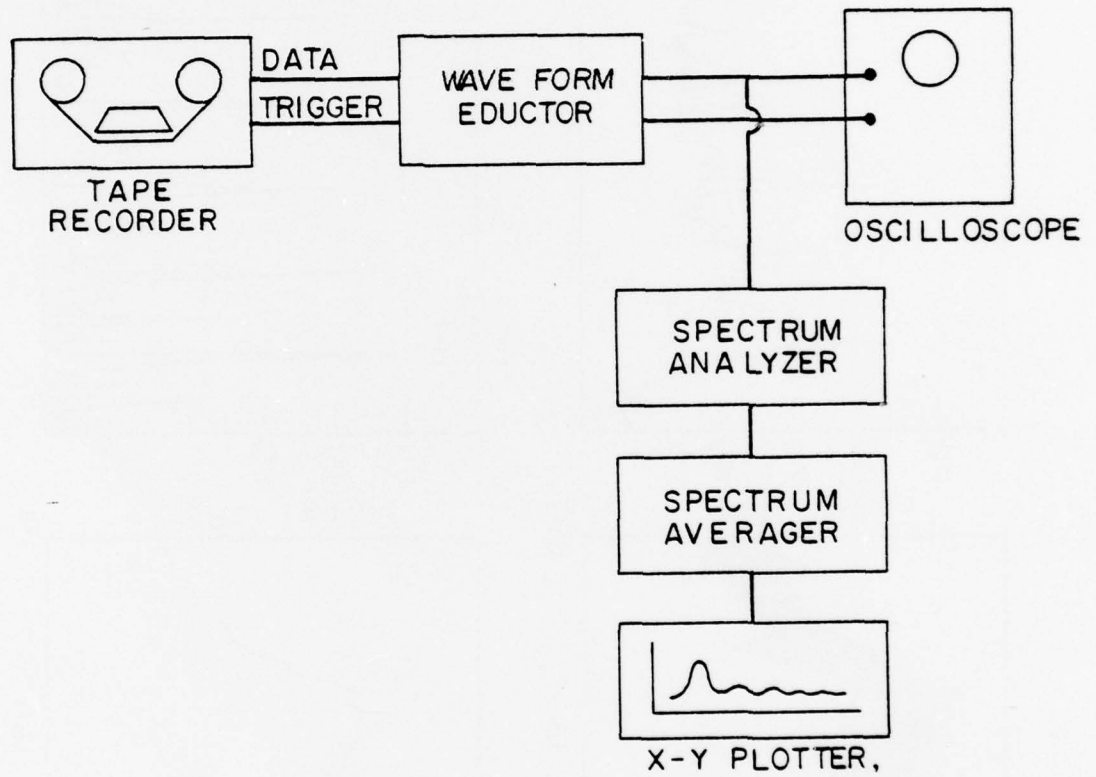
FIGURE 2.12

SCHEMATIC OF INSTRUMENTATION FOR PROCESSING ROTATIONAL NOISE.
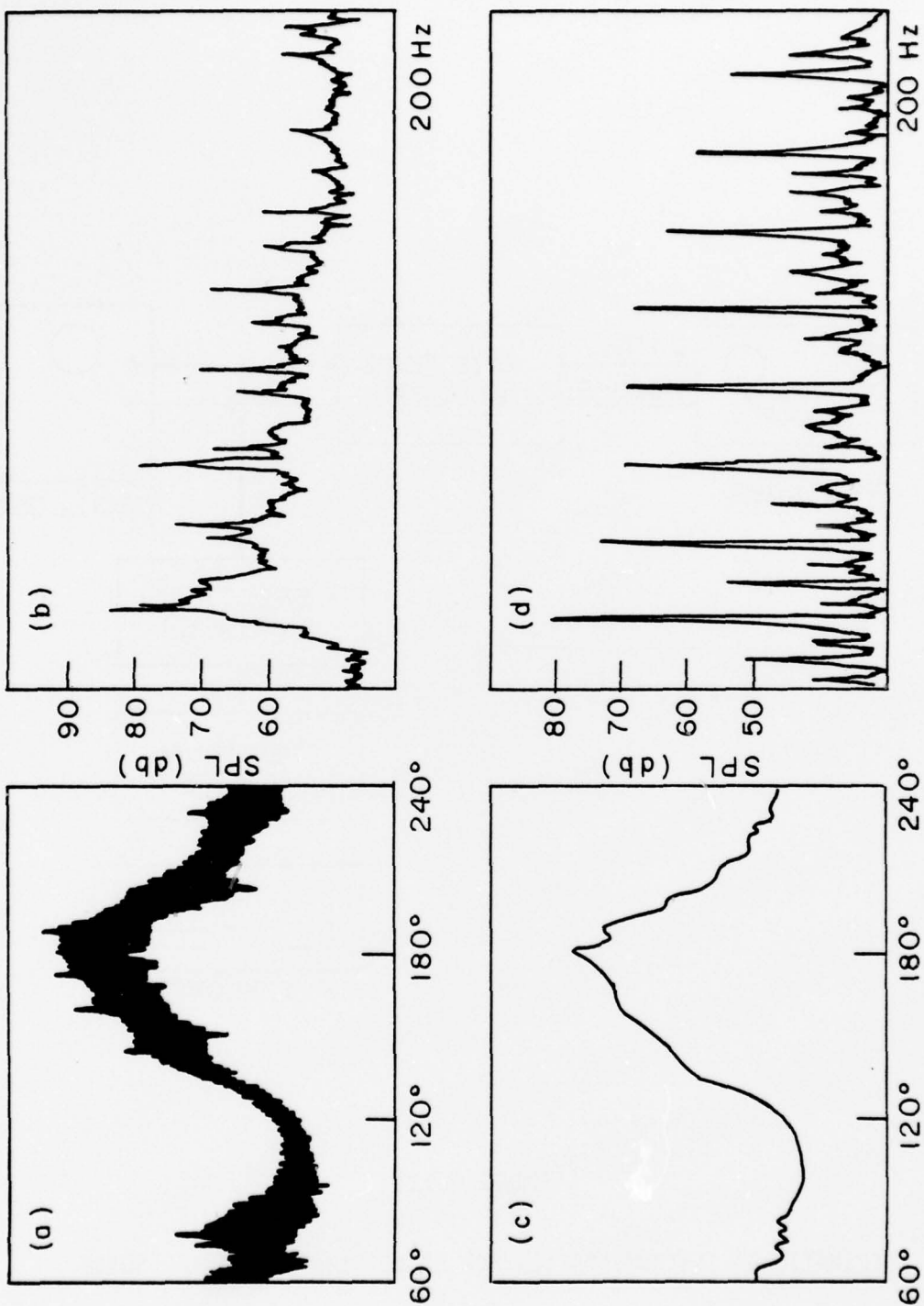
FIGURE 2.13 - ILLUSTRATION OF EFFECT OF PERIODIC SAMPLING TECHNIQUE - (a) WAVEFORM OF RAW DATA
(b) CORRESPONDING NARROWBAND SPECTRA FROM 0 - 200 Hz (c) PROCESSED WAVEFORM and
(d) SUBESQUENT NARROWBAND SPECTRA
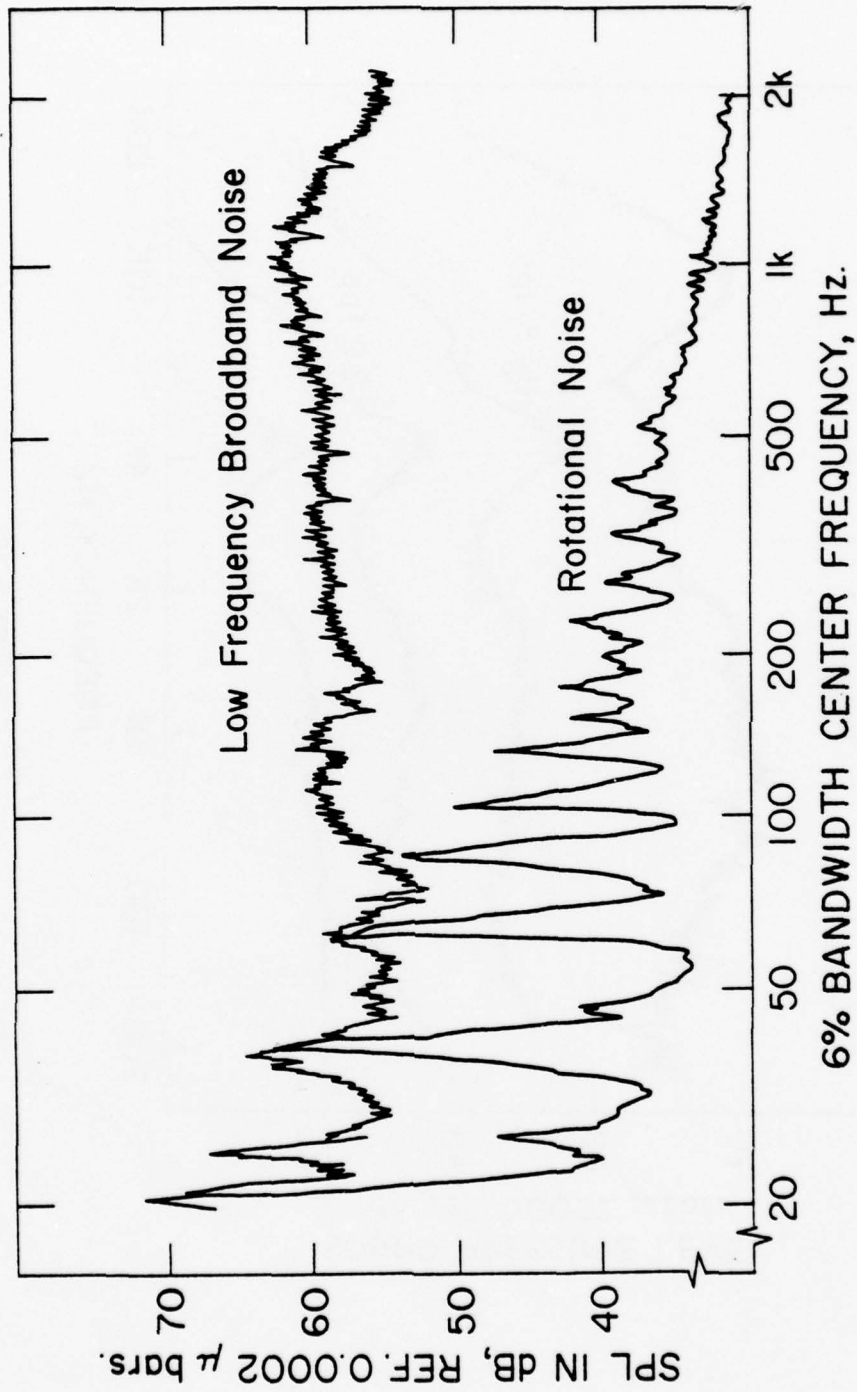
FIGURE 2.14

COMPARISON OF ROTATIONAL NOISE AND LOW FREQUENCY BROADBAND NOISE AT HIGH
FREQUENCIES FOR .75" X 6" TURBULENCE GRID, B = 2, Ω = 672 RPM, U_0 = 44 FPS.

FREQUENCY, HZ
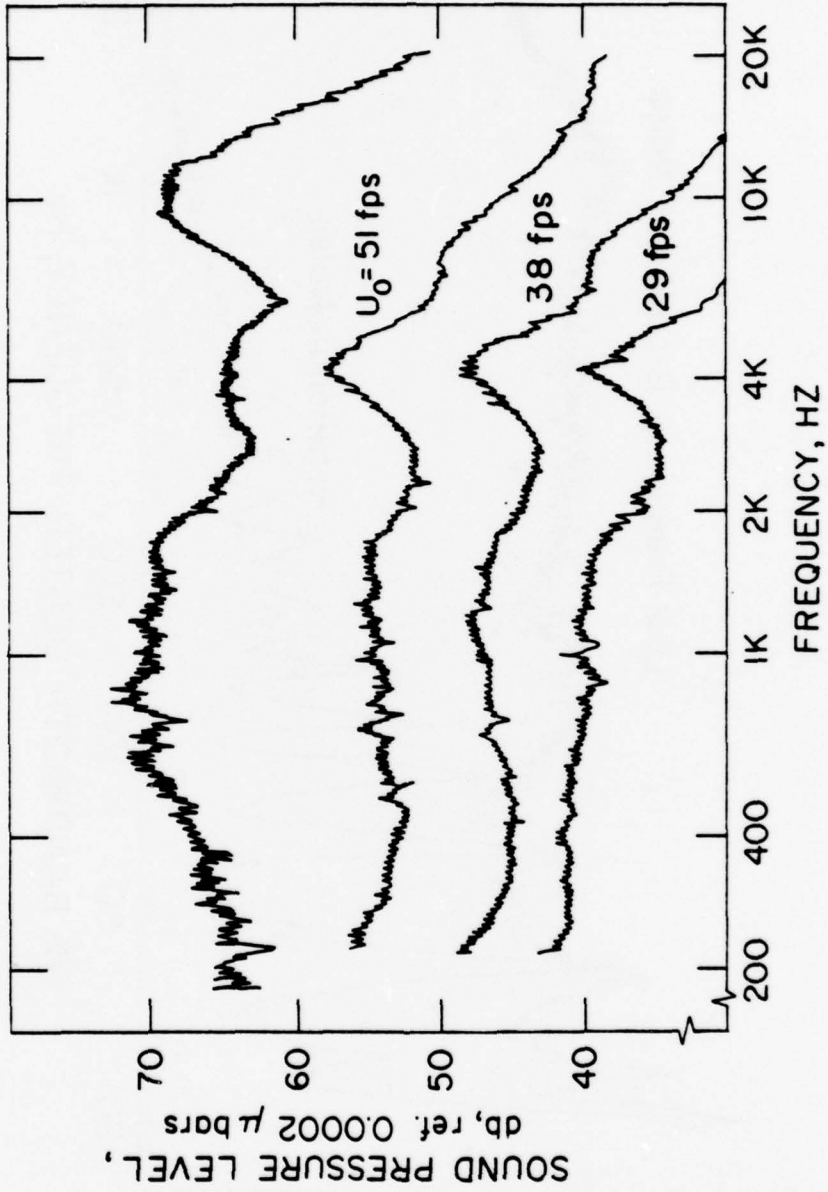
FIGURE 2.15

6% BANDWIDTH BACKGROUND SPECTRA AT VARIOUS TUNNEL SPEEDS FOR 0.75" X 6"
TURBULENCE GRID, TOP CURVE; ROTOR GENERATED NOISE FOR B = 3, Ω = 1000 RPM
and U_0 = 51 FPS.

FREQUENCY, HZ
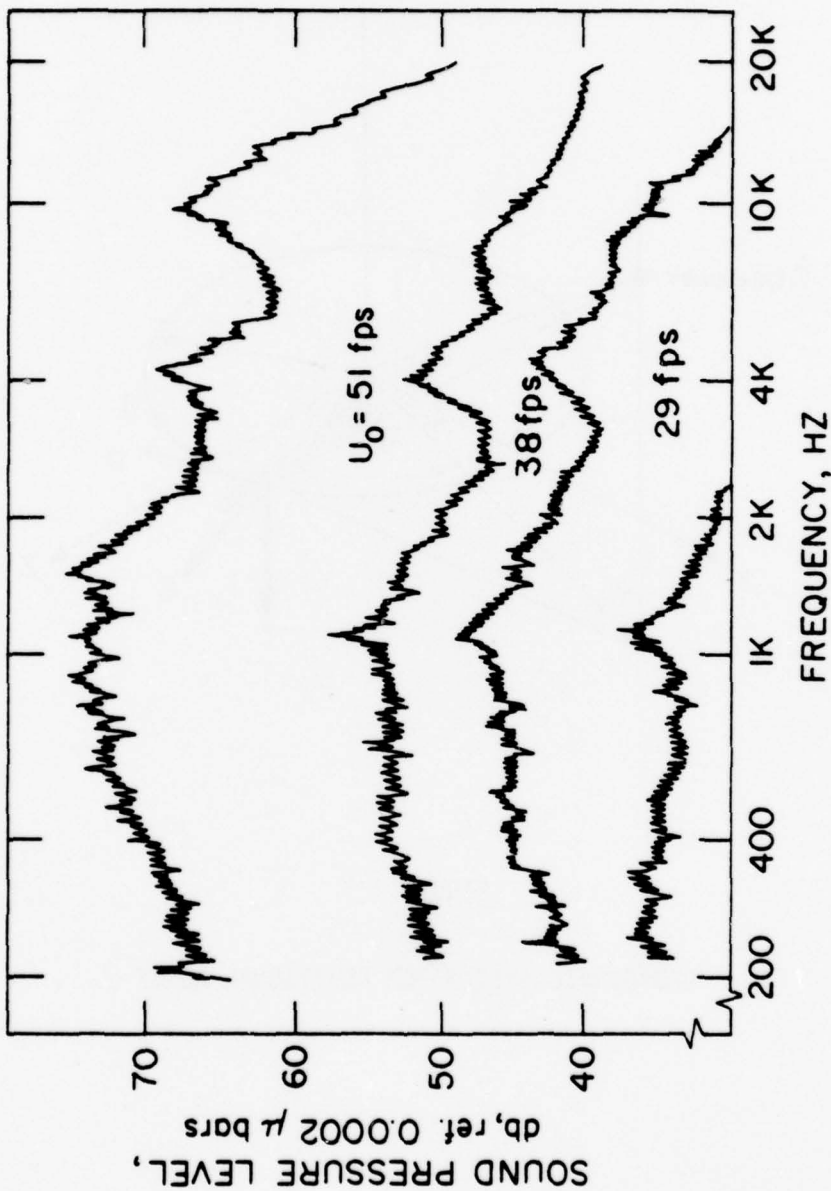
FIGURE 2.16

6% BANDWIDTH BACKGROUND SPECTRA AT VARIOUS TUNNEL SPEEDS FOR 3.5" X 20"
TURBULENCE GRID, TOP CURVE; ROTOR GENERATED NOISE FOR B = 3, Ω = 1000 RPM
and U_0 = 51 FPS.
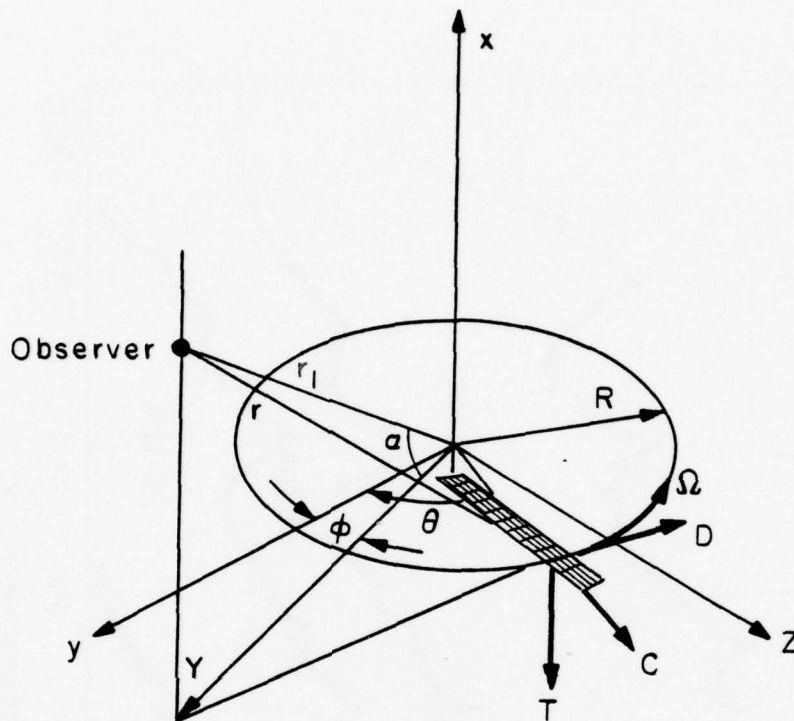
FIGURE 3.1

COORDINATE SYSTEM FOR ROTATIONAL NOISE
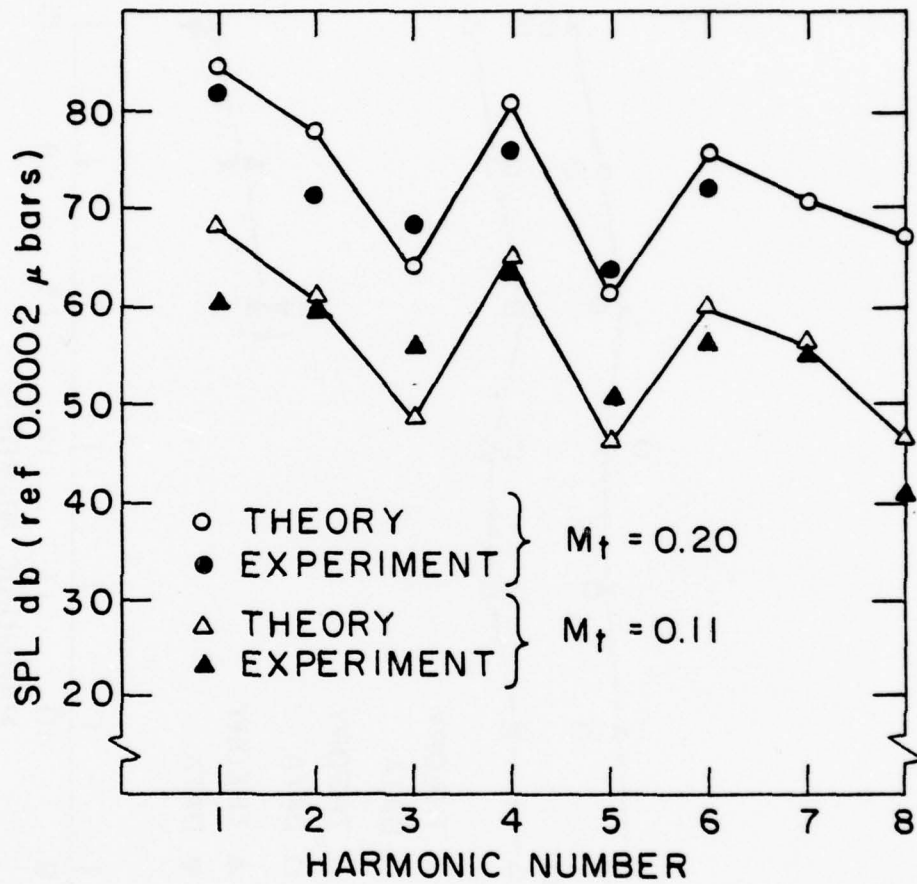
FIGURE 3.2

MACH NUMBER SCALING FOR LOWER HARMONICS OF A TWO-BLADED ROTOR ON AXIS
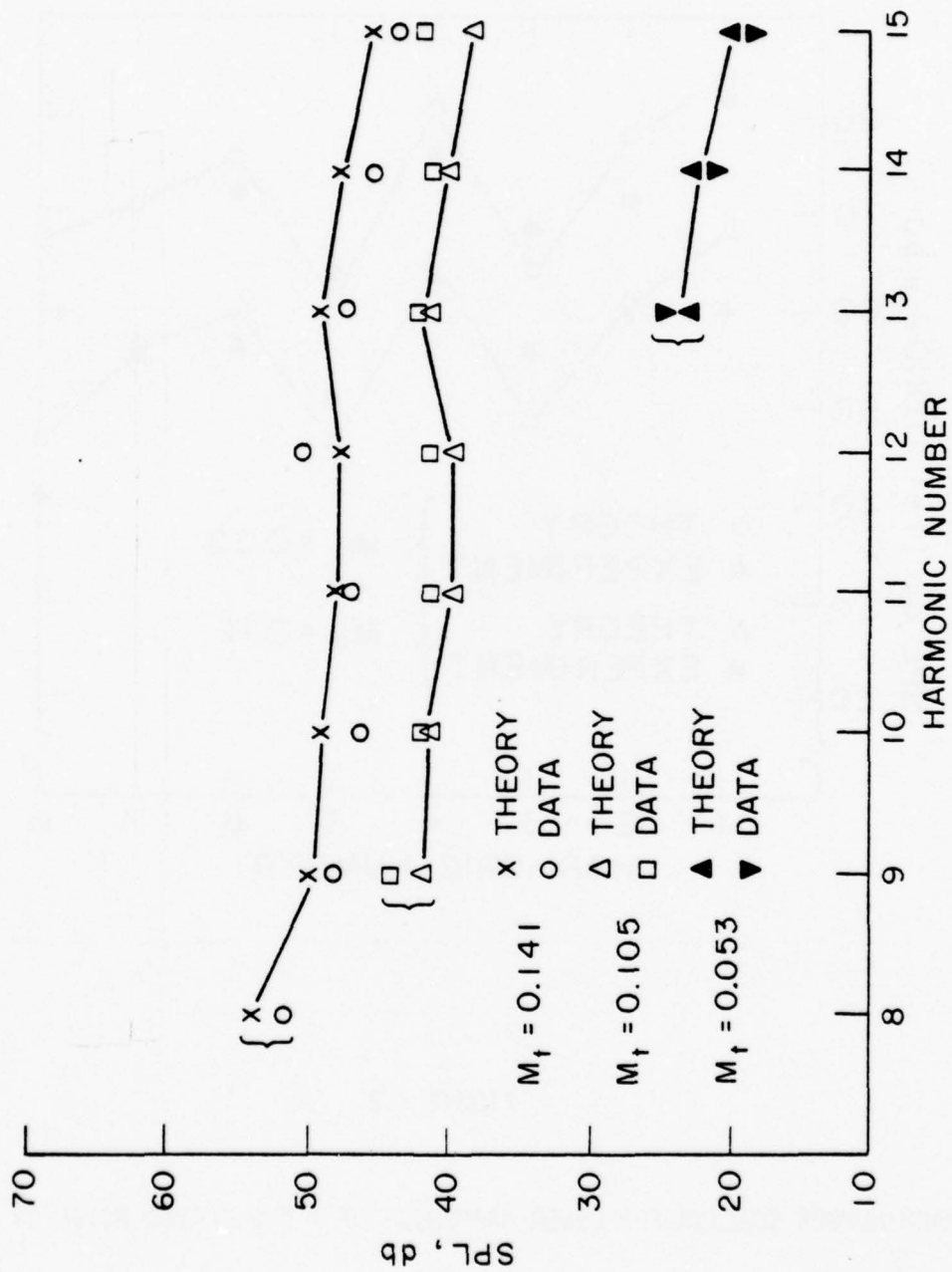
FIGURE 3.3

MACH NUMBER SCALING FOR HIGHER HARMONICS OF A TWO-BLADED ROTOR ON AXIS
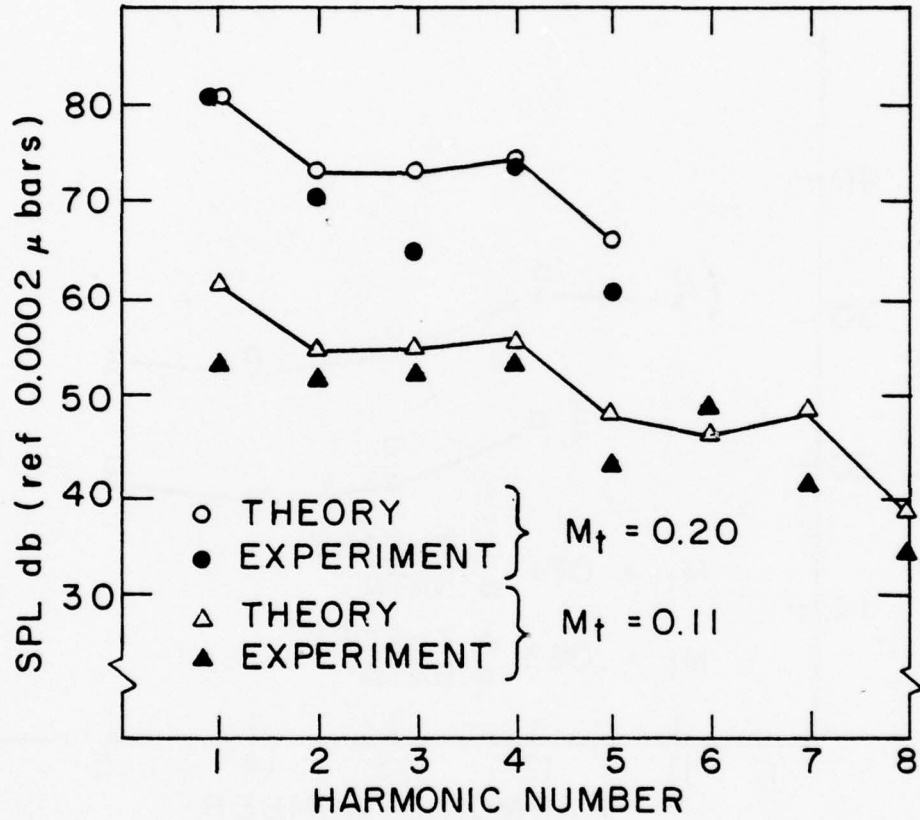
FIGURE 3.4

MACH NUMBER SCALING FOR LOWER HARMONICS

OF A TWO-BLADED ROTOR OFF AXIS
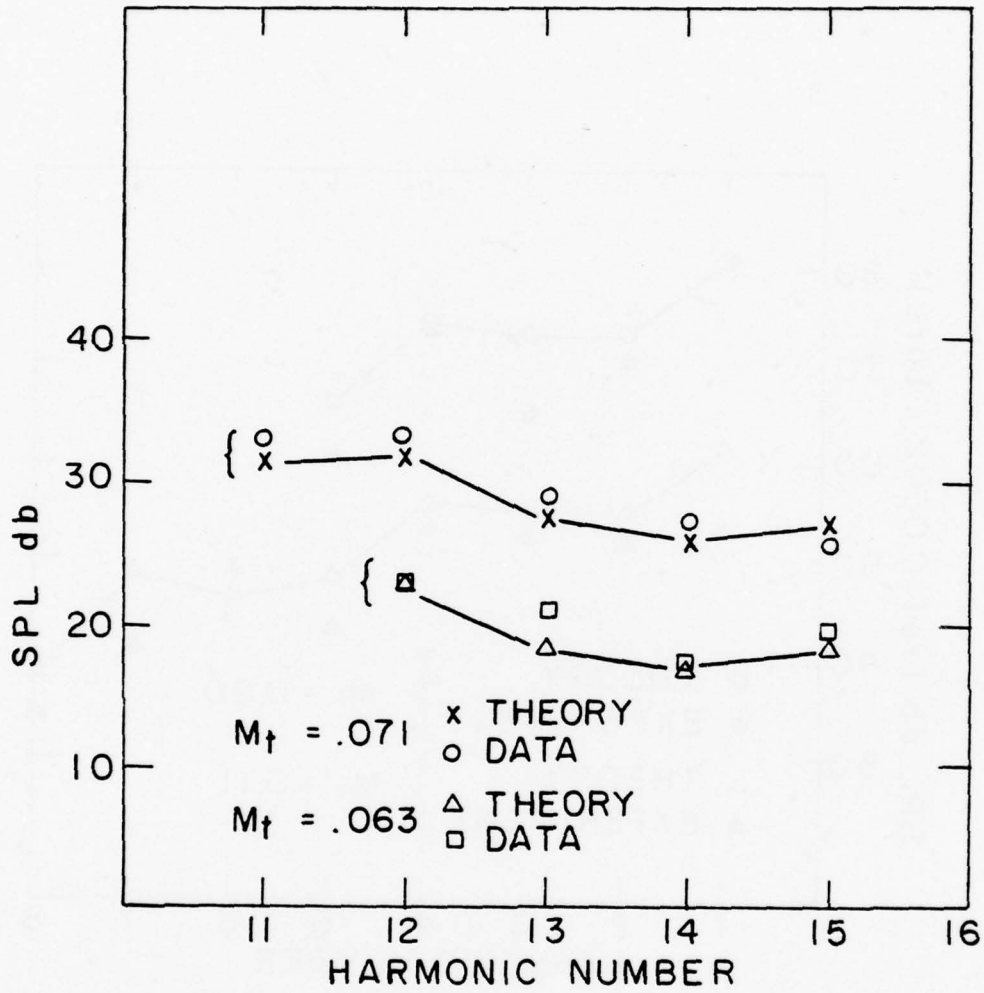
FIGURE 3.5

MACH NUMBER SCALING FOR HIGHER HARMONICS

OF A TWO-BLADED ROTOR OFF AXIS
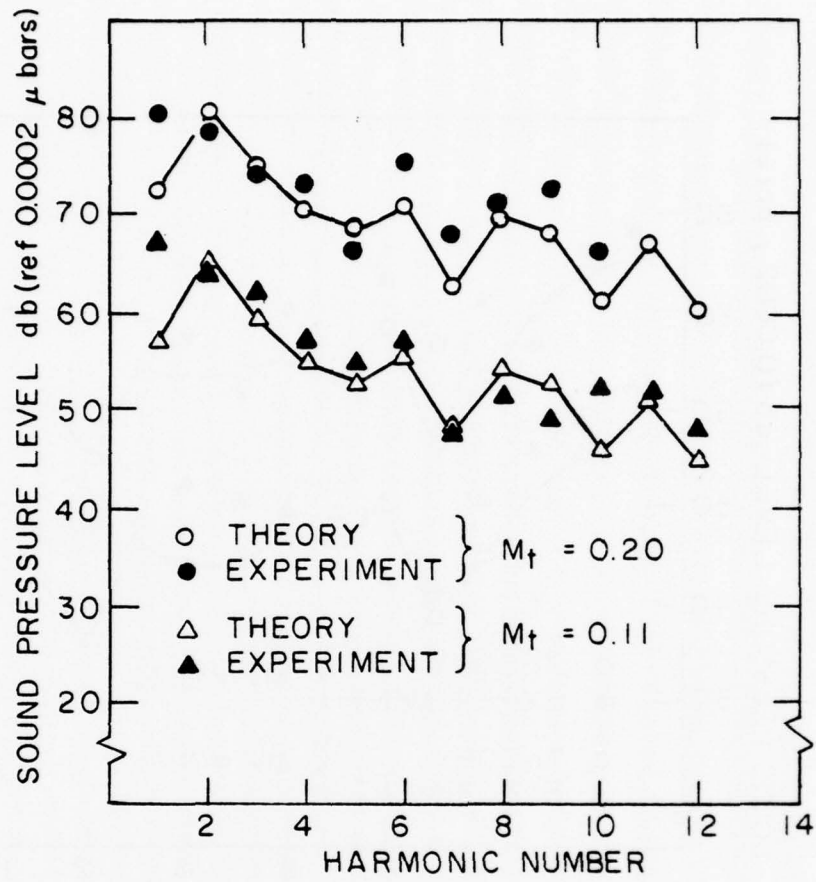
FIGURE 3.6

MACH NUMBER SCALING FOR ROTATIONAL HARMONICS

OF A THREE-BLADED ROTOR ON AXIS
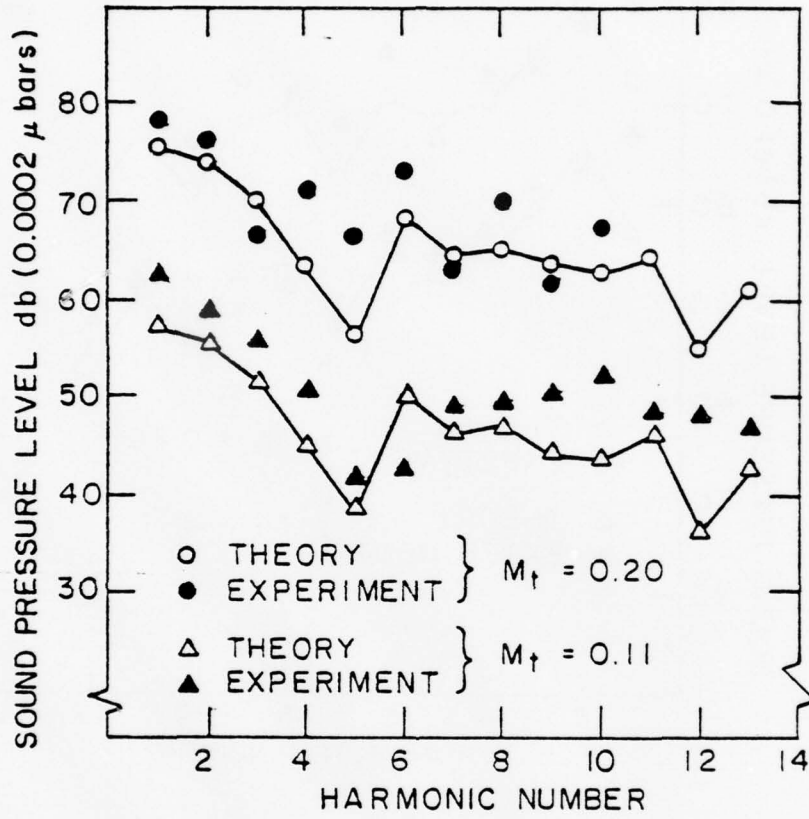
FIGURE 3.7

MACH NUMBER SCALING FOR LOWER HARMONICS

OF A THREE BLADED ROTOR OFF AXIS
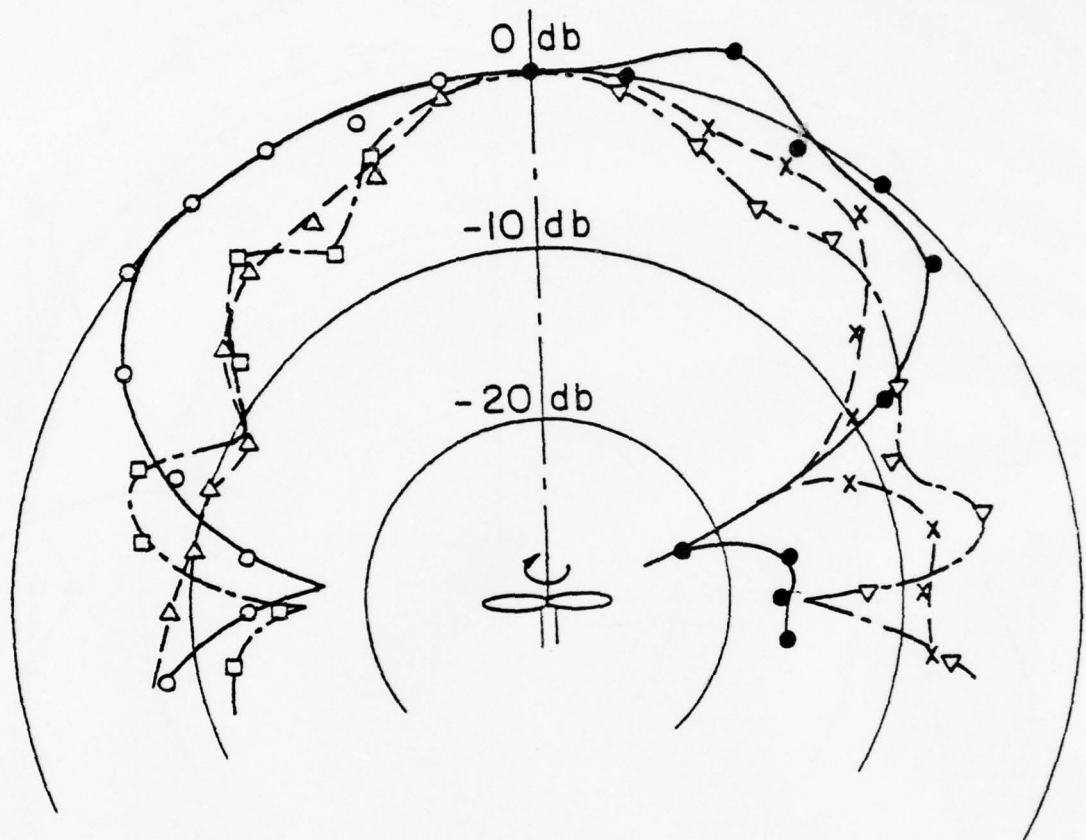
FIGURE 3.8

DIRECTIVITY OF LOWER HARMONICS OF A TWO-BLADED ROTOR
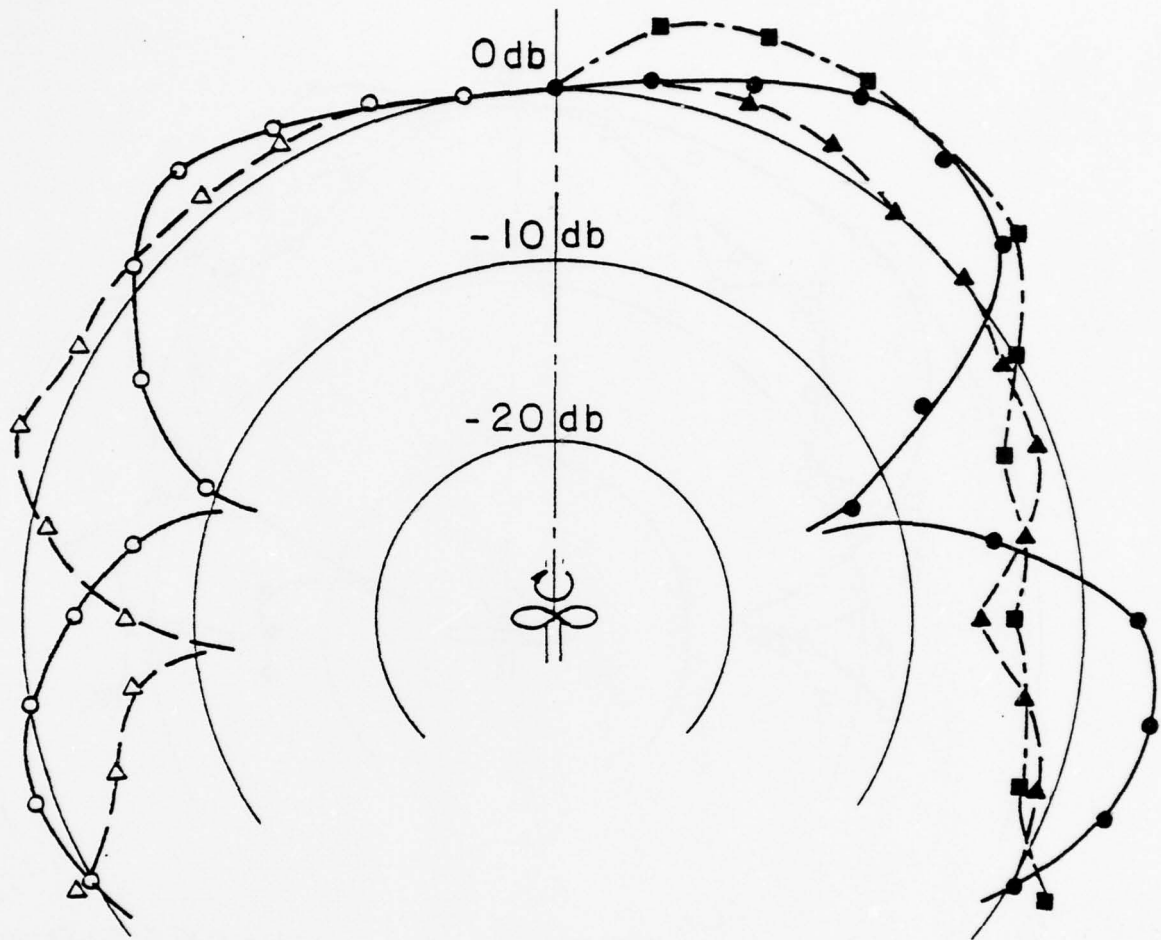
SEVENTH HARMONIC
EIGTH HARMONIC
NINETH HARMONIC
TENTH HARMONIC
ELEVENTH HARMONIC

U = 88 Ft/sec
Ω = 1100 RPM

FIGURE 3.9

DIRECTIVITY OF HIGHER HARMONICS OF A TWO-BLADED ROTOR
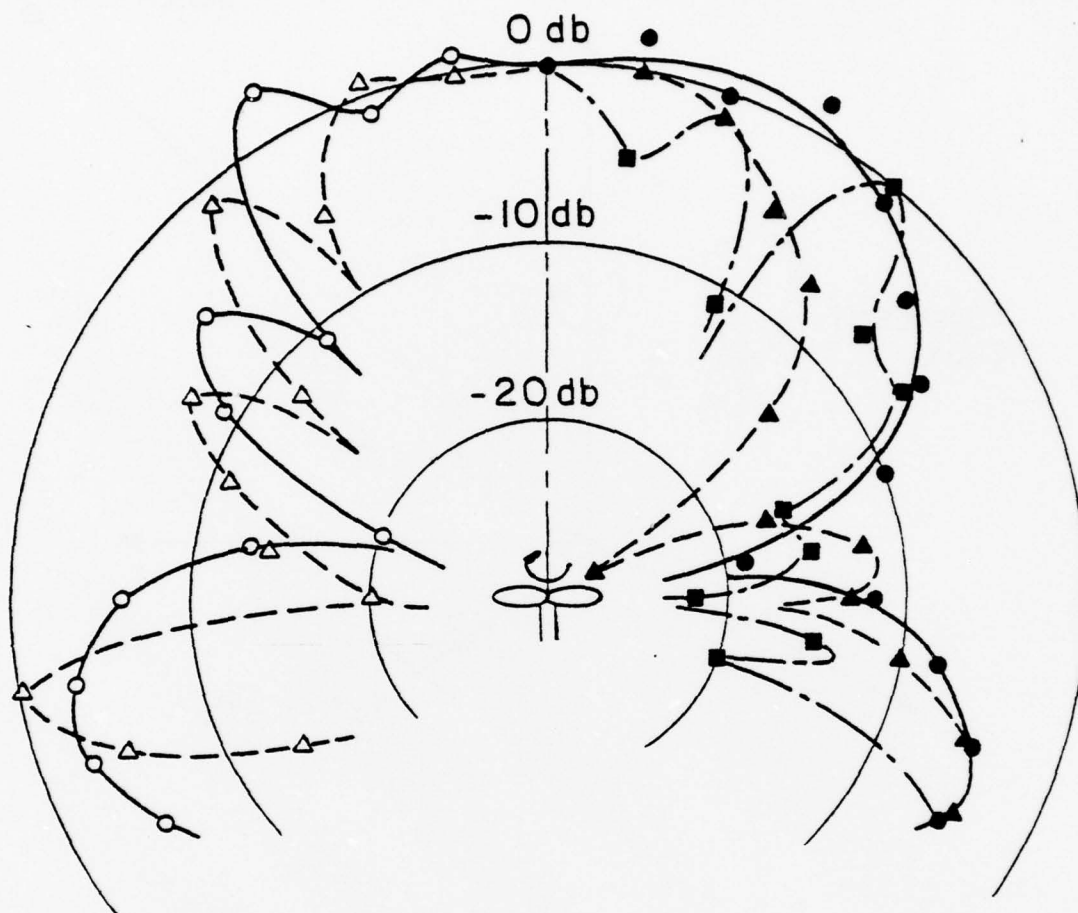
FIGURE 3.10

DIRECTIVITY OF HARMONICS OF A THREE-BLADED ROTOR
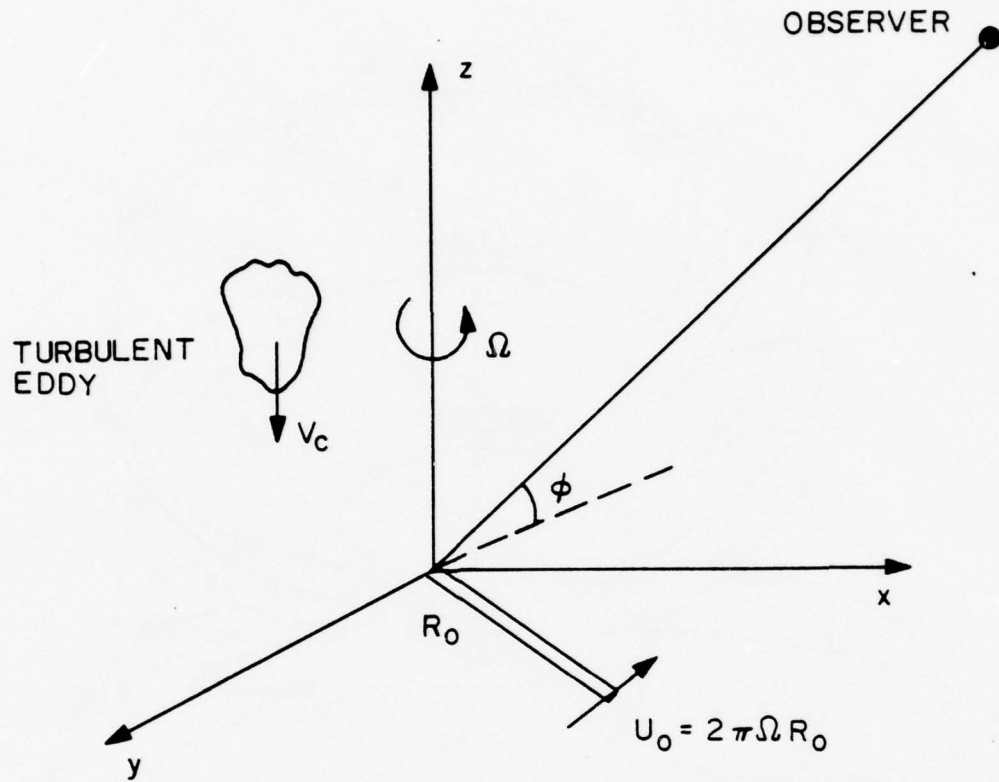
FIGURE 4.1

ROTOR GEOMETRY AND THE COORDINATE SYSTEM USED
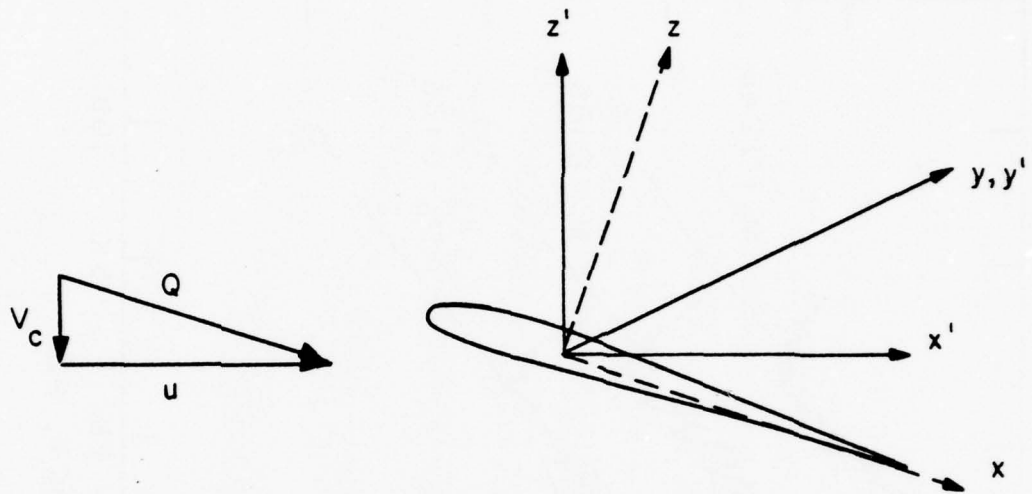
FIGURE 4.2

COORDINATE SYSTEM
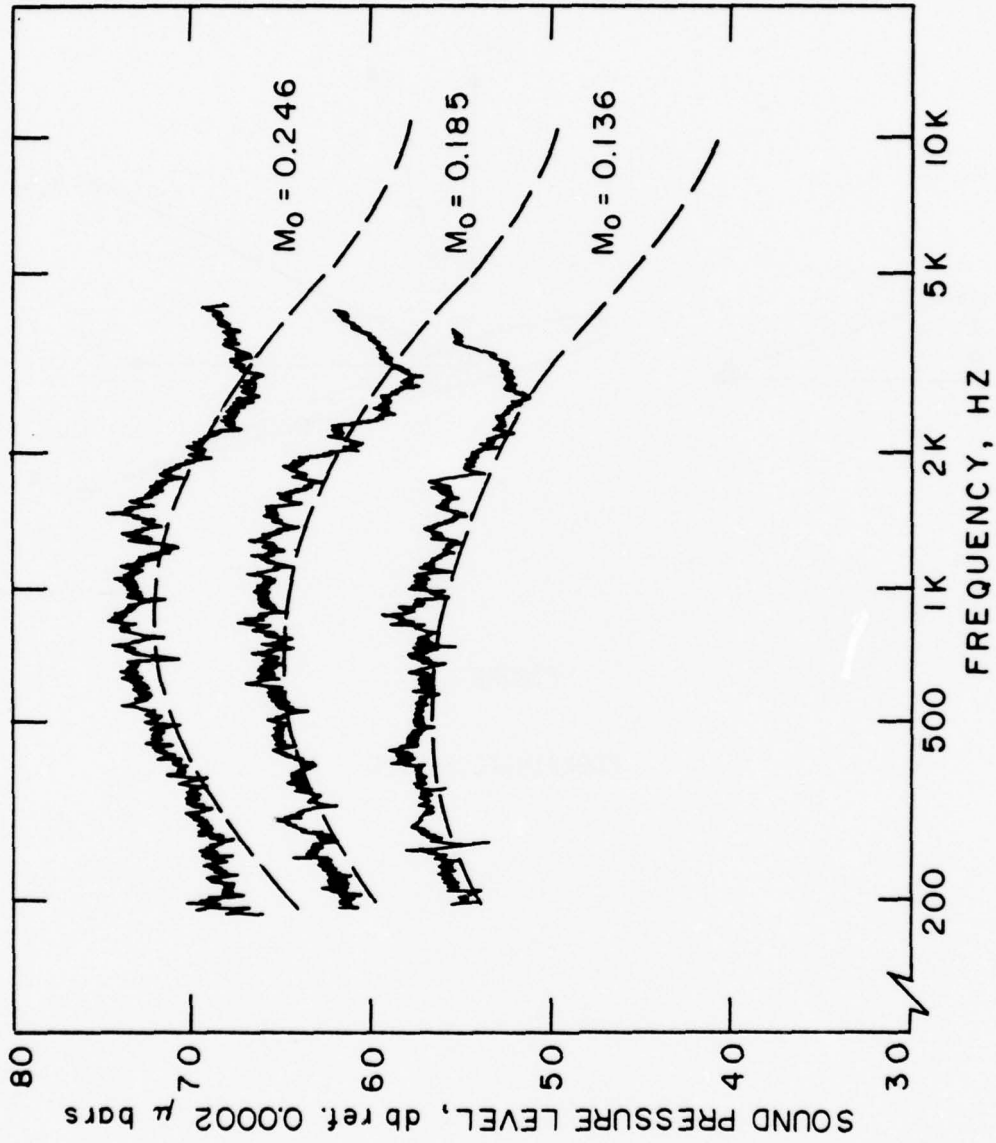
FIGURE 4.3

EFFECT OF MACH NUMBER ON PREDICTED AND MEASURED LOW FREQUENCY BROADBAND
NOISE FOR THE LARGER GRID WITH A Λ_f = 5.0 INCHES
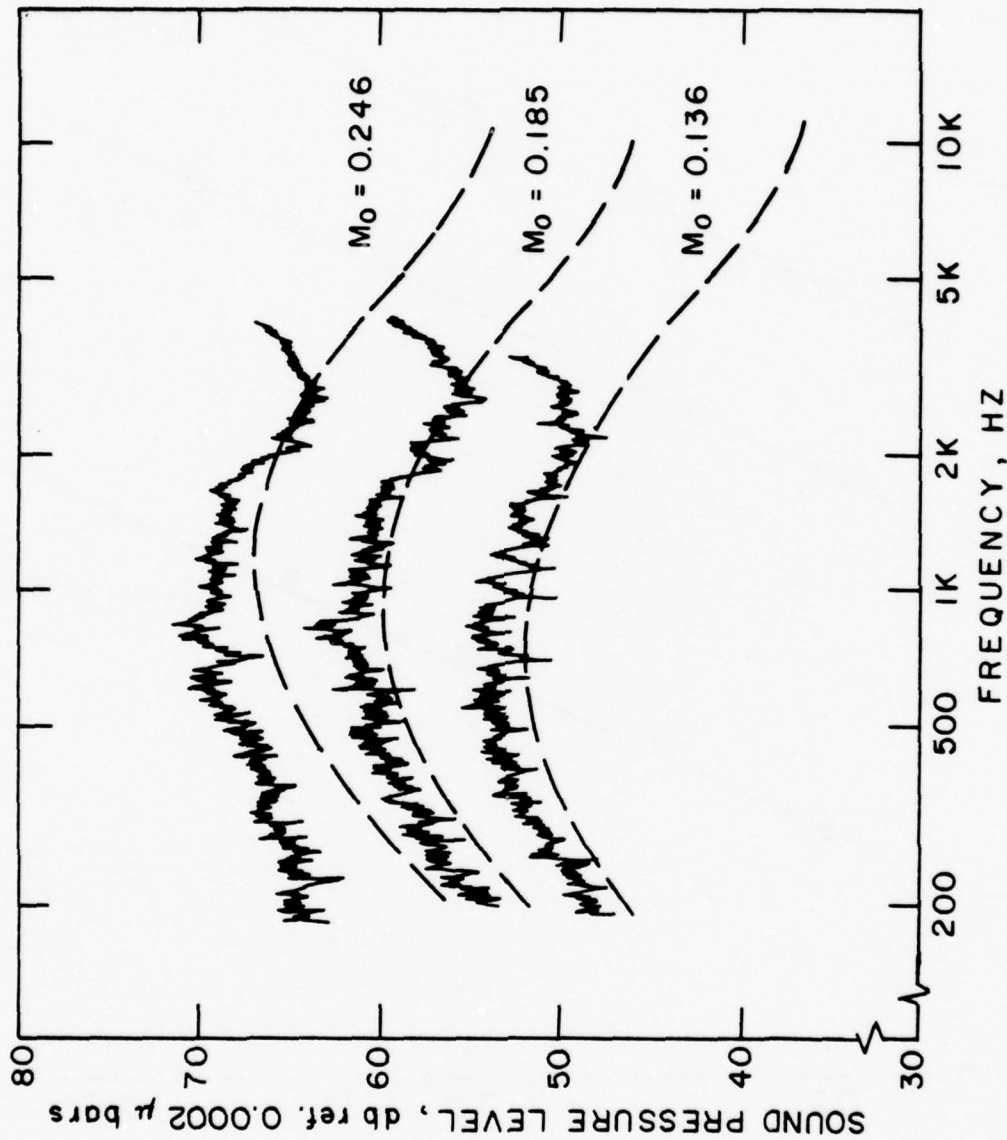
FIGURE 4.4

EFFECT OF MACH NUMBER ON PREDICTED AND MEASURED LOW FREQUENCY BROADBAND
NOISE FOR THE SMALLER GRID WITH A Λ_f = 3.3 INCHES
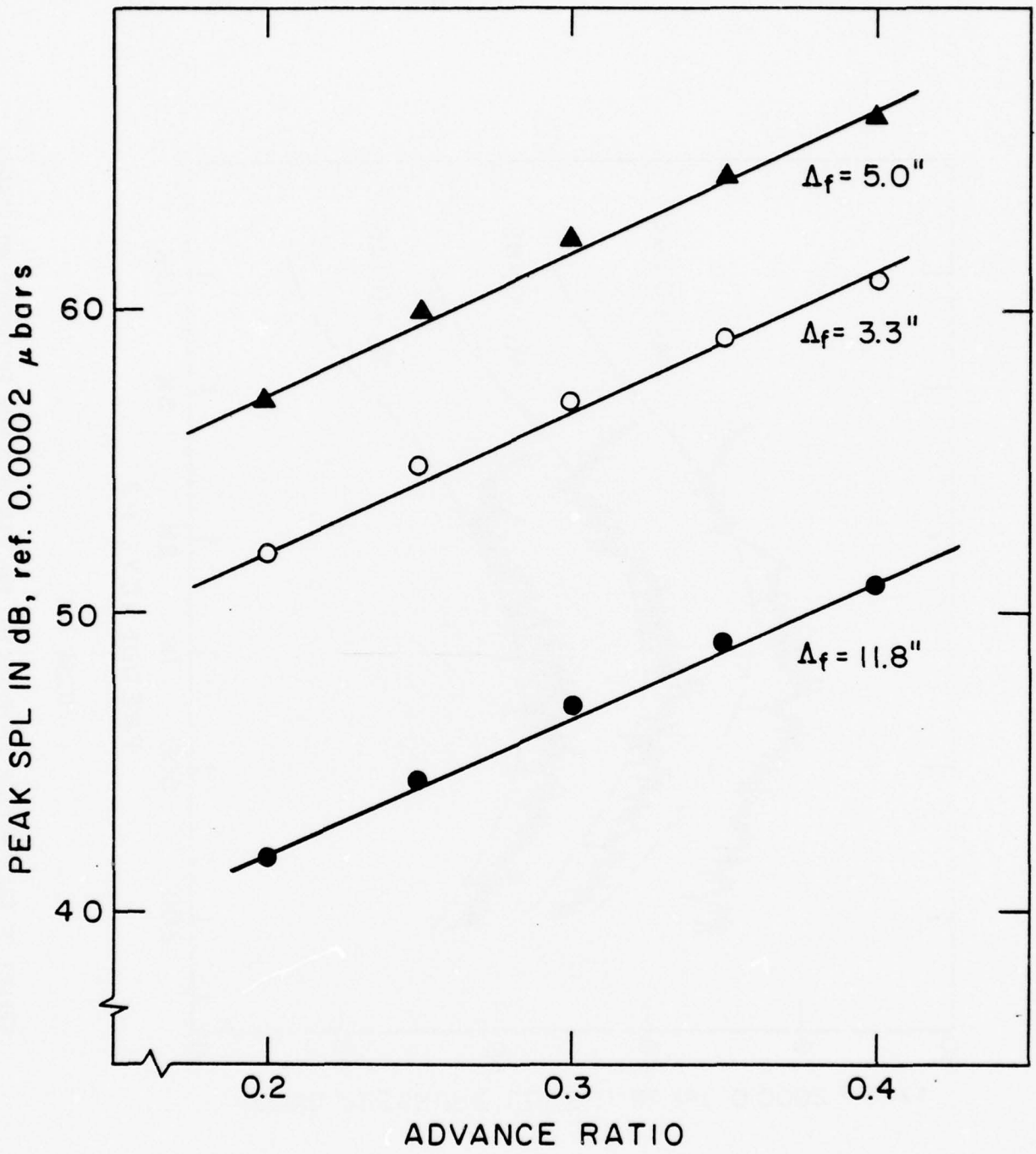
FIGURE 4.5

EFFECT OF ADVANCE RATIO ON THE PEAK INTENSITY
OF LOW FREQUENCY BROADBAND NOISE
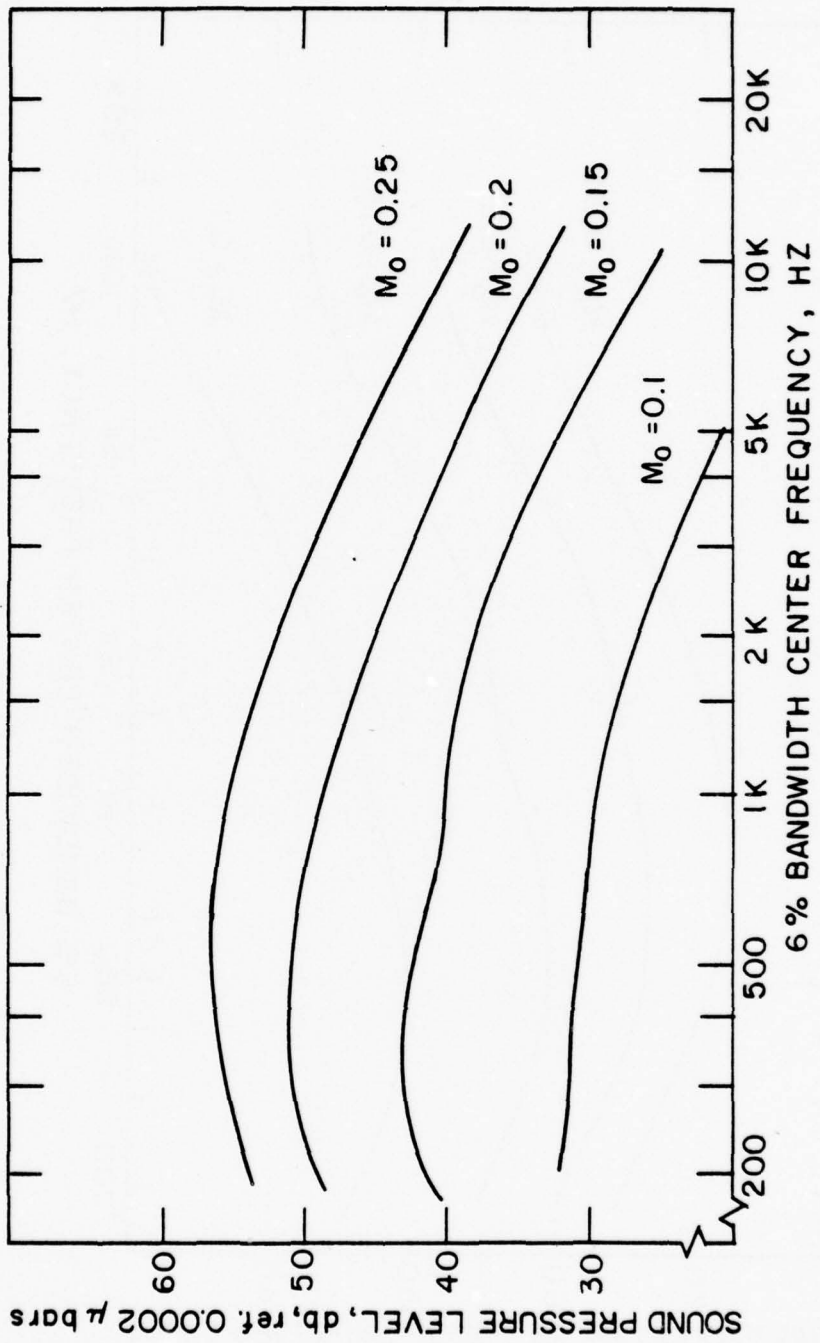
FIGURE 4.6

EFFECT OF MACH NUMBER ON PREDICTED LOW FREQUENCY BROADBAND NOISE SPECTRA FOR

$\Lambda_f = 11.8$ INCHES
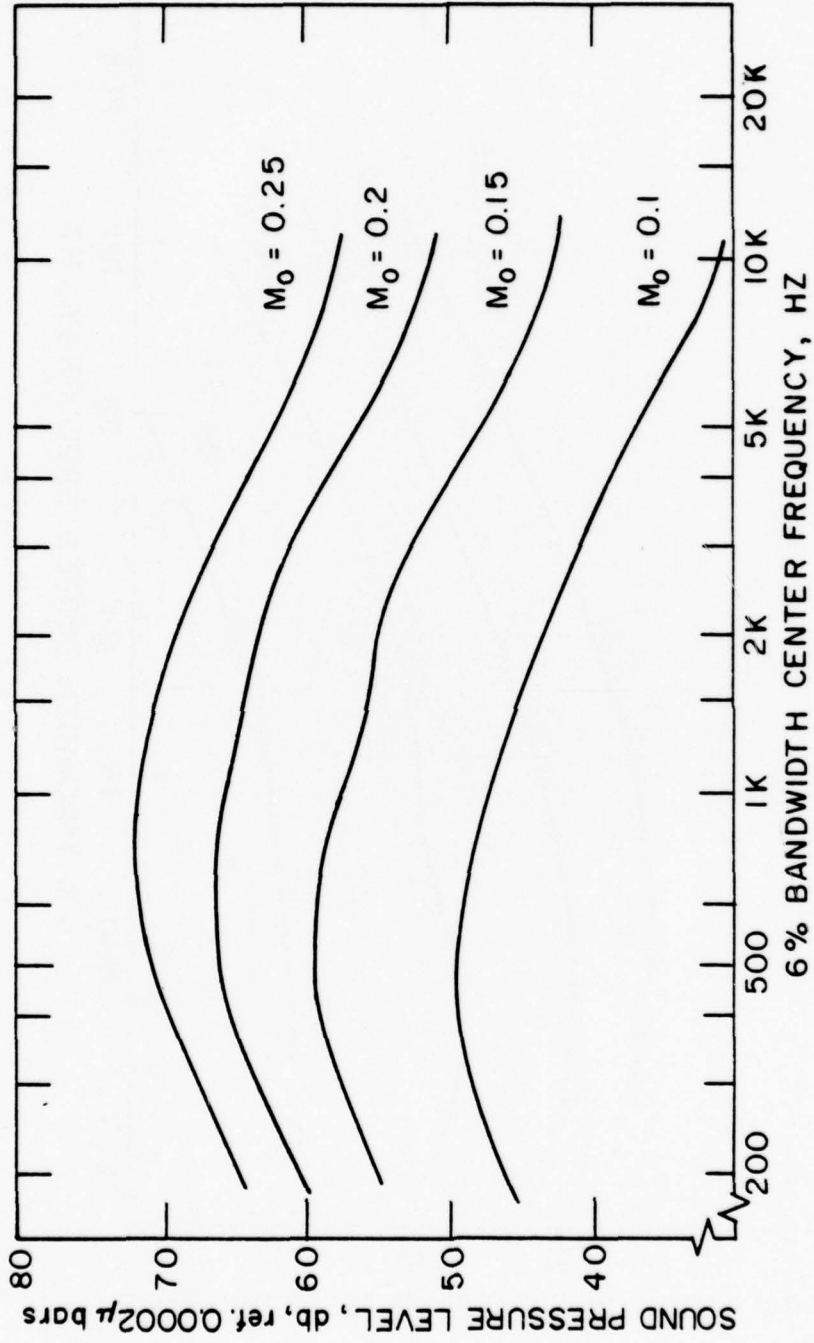
FIGURE 4.7

EFFECT OF MACH NUMBER ON PREDICTED LOW FREQUENCY BROADBAND NOISE SPECTRA FOR

$\Lambda_f = 5.0$ INCHES
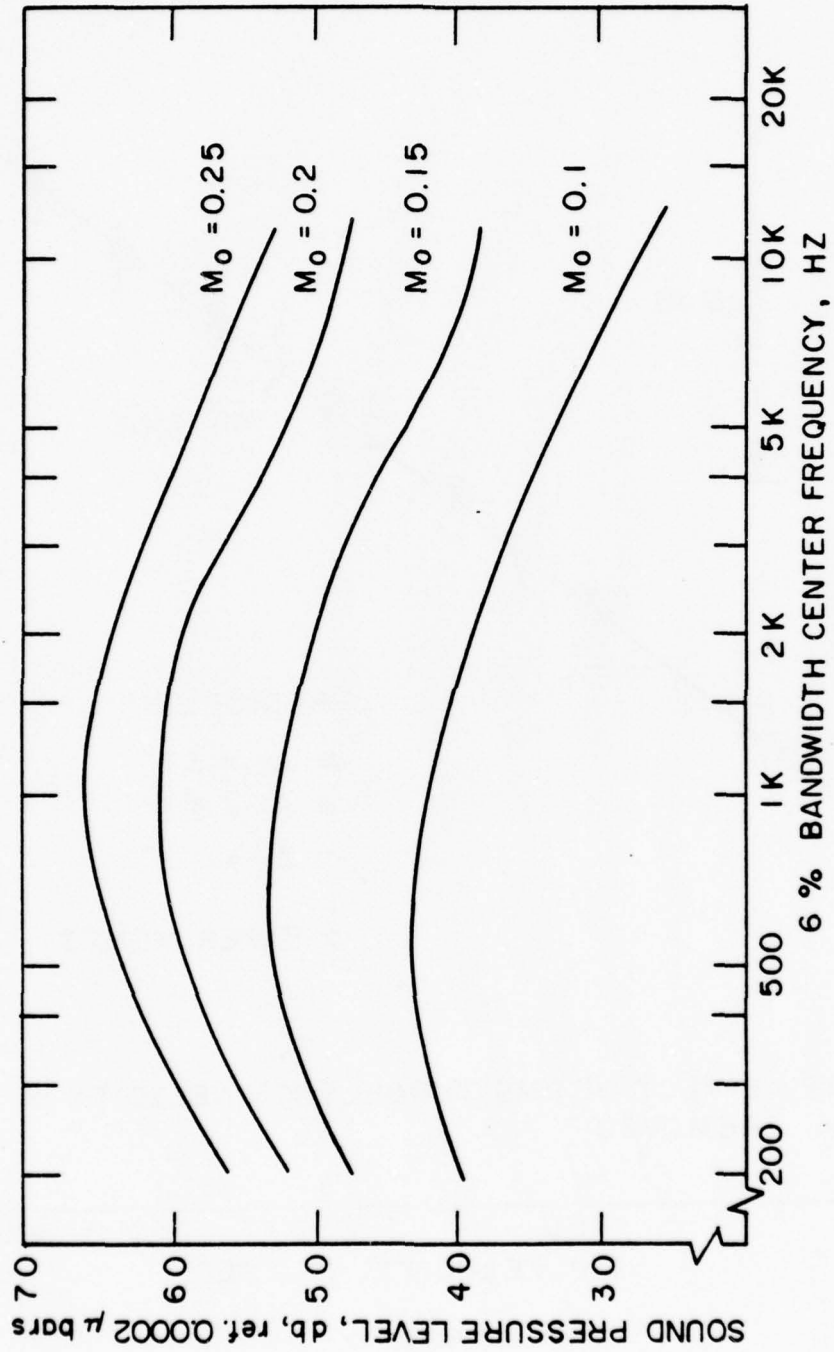
FIGURE 4.8

EFFECT OF MACH NUMBER ON PREDICTED LOW FREQUENCY BROADBAND NOISE SPECTRA

FOR $\Lambda_f = 3.3$ INCHES
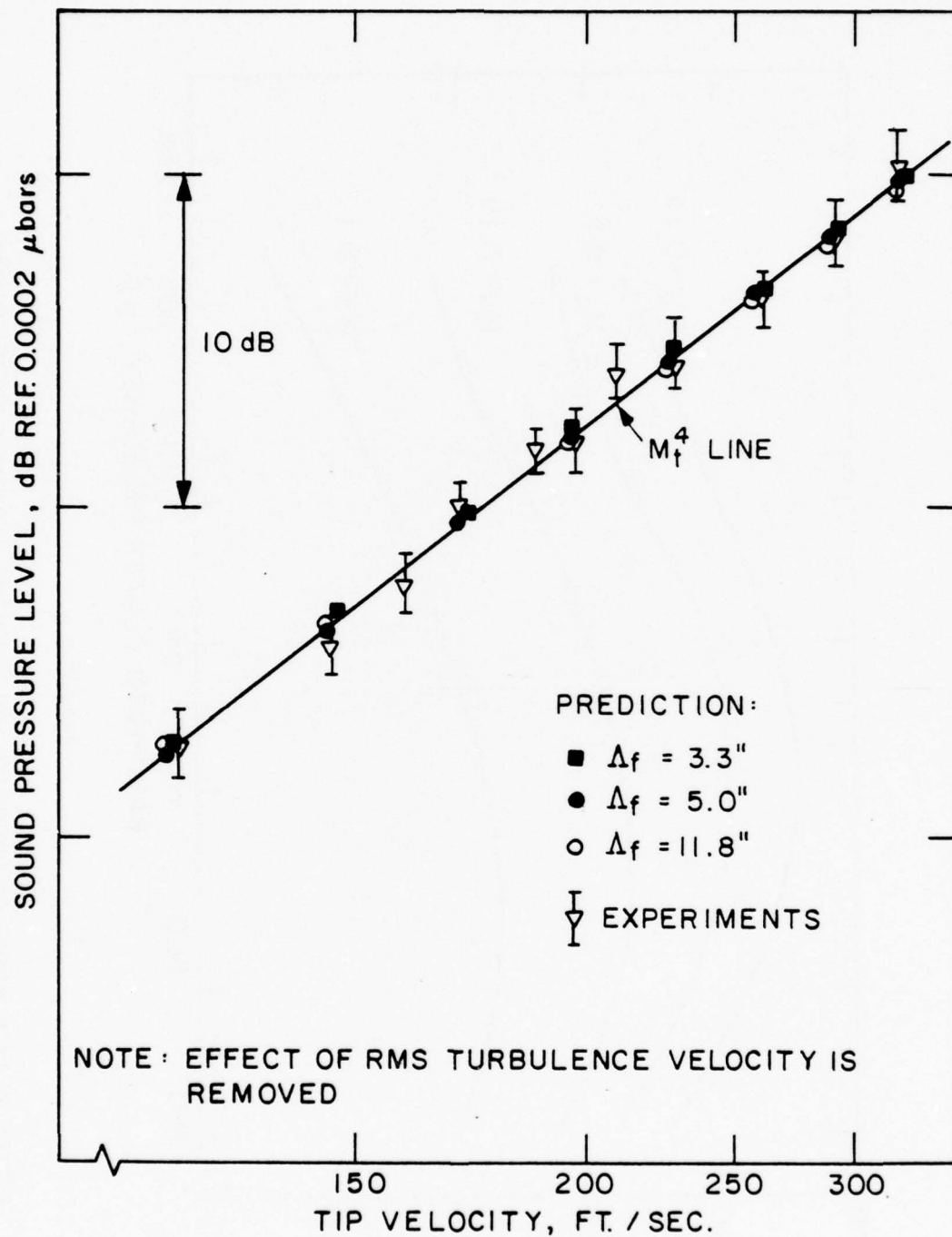
FIGURE 4.9

EFFECT OF TIP VELOCITY ON PREDICTED AND MEASURED PEAK LOW FREQUENCY
BROADBAND NOISE INTENSITY
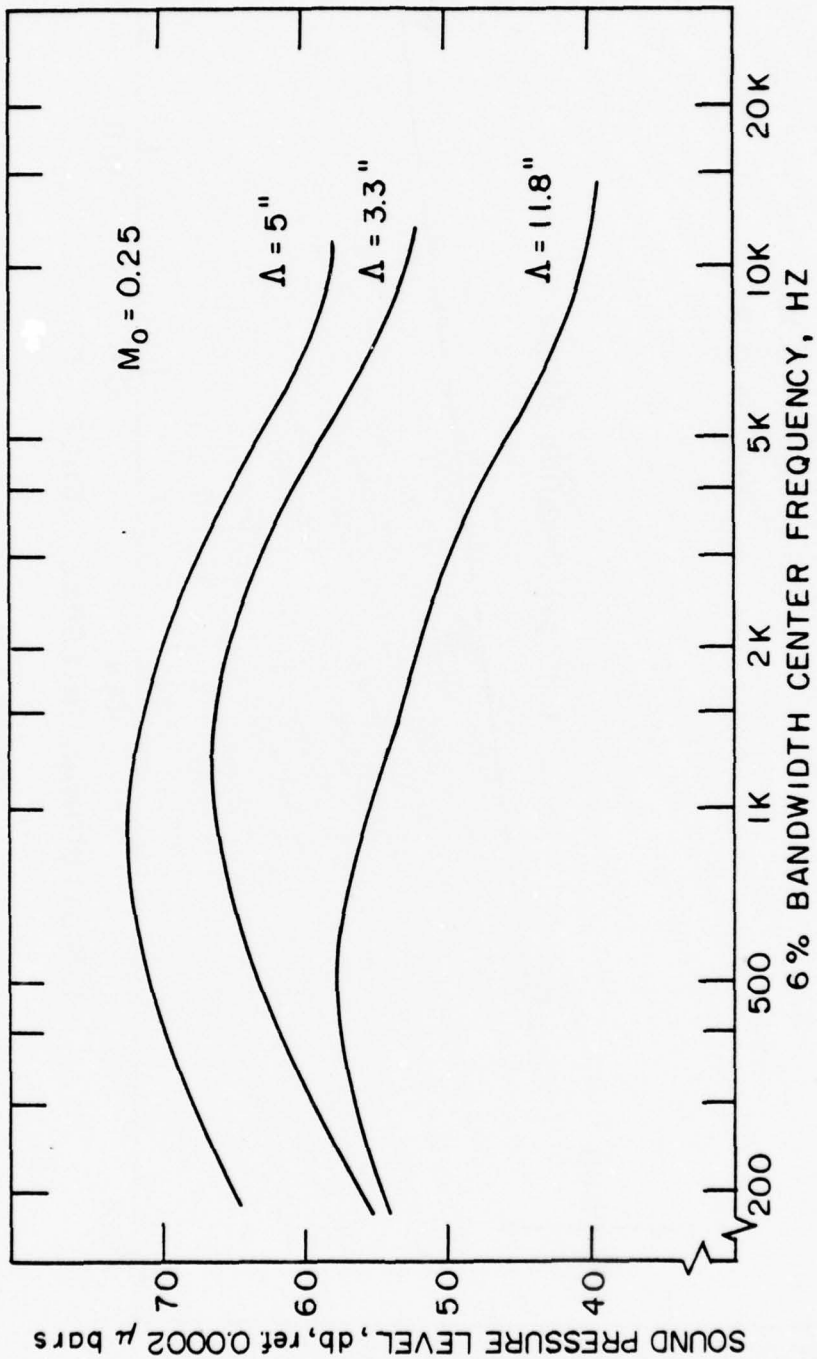
FIGURE 4.10

EFFECT OF INTEGRAL SCALE ON PREDICTED LOW FREQUENCY BROADBAND NOISE SPECTRA FOR M_0 = 0.25
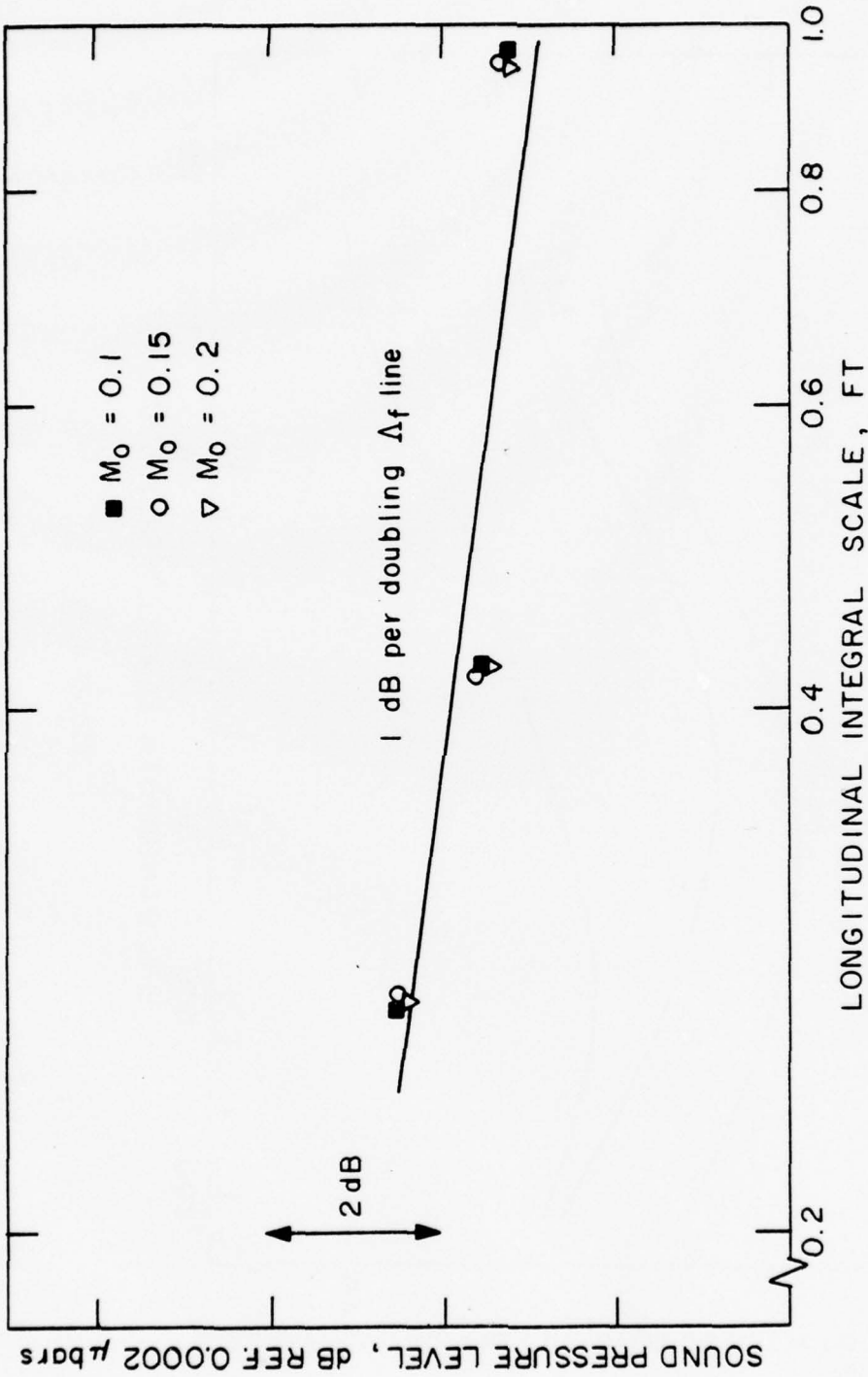
FIGURE 4.11

EFFECT OF TURBULENCE SCALE ON THE PEAK INTENSIGY OF LOW FREQUENCY BROADBAND NOISE
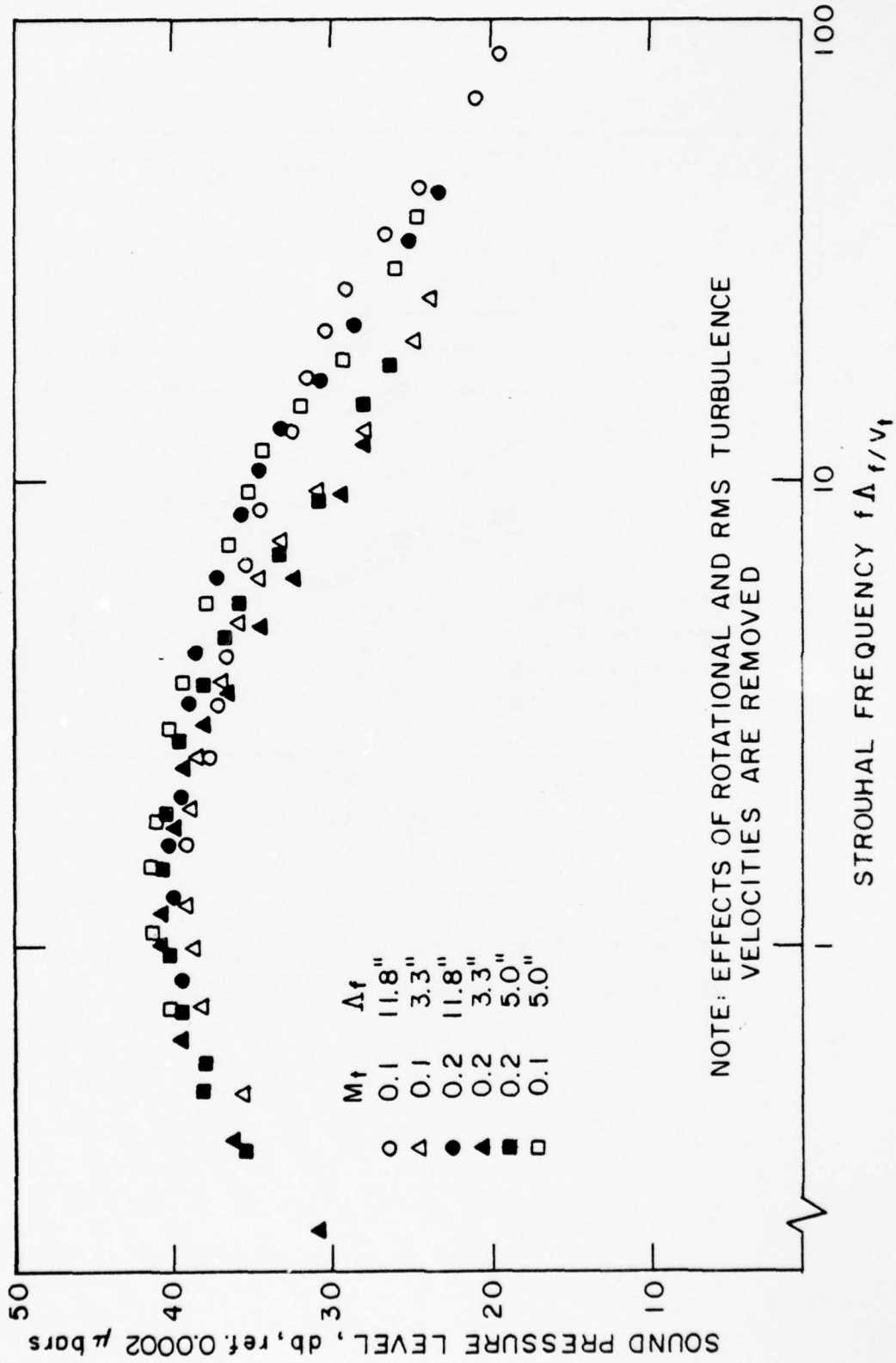
FIGURE 4.12

SPECTRUM OF LOW FREQUENCY BROADBAND NOISE AS A FUNCTION OF NON DIMENSIONAL FREQUENCY

NOTE: EFFECTS OF ROTATIONAL AND RMS TURBULENCE
VELOCITIES ARE REMOVED

STROUHAL FREQUENCY $f \Lambda_f / v_t$

	M_t	Λ_f
○	0.1	11.8"
△	0.1	3.3"
●	0.2	11.8"
▲	0.2	3.3"
■	0.2	5.0"
□	0.1	5.0"

SOUND PRESSURE LEVEL, db, ref. 0.0002 μ bars
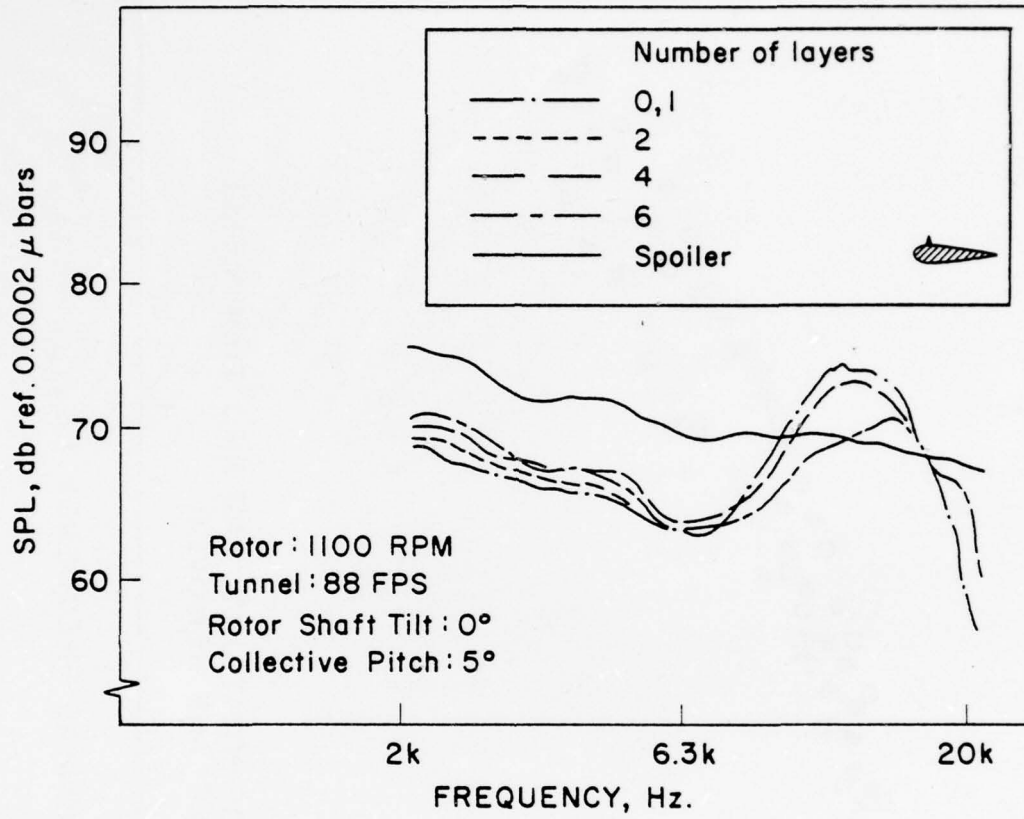
FIGURE 5.1

THE EFFECT OF SUCTION SURFACE SERRATION ON
6% BANDWIDTH HIGH FREQUENCY BROADBAND NOISE
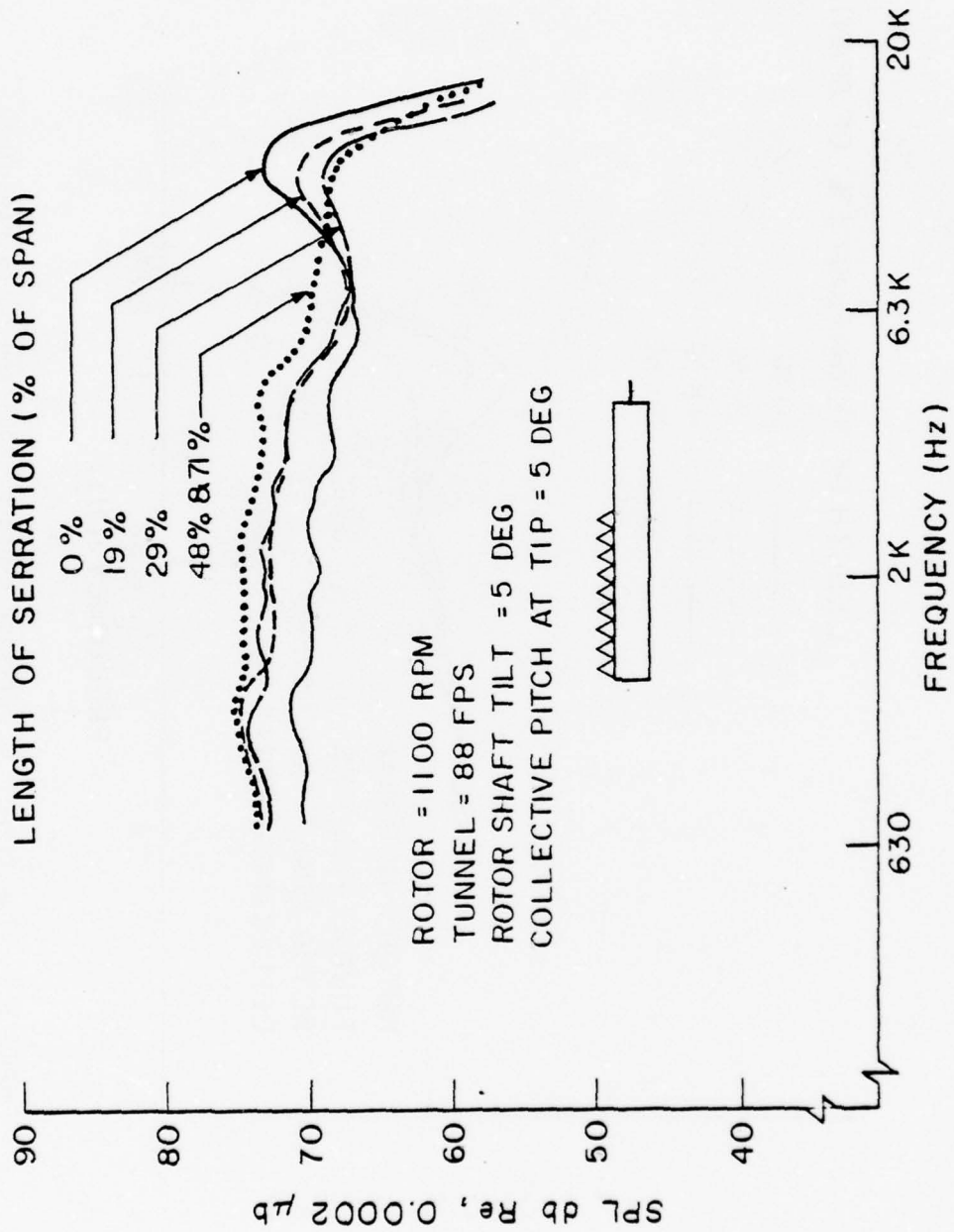
FIGURE 5.2   THE EFFECT OF LEADING EDGE SERRATION ON 6% BANDWIDTH HIGH FREQUENCY BROADBAND NOISE SPECTRA
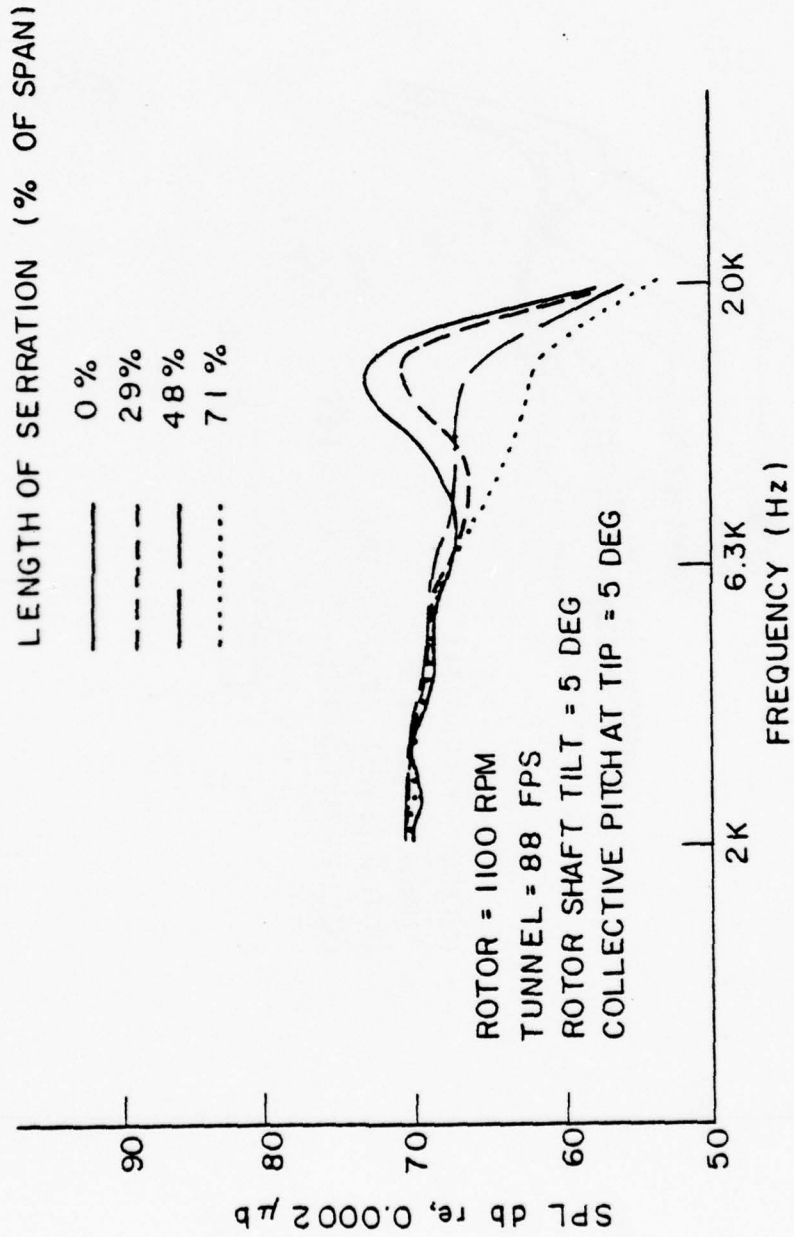
FIGURE 5.3   THE EFFECT OF PRESSURE SURFACE SERRATION ON 6% BANDWIDTH
HIGH FREQUENCY BROADBAND NOISE SPECTRA.
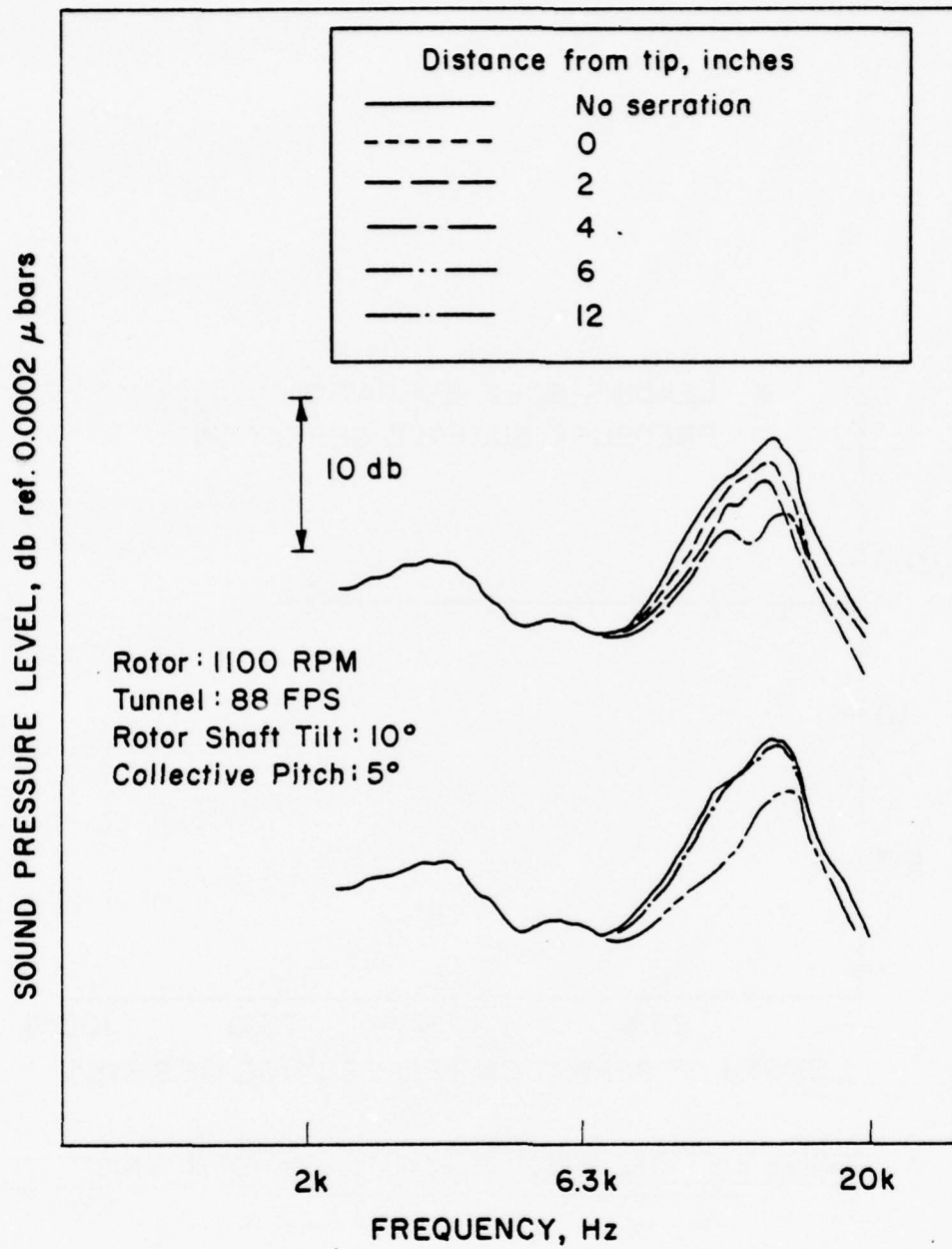
FIGURE 5.4   THE EFFECT OF 4-INCH SERRATION ON 6% BANDWIDTH
HIGH FREQUENCY BROADBAND NOISE SPECTRA.
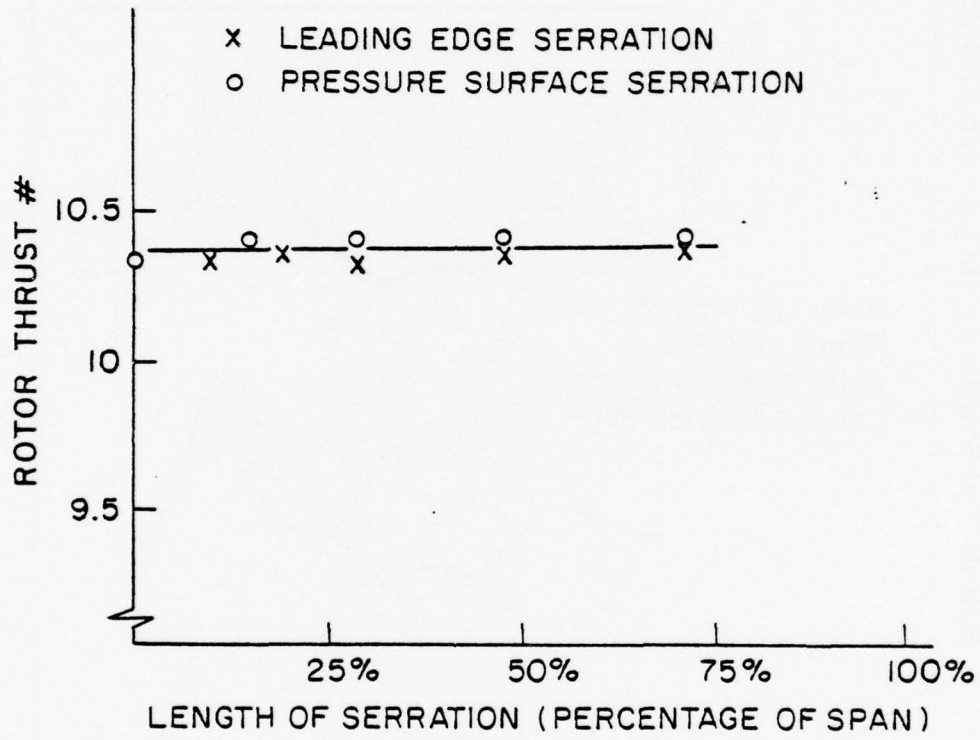
FIGURE 5.5   THE EFFECT OF SERRATION ON ROTOR THRUST
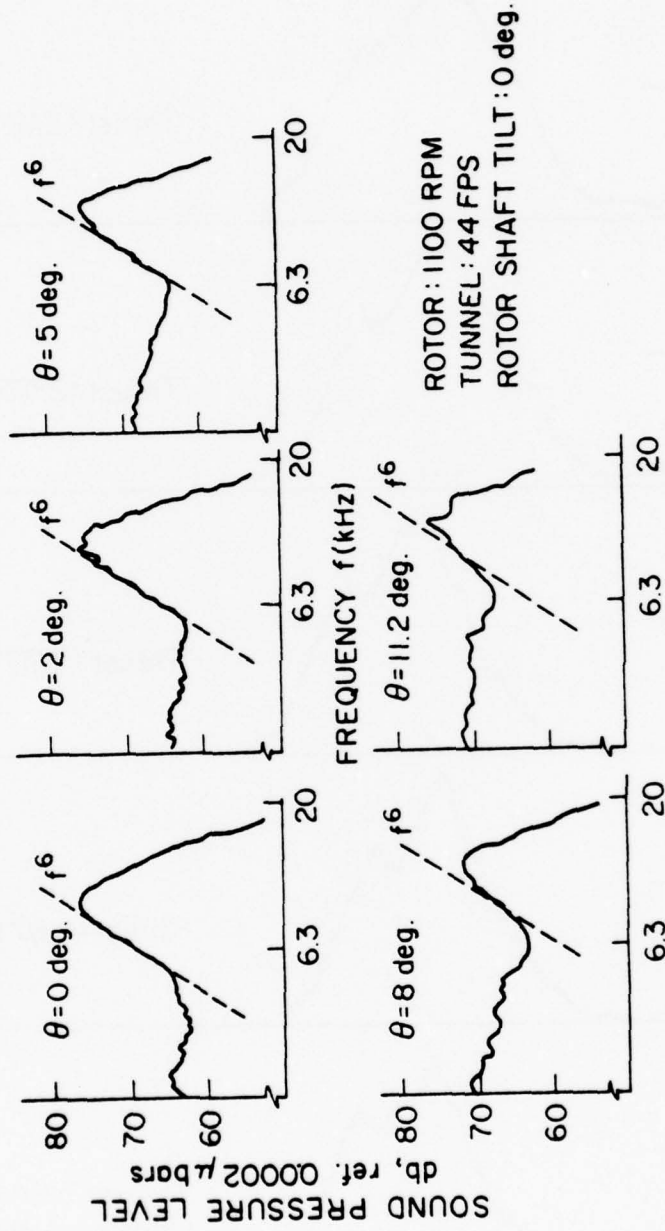
FIGURE 5.6 THE EFFECT OF ROTOR COLLECTIVE PITCH ON 6% BANDWIDTH
HIGH FREQUENCY BROADBAND NOISE SPECTRA.
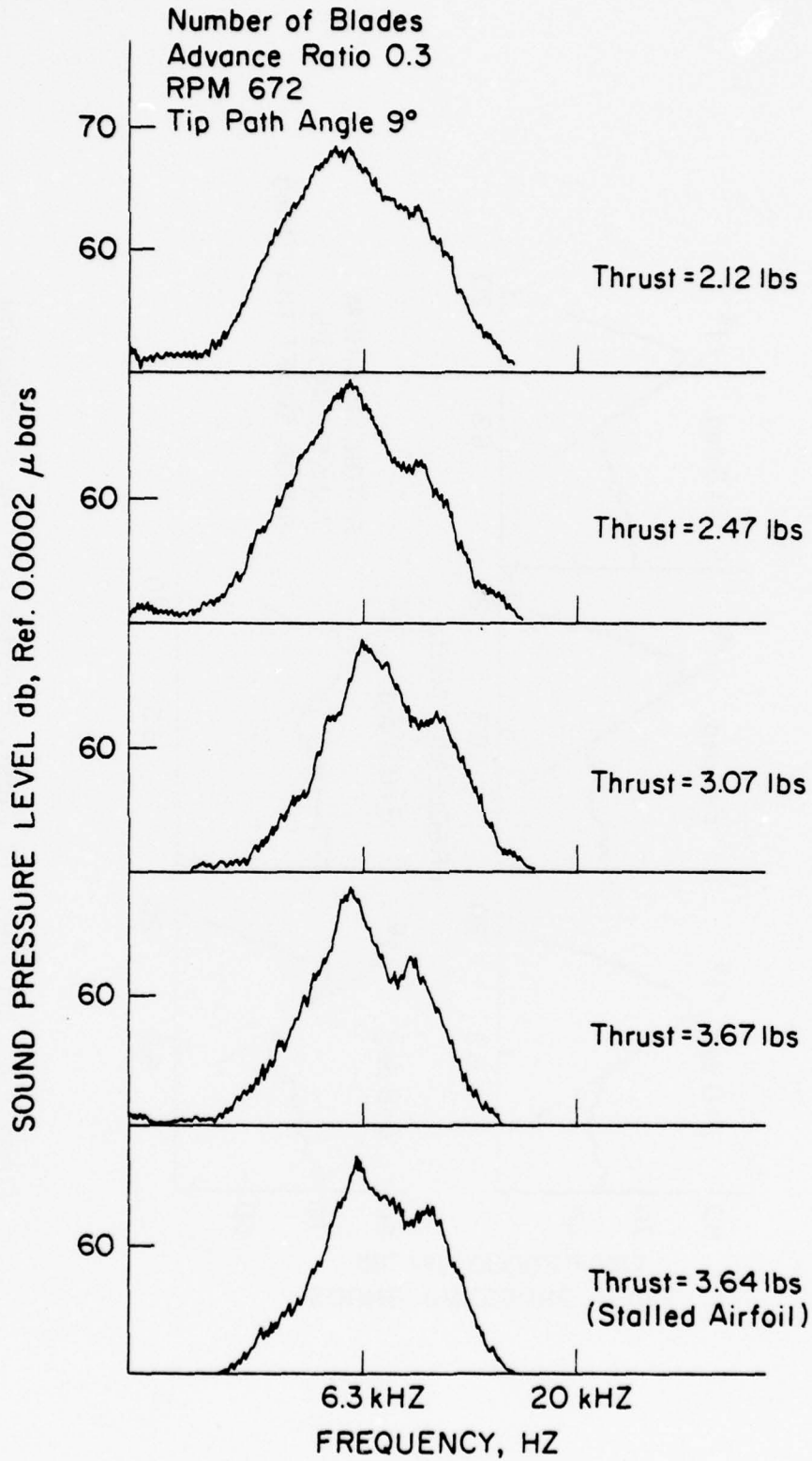
FIGURE 5.7   EFFECT OF STEADY THRUST ON HIGH FREQUENCY
BROADBAND NOISE.
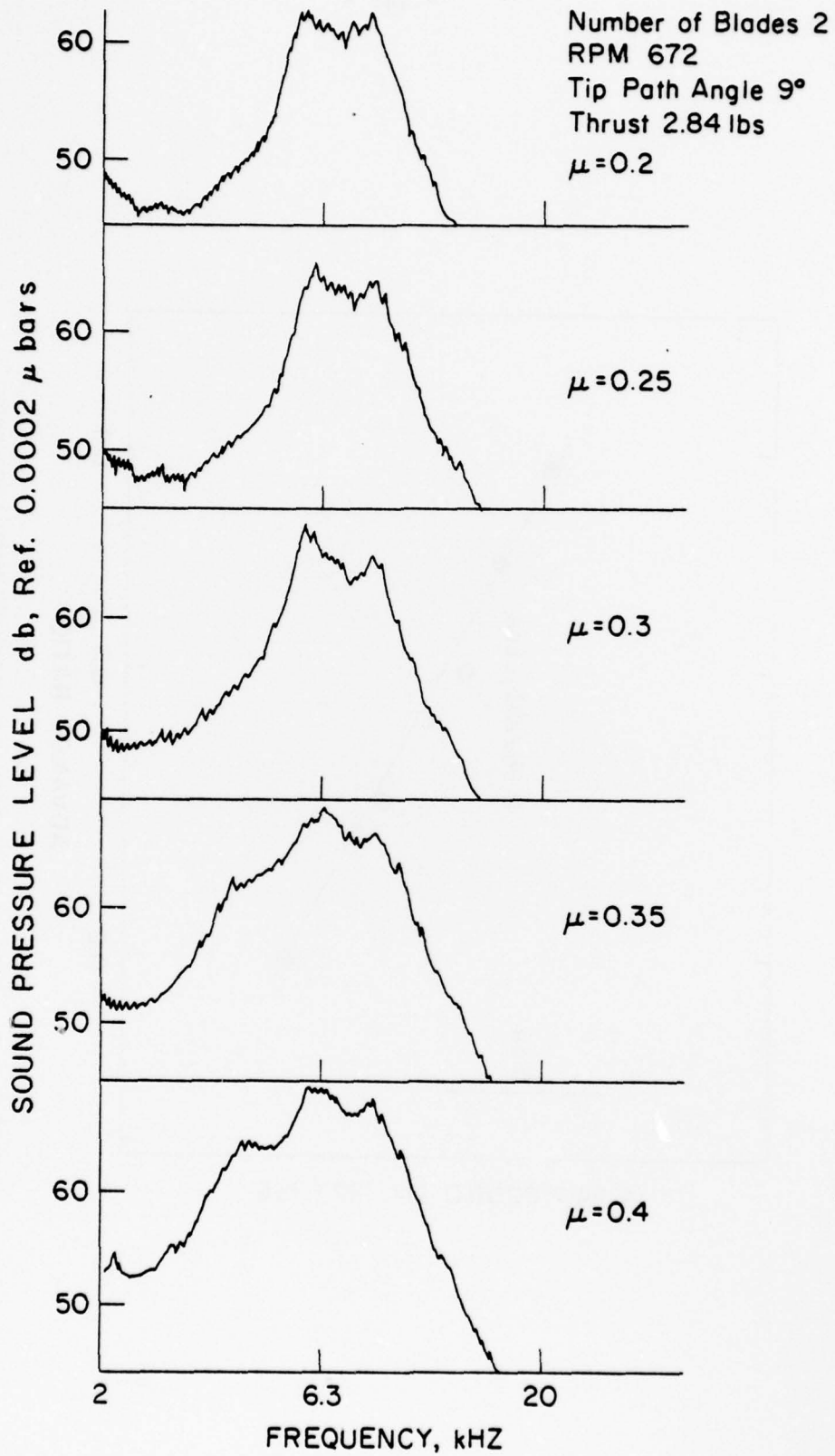
FIGURE 5.8   EFFECT OF ADVANCE RATIO ON HIGH FREQUENCY
BROADBAND NOISE.
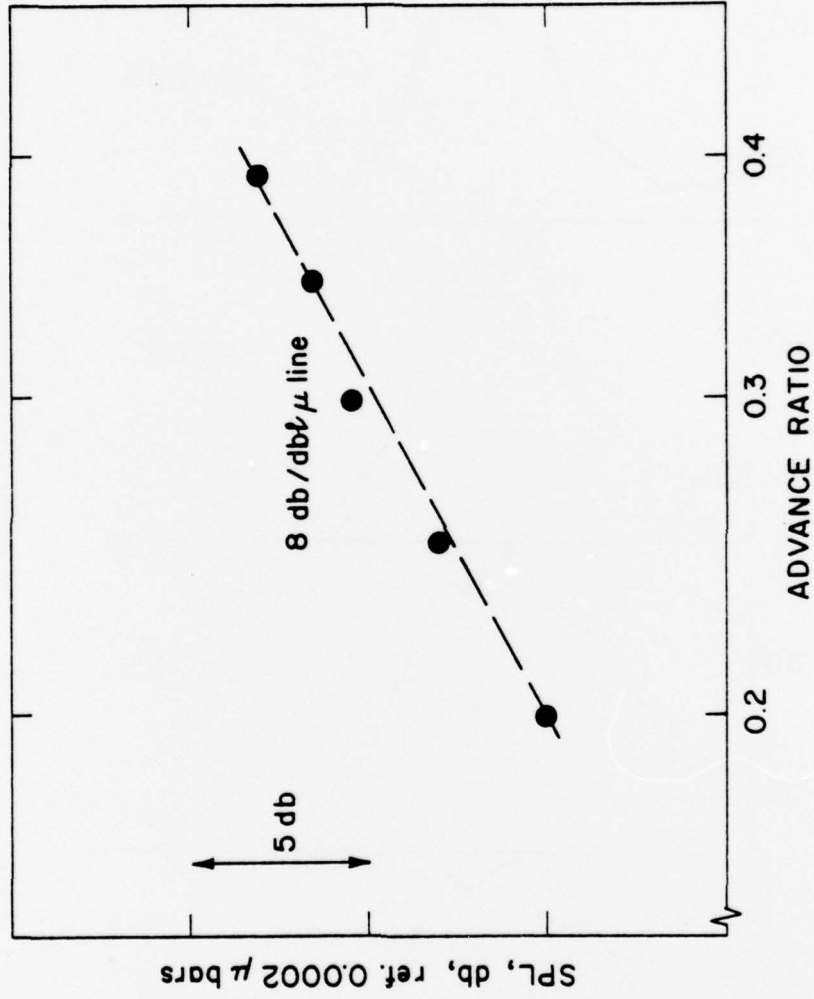
FIGURE 5.9   VARIATION OF PEAK INTENSITY OF HIGH FREQUENCY
BROADBAND NOISE WITH ADVANCE RATIO.
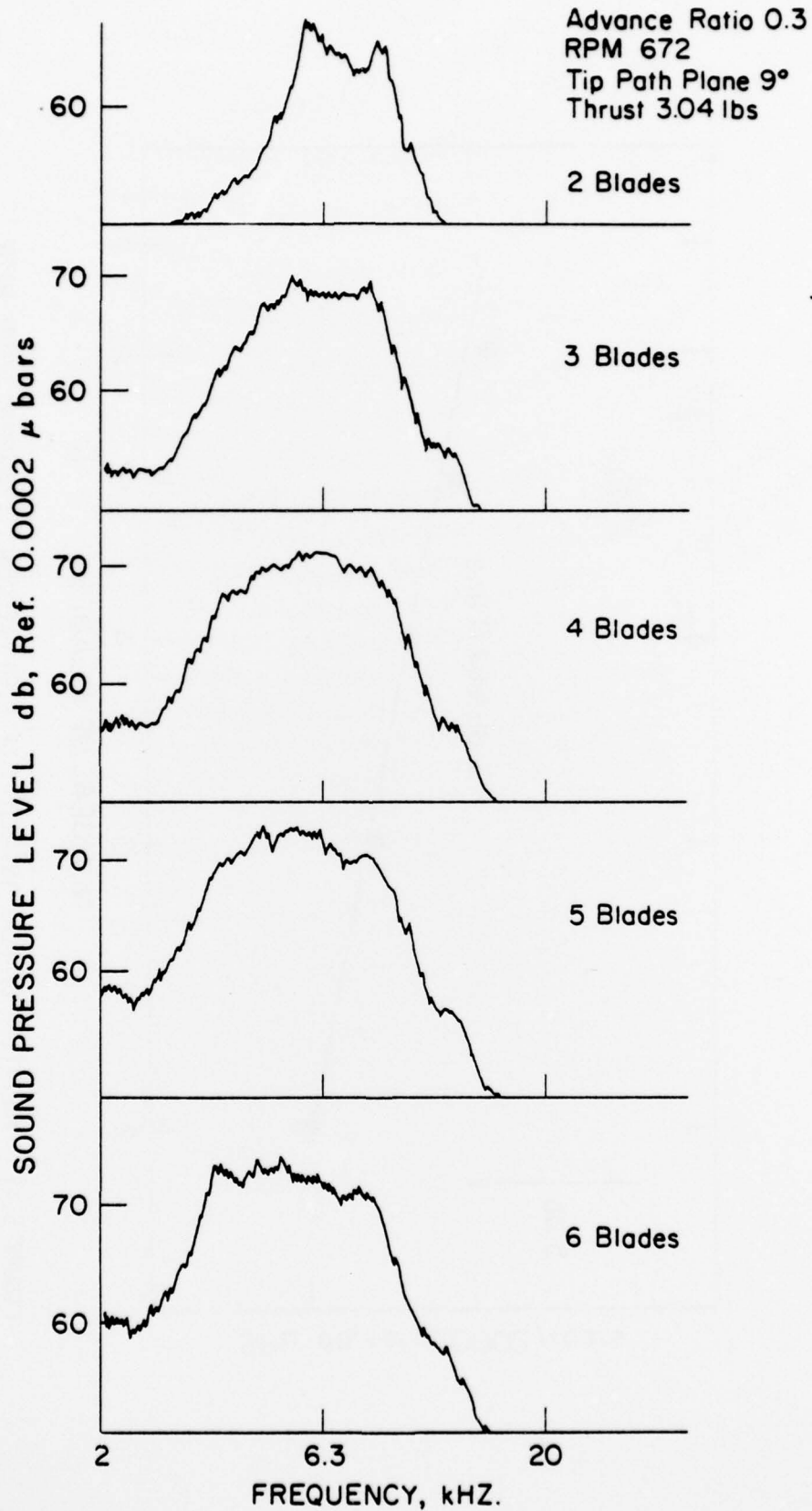
FIGURE 5.10   EFFECT OF NUMBER OF BLADES ON HIGH
FREQUENCY BROADBAND NOISE.
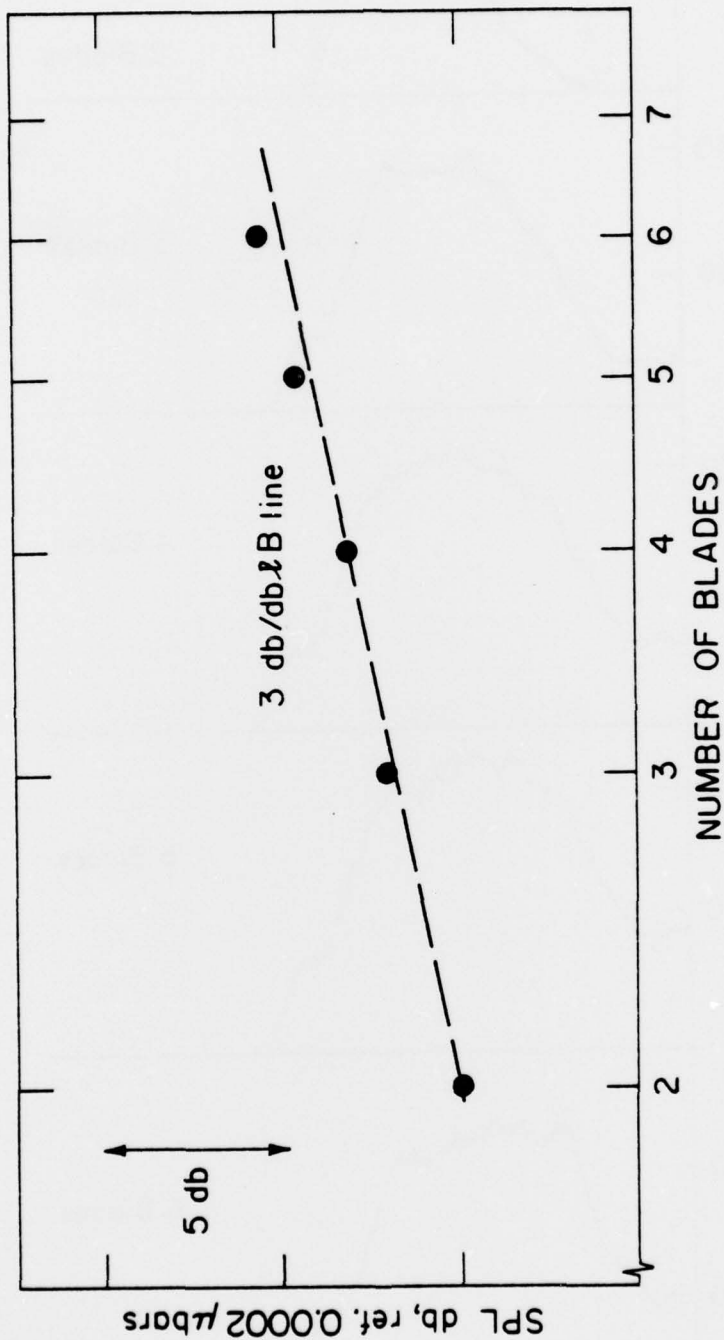
FIGURE 5.11   VARIATION OF PEAK INTENSITY OF HIGH FREQUENCY BROADBAND NOISE WITH
NUMBER OF BLADES.
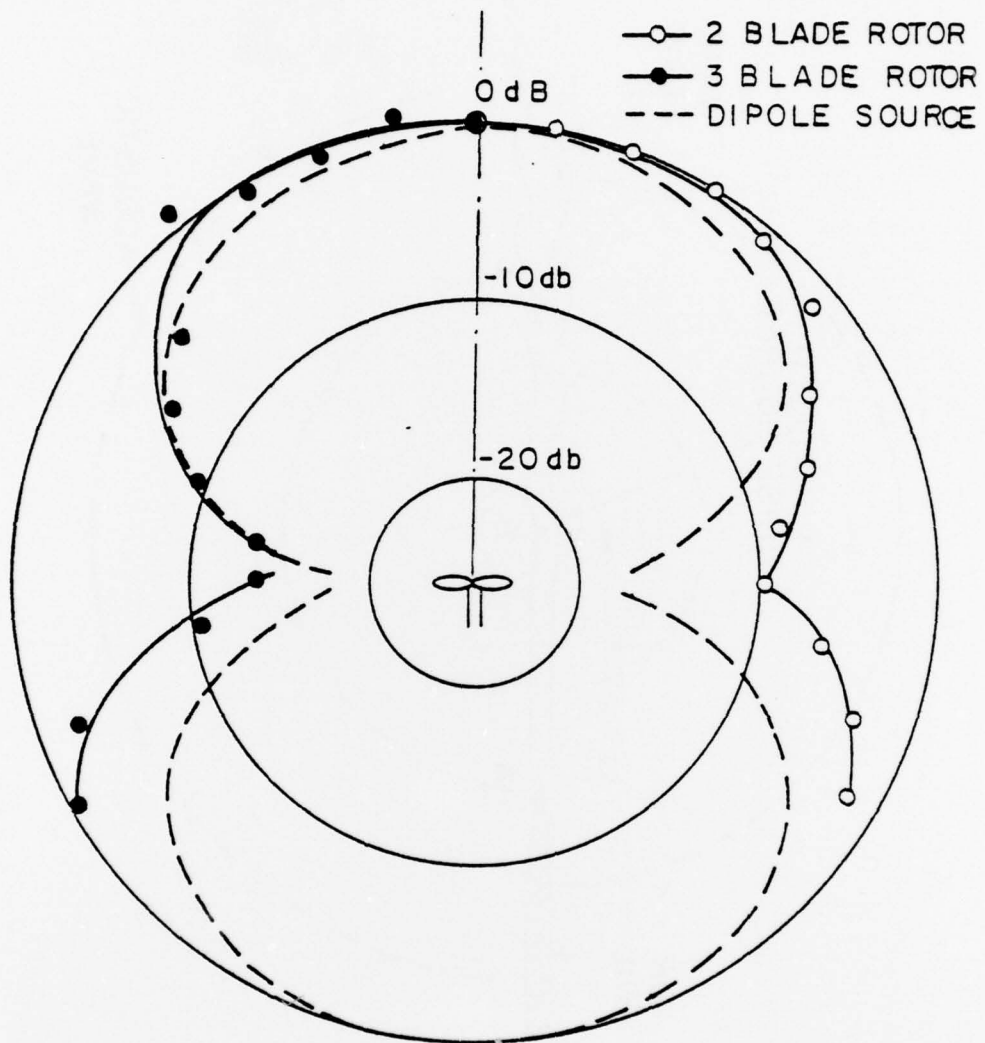
FIGURE 5.12   DIRECTIVITY OF HIGH FREQUENCY BROADBAND NOISE.
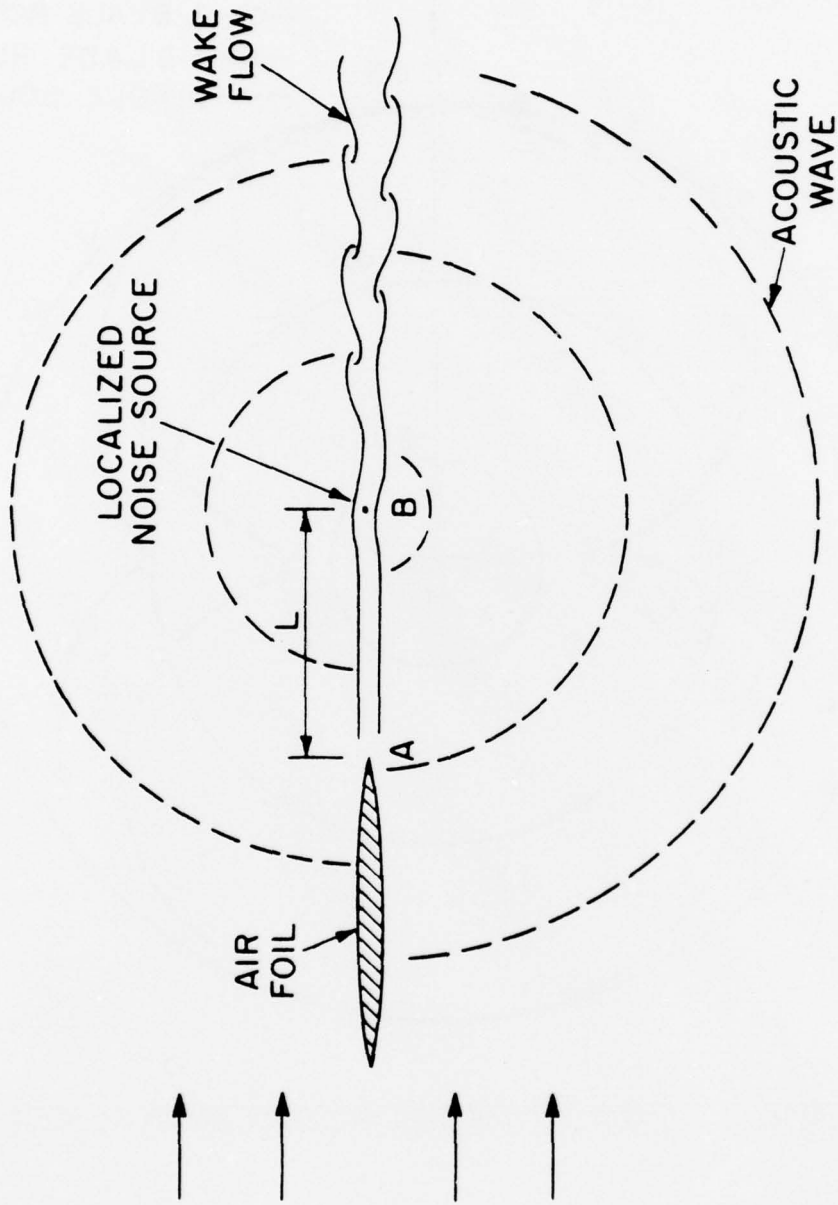
FIGURE 5.13   WAKE FLOW PATTERN BEHIND AN AIRFOIL.
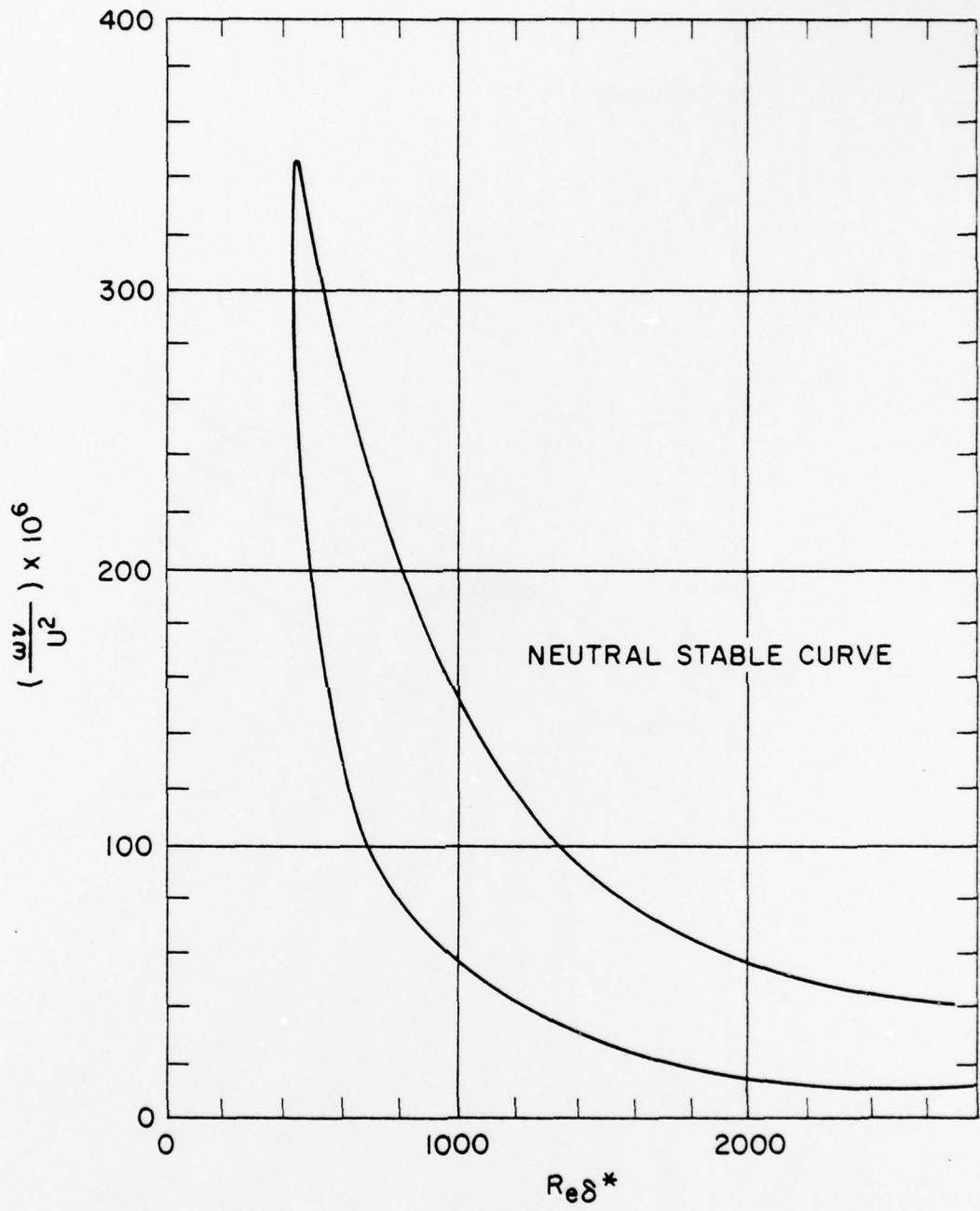
FIGURE 5.14   NEUTRAL STABILITY CONTOUR FOR BLASIUS PROFILE.
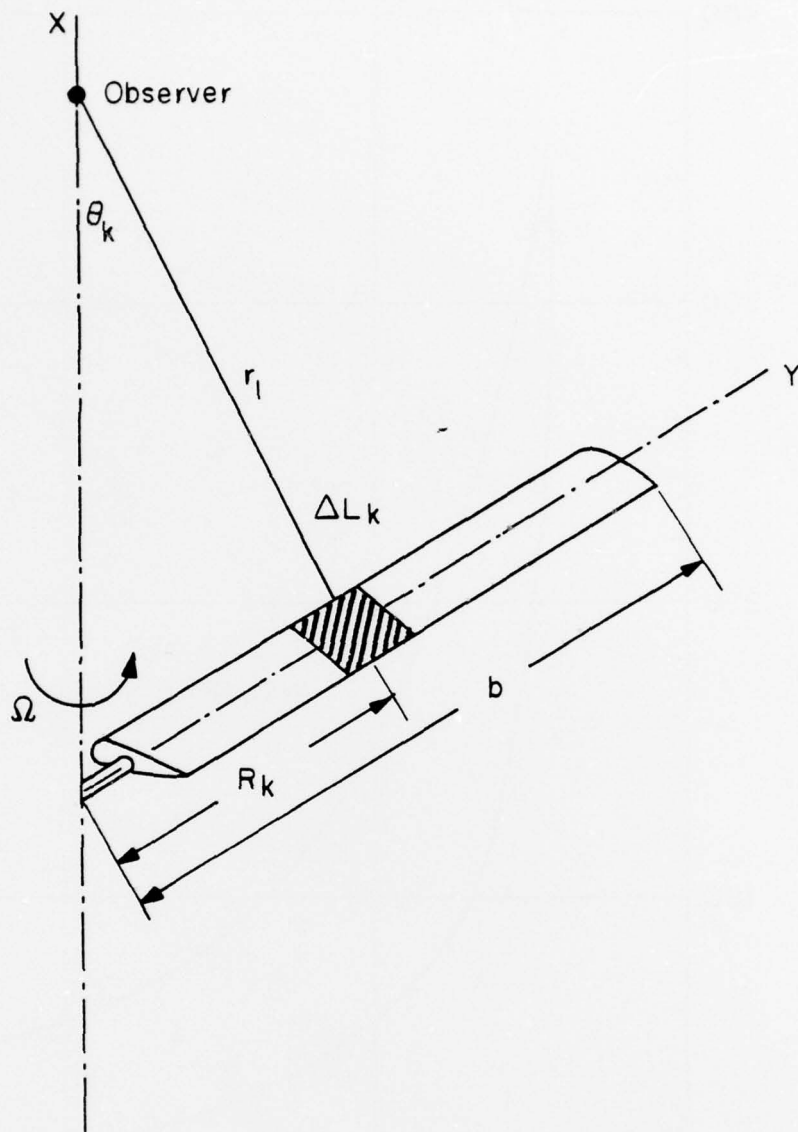
FIGURE 5.15

COORDINATE SYSTEM FOR HIGH FREQUENCY BROADBAND NOISE
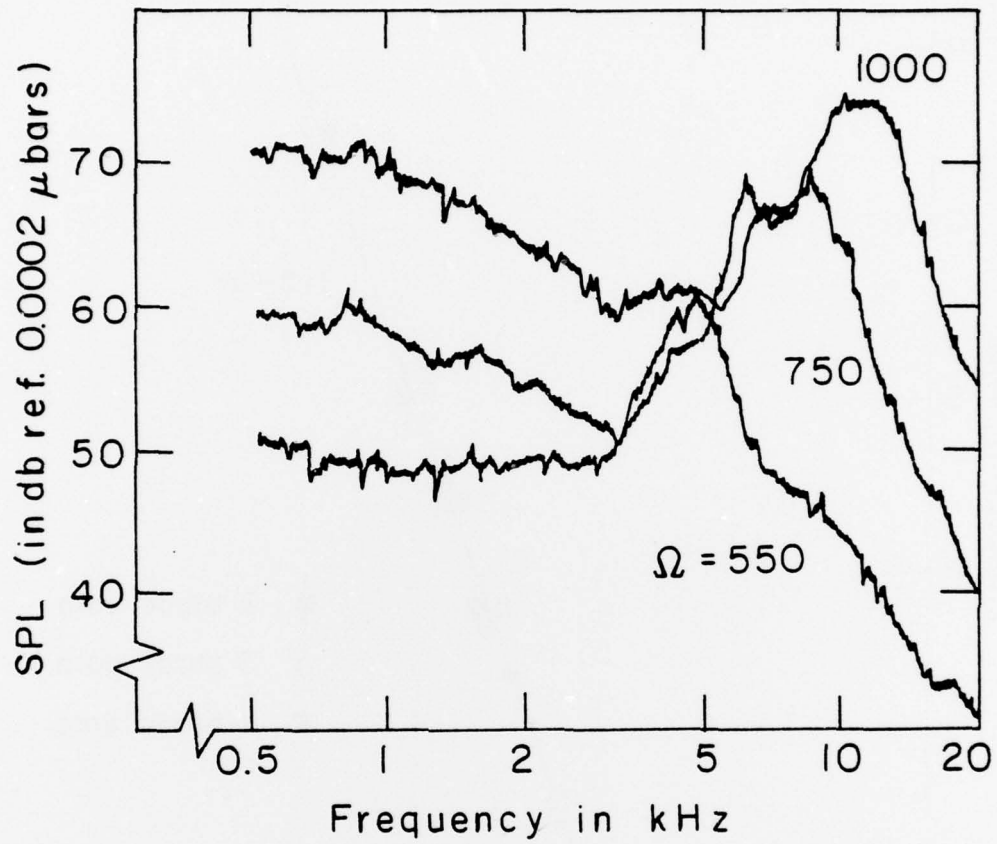
FIGURE 5.16

TYPICAL SPECTRA OF HIGH FREQUENCY BROADBAND NOISE AT
VARIOUS ROTATIONAL SPEEDS
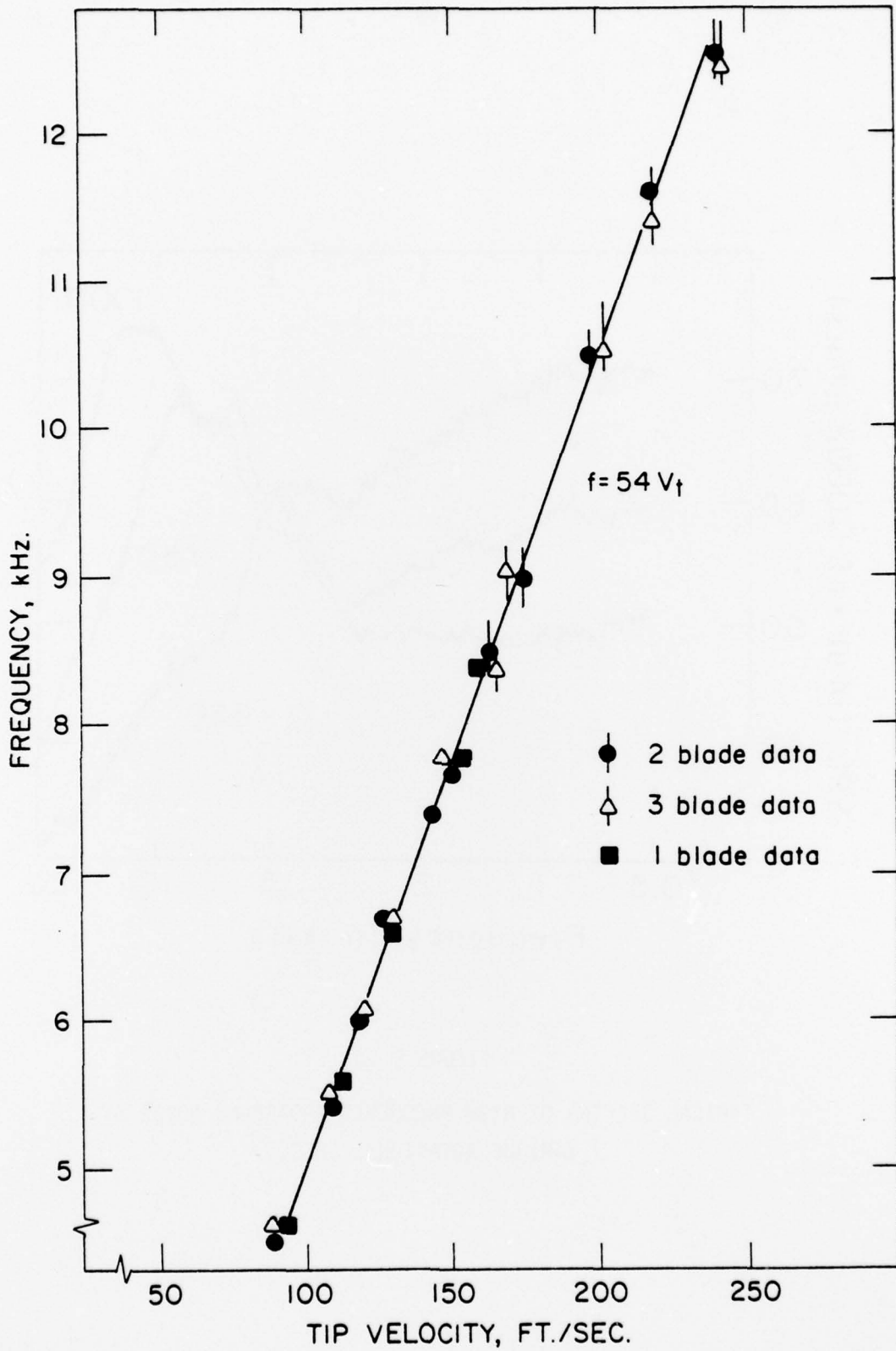
FIGURE 5.17

PEAK FREQUENCY LOCATION AS A FUNCTION OF BLADE TIP SPEED
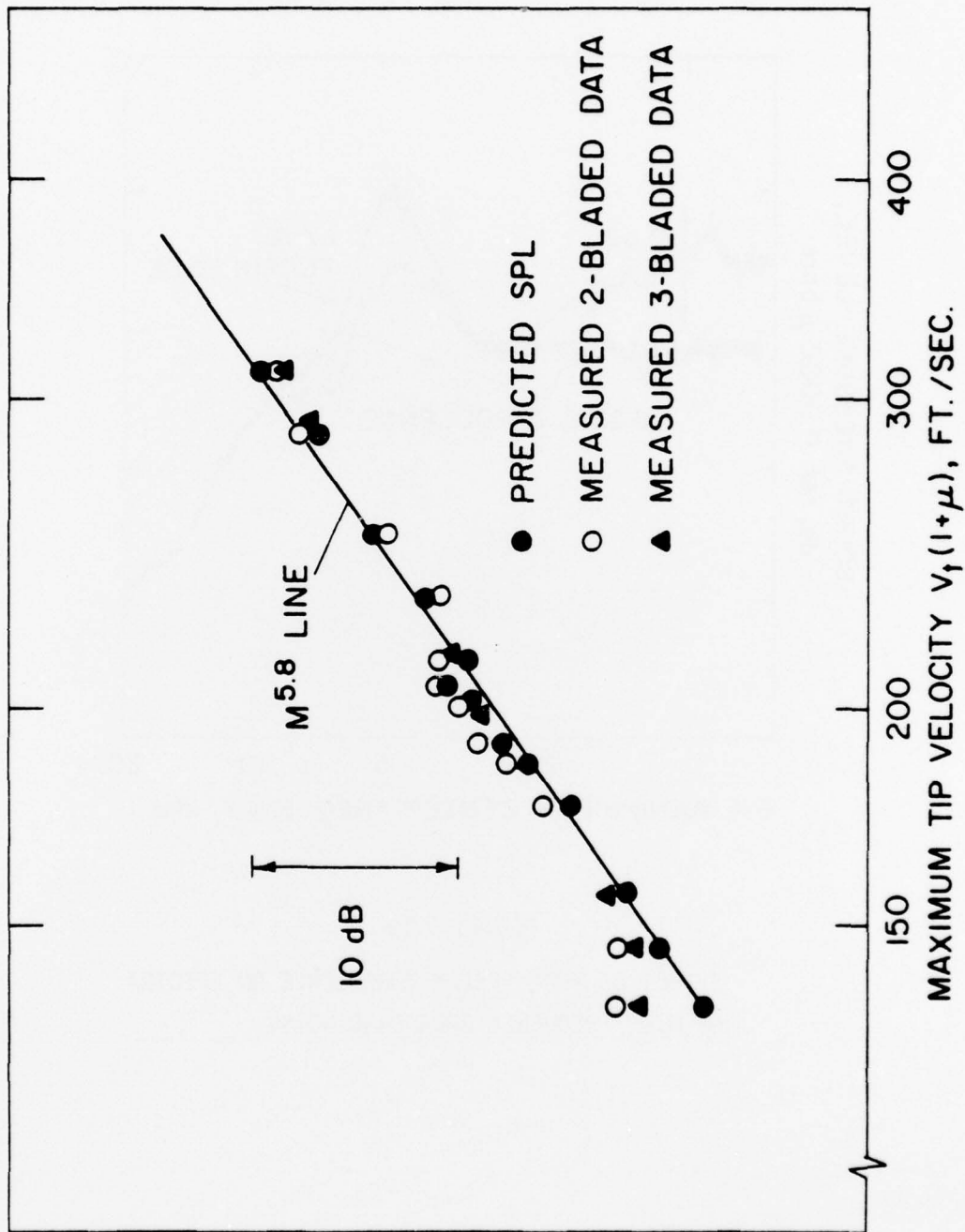
FIGURE 5.18

VELOCITY SCALING OF HIGH FREQUENCY BROADBAND NOISE
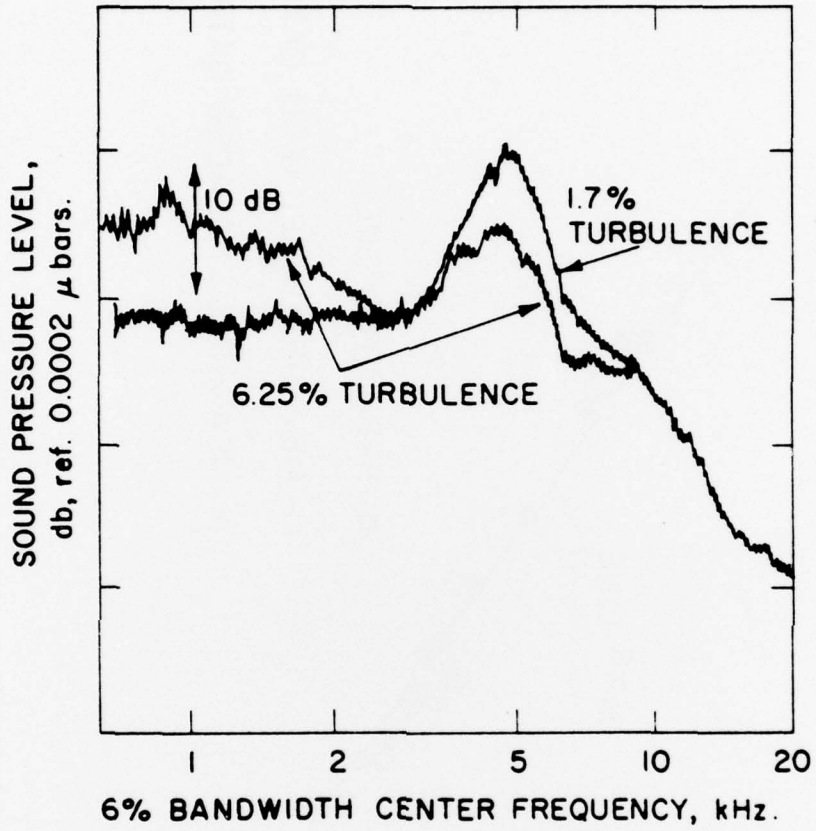
FIGURE 5.19

EFFECT OF FREE STREAM TURBULENCE ON SPECTRA
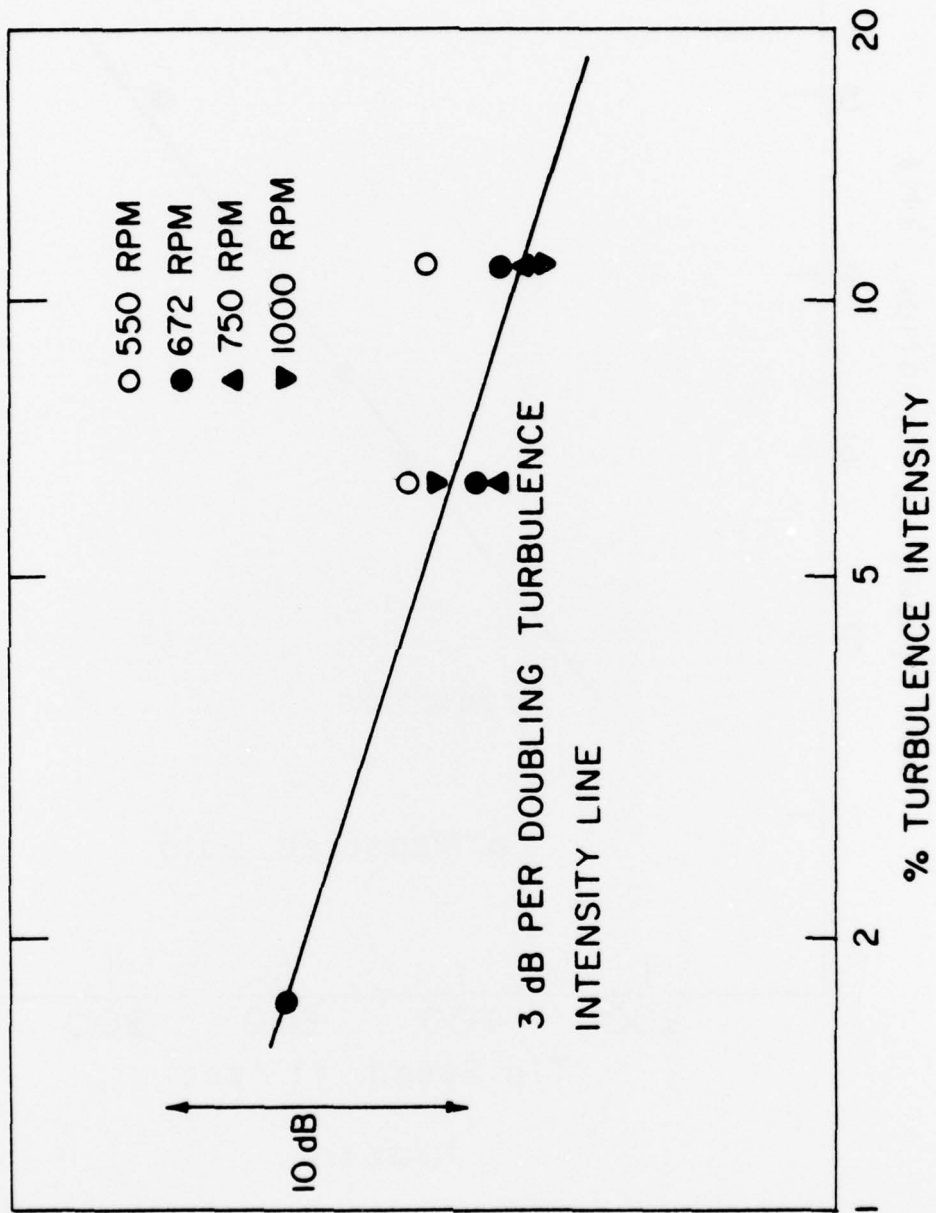OF HIGH FREQUENCY BROADBAND NOISE

FIGURE 5.20

EFFECT OF FREE STREAM TURBULENCE ON PEAK INTENSITY OF HIGH FREQUENCY BROADBAND NOISE
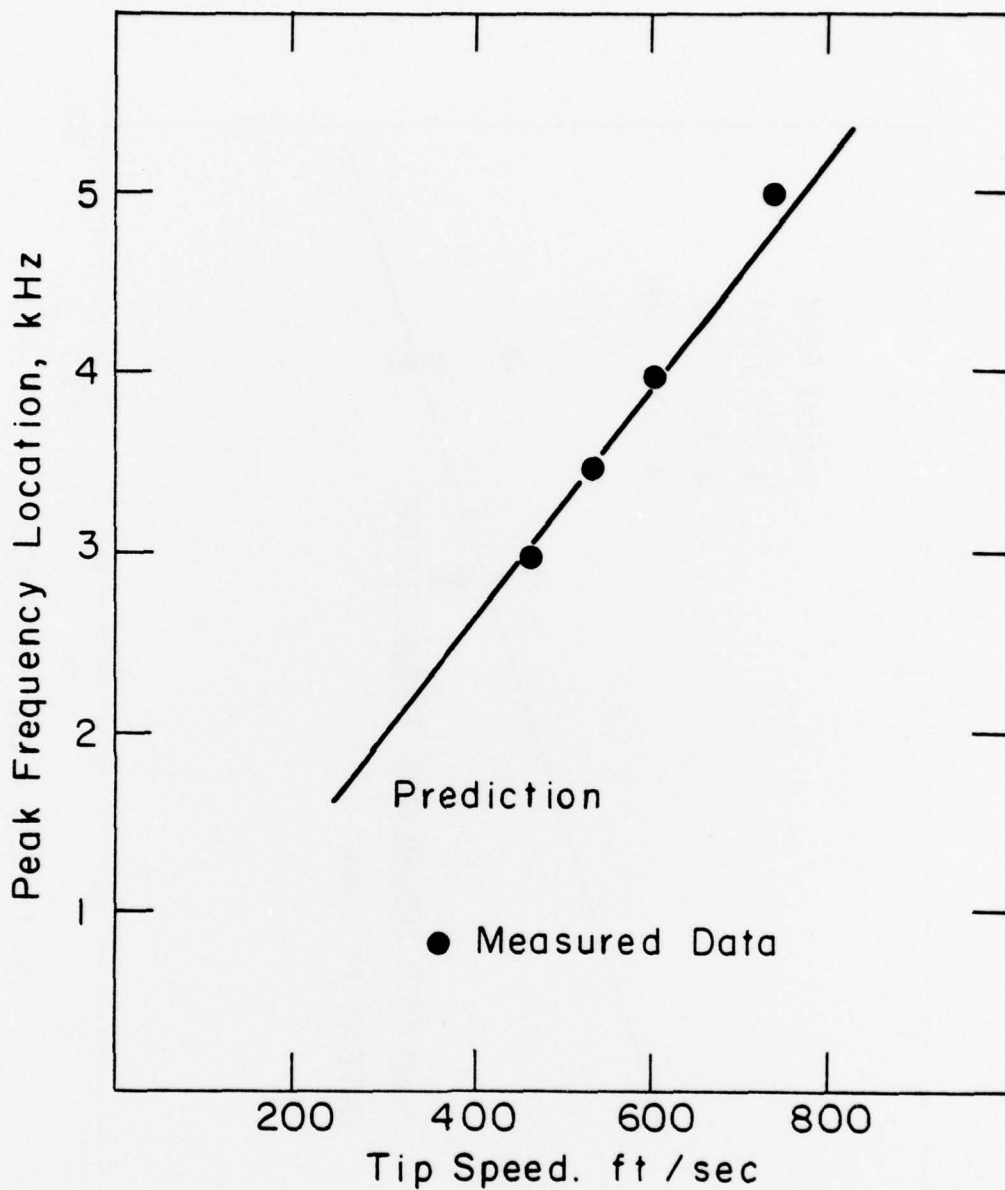
FIGURE 6.1

COMPARISON OF THE PREDICTED PEAK FREQUENCY WITH MEASURED
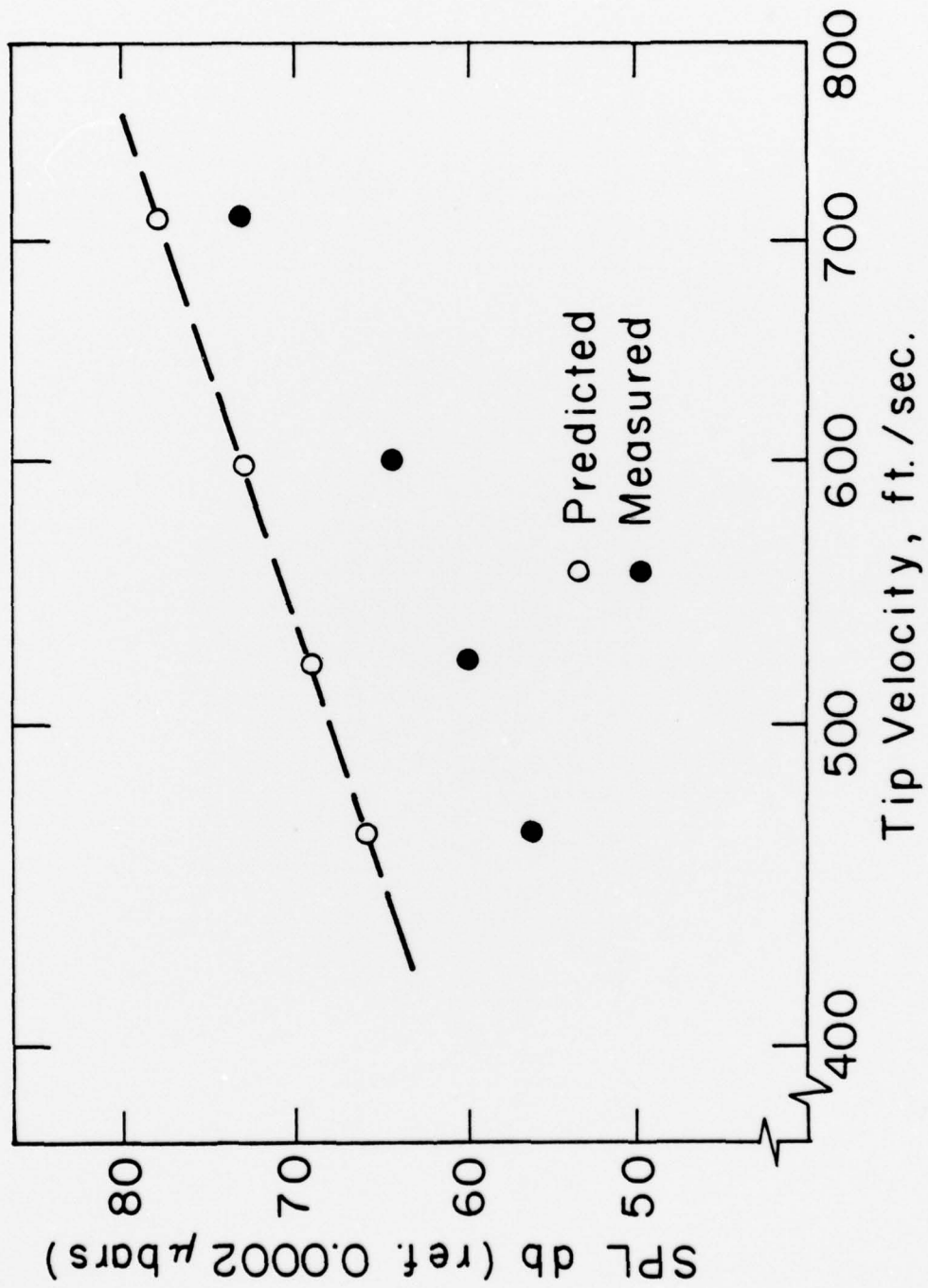
FULL SCALE ROTOR DATA

FIGURE 6.2

COMPARISON BETWEEN PREDICTED AND MEASURED FULL SCALE ROTOR SOUND PRESSURE LEVELS